RESEARCH DEPARTMENT

TECHNICAL REPORT No. 59

DIABATIC NONLINEAR NORMAL MODE INITIALISATION FOR A SPECTRAL MODEL WITH A HYBRID VERTICAL COORDINATE

by

W. Wergen*

Current affiliation:
Deutscher Wetterdienst,
Offenbach.
Federal Republic of Germany

January 1987

Abstract

The normal modes for a baroclinic global spectral model with a hybrid vertical coordinate are derived. A method for incorporating diabatic effects into the initialisation process is presented. The performance of the scheme is discussed. The problem of the systematic rejection of tropical surface pressure information is shown to be associated with an inappropriate initialisation condition for the atmospheric tides. A modified initialisation scheme is proposed and its effectiveness is demonstrated. Finally, experiments on the use of a cut-off period and on the number of vertical modes to be initialised are discussed.

1. INTRODUCTION

Nonlinear normal mode initialisation (NMI) has by now become a widely used technique to control unwanted inertia gravity wave activity in a primitive equation model. Linear NMI was first outlined by Hinkelmann (1951). It was further developed by Dickinson and Williamson (1972), and Williamson (1976). Machenhauer (1977) and Baer (1977) extended the technique to include nonlinear terms. The method was applied operationally to the global, 15 level grid-point model of the European Centre for Medium Range Weather Forecasts (Temperton and Williamson, 1979). Several other forecasting centres have also implemented this technique (Australia, Canada, France, Japan, USA).

While the normal mode approach has solved some of the long standing problems, namely the initialisation of long waves, initialisation in the tropics, and initialisation in the presence of mountains, some problems remained. Perhaps the most serious drawback was the neglect of diabatic processes, which led to a marked reduction of divergent circulations in the tropics. (Bengtsson, 1981). Although physical tendencies can in principle be included in NMI, operational experience (Temperton and Williamson, 1979) showed that the iteration process used to solve the nonlinear initialisation condition diverged when doing so. Therefore, early implementations neglected diabatic forcing terms.

Several methods have been suggested in order to overcome the problem. The simplest approach is to exclude the modes which describe the large scale tropical divergent circulation from the initialisation (Puri and Bourke, 1982). This method by definition retains the analysed divergent circulation. Unfortunately, it also no longer allows the control of noise in the modes not being initialised. We shall come back to this point in Section 6. As an alternative, a method for incorporating diabatic forcing in the initialisation process has been developed at ECMWF and implemented into the then operational grid point model on 21 September 1982. In Section 4, we will discuss the rationale behind the approach chosen and present details of the implementation. There will also be a discussion of the performance of the scheme since its operational introduction.

Another area of possible concern are systematic changes of the analysed fields brought about by the initialisation. For example, the standard normal mode

initialisation scheme tends to reject part of the analysed tropical surface pressure information. In section 5, we will discuss the reason for this and propose a method to overcome the problem. Finally, we shall take the opportunity to discuss some additional experiments on the use of a cut-off period and on the number of vertical models to be initialised.

Some of the above mentioned modifications to the initialisation were originally designed and tested with the ECMWF grid point model. On 21 April 1983 a spectral model with a hybrid vertical coordinate was introduced as operational model. The normal mode initialisation scheme required for this model is slightly different from others as the hybrid vertical coordinate leads to a slightly more complicated vertical structure equation. Although thematically unrelated, we present the non linear initialisation scheme for such a model together with the other topics mentioned above. This also allows a discussion as to what extent conclusions drawn from the grid point model are still applicable for the latest version of the operational spectral model.

To summarise, the purpose of this paper is fourfold:

- to present a nonlinear normal mode initialisation scheme for a spectral model with a hybrid vertical coordinate.
- to describe and assess a method for incorporating physical tendencies into the initialisation process.
- to present a scheme which helps to reduce initialisation changes to the tropical surface pressure.
- to discuss some experiments with modifications to the operational scheme.

2. NORMAL MODES OF A HYBRID SPECTRAL MODEL

Normal modes are the free solutions of the linearised model equations. In order to end up with manageable matrices it is necessary to assume simple basic states. For a basic state at rest and a horizontally homogeneous mean temperature the problem can be separated into a vertical and a horizontal part.

2.1 Vertical Treatment

The nonlinear normal mode initialisation method for a global spectral model with a standard sigma coordinate was first outlined by Andersen (1977). In the following we shall present a scheme for a model with a generalised hybrid vertical coordinate. This coordinate system resembles the usual sigma coordinate close to the ground, but reduces smoothly to a pressure coordinate at stratospheric levels (Simmons and Burridge, 1981). The hybrid system requires a slightly different linearisation process of the model equations which results in a more complicated vertical structure equation. All the remaining steps in the initialisation process are identical to the usual sigma type model.

2.1.1 Basic equations and coordinate system

The vertical normal modes are the eigensolutions of the vertical structure equation. This equation is obtained by a combination of the linearised first law of thermodynamics together with the hydrostatic and the continuity equation. For a general, terrain following coordinate η, which is a monotonic function of pressure p and dependent on its surface value p_s, these equations are given by (Kasahara, 1974).

$$\frac{\partial T}{\partial t} + \vec{v}.\nabla T + \dot{\eta}\frac{\partial T}{\partial \eta} - \frac{\kappa T \omega}{p} = Q \qquad (1)$$

$$\frac{\partial \phi}{\partial \eta} = -\frac{RT}{p}\frac{\partial p}{\partial \eta} \qquad (2)$$

$$\frac{\partial}{\partial \eta}\frac{\partial p}{\partial t} + \nabla.\vec{v}\frac{\partial p}{\partial \eta} + \frac{\partial}{\partial \eta}\left(\dot{\eta}\frac{\partial p}{\partial \eta}\right) = 0 \qquad (3)$$

Where T is temperature, t the time, $\vec{v}$ the horizontal velocity vector, ∇ the horizontal gradient equator. $\dot{\eta}$ is the generalised vertical velocity with the boundary conditions $\dot{\eta}=0$ at the lower ($\eta=1$) and upper ($\eta=0$) boundaries, $\kappa=R/c_p$ where R is the gas constant and c_p the specific heat at constant pressure, ϕ is the geopotential, p the pressure.

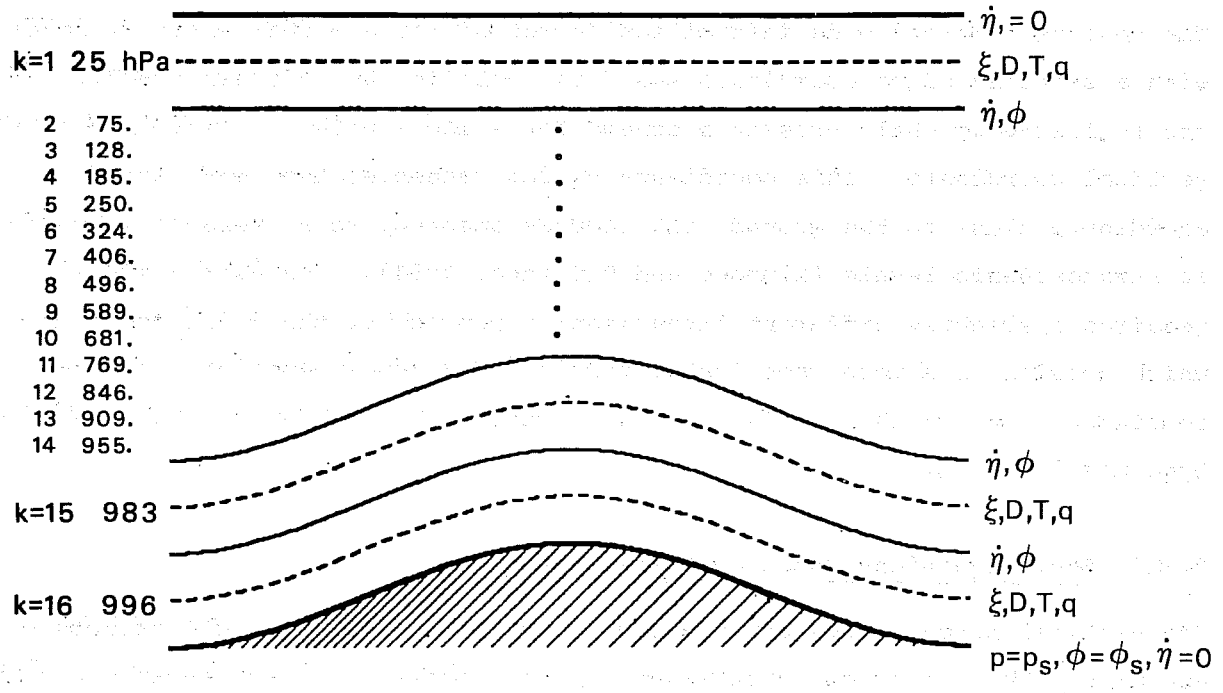

Fig. 1 Vertical distribution of model levels and staggering of variables for the 16 level version of the ECMWF model. Rounded pressure values are calculated with a surface pressure of 1000 hPa.

Equations for the surface pressure tendency and for the generalised vertical velocity can be obtained by integrating (3)

$$\frac{\partial \ell n p_s}{\partial t} = - \frac{1}{p_s} \int_0^1 \nabla.(\vec{v} \frac{\partial p}{\partial \eta}) \, d\eta \tag{4}$$

$$\dot{\eta} \frac{\partial p}{\partial \eta} = - \frac{\partial p}{\partial p_s} \frac{\partial p_s}{\partial t} - \int_0^\eta \nabla.(\vec{v} \frac{\partial p}{\partial \eta}) d\eta \tag{5}$$

For the pressure coordinates vertical velocity ω we get

$$\omega = - \int_0^\eta \nabla.(\vec{v} \frac{\partial p}{\partial \eta}) \, d\eta + \vec{v}.\nabla p \tag{6}$$

Next we define a hybrid vertical coordinate system with K levels. Fig. 1 shows the vertical distribution of model levels and the staggering of the variables for the 16 level model operational until 12.5.86.

The three bottom levels are pure σ-levels whereas the two top levels are pressure levels with a smooth transition in between. Half level pressure values for $k<0, \ldots K$ are defined by:

$$p_{k+\frac{1}{2}} = A_{k+\frac{1}{2}} + B_{k+\frac{1}{2}} \, p_s \tag{7}$$

where p_s is the surface pressure. The constants $A_{k+\frac{1}{2}}$ and $B_{k+\frac{1}{2}}$ must satisfy: $A_{\frac{1}{2}}=B_{\frac{1}{2}}=A_{K+\frac{1}{2}}=0$; $B_{K+\frac{1}{2}}=1$. Note that (7) corresponds to an implicit definition of the general η coordinate. Unlike in a pure pressure coordinate, where the pressure differences between adjacent levels is horizontally constant or in a pure σ coordinate where $\Delta\sigma$ is constant, the pressure difference Δp_k between level $k+\frac{1}{2}$ and $k-\frac{1}{2}$ in a hybrid coordinate model is a function of the horizontal coordinate through the variable surface pressure. This has implications for the linearisation of the model equations.

2.1.2 Vertical Structure Equation

For the linearisation of (1)-(6) we choose a basic state at rest. The basic state temperature $\bar{T}$ is independent of the horizontal position. It varies only in the vertical

$$T'=T-\bar{T} \tag{8}$$

As the pressure difference Δp_k between adjacent coordinate surfaces varies horizontally we also have to introduce a basic state surface pressure $\bar{p}_s$. The linearisation process follows the derivation of the semi-implicit time scheme as presented by Simmons and Burridge (1981). We linearise about $\ell n \bar{p}_s$, as $\ell n \bar{p}_s$ is the predictive variable of the model. We define $\ell n p'_s$ arbitrarily as

$$\ell n p'_s = \ell n p_s - \ell n \bar{p}_s \tag{9}$$

The variation with surface pressure of any variable F in a coordinate surface k can be expressed in a Taylor series as:

$$F_k(\ell n p_s) = F_k(\ell n \bar{p}_s) + \frac{\partial F_k}{\partial \ell n p_s}\Big|_{p_s=\bar{p}_s} \ell n p_s' + r_1 \qquad (10)$$

where r_1 is a residual of at most order $(\ell n p_s')^2$ which will be dropped in the linearisation process.

The finite difference analog of the hydrostatic equation (2) is (Simmons and Burridge, 1981)

$$\phi_k = \phi_s + \sum_{j=k+1}^{K} RT_j \ell n \frac{p_{j+\frac{1}{2}}}{p_{j-\frac{1}{2}}} + \alpha_k RT_k \; ; \qquad (11)$$

using (8), (9) and (10) this can be expressed as

$$\phi_k = \phi_s + R \sum_{j=k+1}^{K} [\bar{T}_j \ell n \frac{\bar{p}_{j+\frac{1}{2}}}{\bar{p}_{j-\frac{1}{2}}} + \bar{T}_j \bar{p}_s \ell n p_s' \left(\frac{\partial \ell n p_{j+\frac{1}{2}}}{\partial p_s} - \frac{\partial \ell n p_{j-\frac{1}{2}}}{\partial p_s}\right)\Big|_{p_s=\bar{p}_s} \qquad (12)$$

$$+ T'(\ell n \frac{\bar{p}_{j+\frac{1}{2}}}{\bar{p}_{j-\frac{1}{2}}})] + R\bar{\alpha}_k \bar{T}_k + R\bar{\alpha}_k T_k' + R\bar{p}_s \frac{\partial \alpha_k}{\partial p_s}\Big|_{p_s=\bar{p}_s} \bar{T}_k \ell n p_s' + N_\phi$$

Here, α_k is a variable to be specified later. The notation $\bar{p}_{j+\frac{1}{2}}$ and $\bar{\alpha}_k$ indicates that these quantities are to be evaluated for the reference surface pressure $\bar{p}_s$. N_ϕ is the sum of all the nonlinear terms. Combining the variables at each of the K levels of the model into column vectors yields a matrix form for (12)

$$\underline{\phi} = \underline{\phi}_s + \underline{\phi}_r + \underline{\underline{g}}\underline{T}' + \ell n p_s' \underline{b} + \underline{N}_\phi \; ; \qquad (13)$$

$\underline{\phi}_s$ is a vector with identical elements ϕ_s, $\underline{\phi}_r$ contains the contributions from the basic state which are independent of time and of the horizontal coordinate, $\underline{N}_\phi$ is the vector of the nonlinear terms. The elements of the matrix $\underline{\underline{g}}$ are given by

$$g_{j,k} = \begin{cases} 0 & k<j \\ R\bar{\alpha}_k & k=j \\ R\ell n \dfrac{\bar{p}_{k+\frac{1}{2}}}{\bar{p}_{k-\frac{1}{2}}} & k>j \end{cases}$$

The elements of the vector $\underline{b}$ are defined as

$$b_j = R\bar{T}_j \bar{p}_s \frac{\partial \alpha_j}{\partial p_s}\Big|_{p_s=\bar{p}_s} + R \sum_{k=j+1}^{K} \bar{T}_k \bar{p}_s \left(\frac{\partial \ell n p_{k+\frac{1}{2}}}{\partial p_s}\Big|_{p_s=\bar{p}_s} - \frac{\partial \ell n p_{k-\frac{1}{2}}}{\partial p_s}\Big|_{p_s=\bar{p}_s}\right)$$

The finite difference analogue of the surface pressure tendency equation (9) is

$$\frac{\partial \ell n p_s}{\partial t} = - \frac{1}{p_s} \sum_{j=1}^{K} \nabla . \vec{v}_j \Delta p_j \qquad (14)$$

This can be written as

$$\frac{\partial \ell n p_s}{\partial t} = - \underline{s}^T . \underline{D} + \underline{N}_{p_s} \qquad (15)$$

where the elements of vector $\underline{s}$ are given by

$$s_j = \frac{1}{\bar{p}_s} (\bar{p}_{j+\frac{1}{2}} - \bar{p}_{j-\frac{1}{2}})$$

Superscript T indicates the transpose of a vector or matrix. The nonlinear terms are contained in the vector $\underline{N}_{p_s}$; $\underline{D}$ is the vector of the divergences in the K model levels.

For the vertical advection of any variable, F, Simmons and Burridge (1981) propose the energy conserving finite difference analogue

$$(\dot{\eta} \frac{\partial F}{\partial \eta})_k = \frac{1}{2\Delta P_k} [(\frac{\partial p_{k+\frac{1}{2}}}{\partial p_s} \sum_{j=1}^{K} \nabla . \vec{v}_j \Delta p_j - \sum_{j=1}^{k} \nabla . \vec{v}_j \Delta p_j) (F_{k+1} - F_k) + (\frac{\partial p_{k-\frac{1}{2}}}{\partial p_s} \sum_{j=1}^{K} \nabla . \vec{v}_j \Delta p_j - \sum_{j=1}^{k-1} \nabla . \vec{v}_j \Delta p_j) (F_k - F_{k-1})] \qquad (16)$$

Using the basic state variables $\bar{T}$ and $\bar{p}_s$, the vertical advection of temperature can be expressed in vector form as

$$(\dot{\eta} \frac{\partial T}{\partial \eta}) = \underline{\underline{W}} \, \underline{D} + \underline{r}_2 \qquad (17)$$

where $\underline{r}_2$ is the vector of nonlinear terms and the elements of matrix $\underline{\underline{W}}$ are given by

$$w_{j,k} = \frac{1}{2\Delta p_j} [(\bar{T}_{j+1} - \bar{T}_j) (\frac{\partial p_{j+\frac{1}{2}}}{\partial p_s} \Big|_{\bar{p}_s} \Delta p_k - \begin{cases} 0 & k > j \\ \Delta p_k & k \leq j \end{cases}) + (\bar{T}_j - \bar{T}_{j-1} (\frac{\partial p_{j-\frac{1}{2}}}{\partial p_s} \Big|_{\bar{p}_s} \Delta p_k - \begin{cases} 0 & k+1 > j \\ \Delta p_k & k+1 \leq j \end{cases})]$$

For the pressure gradient term Simmons and Burridge (1981) derive the angular momentum preserving finite difference analogue

$$(\frac{RT}{p} \nabla p)_k = \frac{RT_k}{\Delta P_k} (\ell n \frac{p_{k+\frac{1}{2}}}{p_{k-\frac{1}{2}}} \nabla p_{k-\frac{1}{2}} + \alpha_k \nabla (\Delta p_k)) \qquad (18)$$

This can be transformed to

$$\frac{RT_k \nabla p_k}{p_k} = \underline{d}\ \nabla \ell n p_s' + \underline{r}_3 \qquad (19)$$

where $\underline{r}_3$ is the vector of nonlinear terms and the elements of vector $\underline{d}$ are given by

$$d_j = \frac{R\bar{T}_j}{\Delta \bar{p}_j}\left[\ell n \frac{\bar{p}_{j+\frac{1}{2}}}{\bar{p}_{j-\frac{1}{2}}} \frac{\partial p_{j-\frac{1}{2}}}{\partial \ell n p_s}\Big|_{\bar{p}_s} + \bar{\alpha}_j \left(\frac{\partial p_{j+\frac{1}{2}}}{\partial \ell n p_s}\Big|_{\bar{p}_s} - \frac{\partial p_{j-\frac{1}{2}}}{\partial \ell n p_s}\Big|_{\bar{p}_s}\right)\right]$$

Finally, an energy conserving finite difference form of the energy conversion term can be expressed as (Simmons and Burridge, 1981)

$$\left(\frac{\kappa T \omega}{p}\right)_k = -\frac{\kappa T_k}{\Delta p_k}\left[\ell n \frac{p_{k+\frac{1}{2}}}{p_{k-\frac{1}{2}}} \sum_{j=1}^{k-1} \nabla.(\vec{v}_j \Delta p_j) + \alpha_k \nabla.(\vec{v}_k \Delta p_k)\right] +$$

$$\frac{\kappa T_k \vec{v}_k}{\Delta p_k}\left[\ell n \frac{p_{k+\frac{1}{2}}}{p_{k-\frac{1}{2}}} \nabla p_{k-\frac{1}{2}} + \alpha_k \nabla(\Delta p_k)\right] \qquad (20)$$

Noting that terms of the form $T_k \vec{v}_k \nabla p_{k-\frac{1}{2}}$ cannot be linearised when using a resting basic state, (20) can be written as

$$\left(\frac{\kappa T \omega}{p}\right)_k = -\underline{\underline{C}}\ \underline{D} + \underline{r}_4 \qquad (21)$$

where $\underline{r}_4$ is the vector of nonlinear terms and the elements $c_{j,k}$ of matrix $\underline{\underline{C}}$ are given by

$$c_{j,k} = \frac{1}{c_p} \frac{\Delta \bar{p}_k}{\Delta \bar{p}_j} \bar{T}_j g_{k,j}$$

with these notations the thermodynamic equation becomes

$$\frac{\partial \underline{T}}{\partial t} = -(\underline{\underline{C}} + \underline{\underline{W}})\ \underline{D} + \underline{N}_T \qquad (22)$$

where $\underline{N}_T$ is the vector of nonlinear terms.

We define an auxiliary potential h as

$$\underline{h} = \underline{\underline{g}}\ T' + (\underline{b} + \underline{d})\ \ell n p_s' \qquad (23)$$

Differentiating with respect to time yields

$$\frac{\partial \underline{h}}{\partial t} = \underline{\underline{g}} \frac{\partial T'}{\partial t} + (\underline{b}+\underline{d}) \frac{\partial \ell n p_s'}{\partial t} \qquad (24)$$

Using (22) and (15), this can be expressed as

$$\frac{\partial \underline{h}}{\partial t} = -\underline{\underline{B}}\ \underline{D} + \underline{N}_p \qquad (25)$$

with matrix $\underline{\underline{B}}$ being defined as

$$\underline{\underline{B}} = \underline{g}\,(\underline{\underline{C}}+\underline{\underline{W}}) + (\underline{b}+\underline{d})\underline{s}^{T} \qquad (26)$$

The matrix $\underline{\underline{B}}$ in the vertical structure equation (25) is often referred to as vertical structure matrix. In it, the elements in row j give the linear contribution of the divergence in all model levels to the time rate of change of the variable h at level j. $\underline{\underline{B}}$ depends upon the basic state temperature $\bar{T}$ and surface pressure $\bar{p}_s$ and on the vertical discretisation of the model. Explicit expressions for the non linear tendencies $\underline{N}_p$ are not required, as they will later be calculated as the difference between the full tendencies and the linear contribution. Before proceeding with the computation of the normal modes, the variable α_k needs to be specified. Simmons and Burridge (1981) choose it to be

$$\alpha_k = 1 - \frac{p_{k-\frac{1}{2}}}{\Delta p_k}\,\ell n\,\frac{p_{k+\frac{1}{2}}}{p_{k-\frac{1}{2}}} \qquad (27)$$

which reduces the pressure gradient term (18) to the form $RT_k \nabla \ell n p_s$ for the standard σ coordinate system. With this specification the elements of vector $\underline{b}+\underline{d}$ become

$$(\underline{b}+\underline{d})_j = \bar{p}_s\, R\bar{T}\,\frac{\partial \ell n p_{j+\frac{1}{2}}}{\partial p_s}\Big|_{\underline{p}_s} + R\bar{p}_s \sum_{k=j+1}^{K} \bar{T}\left(\frac{\partial \ell n p_{k+\frac{1}{2}}}{\partial p_s}\Big|_{\underline{p}_s} - \frac{\partial \ell n p_{k-\frac{1}{2}}}{\partial p_s}\Big|_{\underline{p}_s}\right) \qquad (28)$$

For an isothermal basic state temperature T_o, the right hand side of (28) reduces to RT_o.

2.1.3 Vertical modes

The vertical modes are the eigenvectors of $\underline{\underline{B}}$. The associated eigenvalues $\bar{\phi}_k$ are called "equivalent depths". As shown by Hoskins and Simmons (1975), they are the squared phase velocities of pure gravity waves for a non-rotating earth corresponding to the vertical structure of the mode in question. Table 1 gives the values of $\bar{\phi}_k$ for the 16 level hybrid model (left) and for the recently introduced 19 level model (right). The 19 level model has increased vertical resolution in the stratosphere. Also given are the pressures at the full model levels for a 1000 hPa surface pressure. The modes have been derived using a basic state at rest with an isothermal (300K) temperature distribution and a reference surface pressure of 800 hPa.

k	p_k in hPa	$\bar{\phi}_k$ in $\frac{m^2}{sec^2}$	p_k in hPa	$\bar{\phi}_k$
1	25	115510	10	117300
2	75	30365	30	39144
3	128	8301.6	50	12909
4	185	3072.1	73	5340.5
5	250	1381.5	103	2636.8
6	324	695.49	141	1450.9
7	406	374.08	190	853.37
8	496	208.49	251	522.62
9	589	117.66	323	327.21
10	681	65.898	406	206.51
11	769	35.888	495	129.82
12	846	18.549	589	80.376
13	909	8.8017	682	48.422
14	955	3.6368	769	27.985
15	983	1.1784	846	15.228
16	996	0.21997	909	7.5808
17			955	3.2806
18			983	1.1072
19			996	0.21251

Table 1: Pressure levels p_k and equivalent depths $\bar{\phi}_k$ for 16 (left) and 19 (right) level model.

The higher vertical modes are associated with very low equivalent depths. Therefore, the higher internal gravity modes have small phase speeds. As initialisation seeks to control the high frequency noise, only the first few vertical models need to be included in the initialisation process. Fig. 2 shows the vertical structure of the first 5 vertical modes for the 16 (Fig. 2a) and the 19 level model (Fig. 2b).

The first mode - also called the external mode - represents fields which are almost constant throughout the atmosphere. Therefore, it describes the

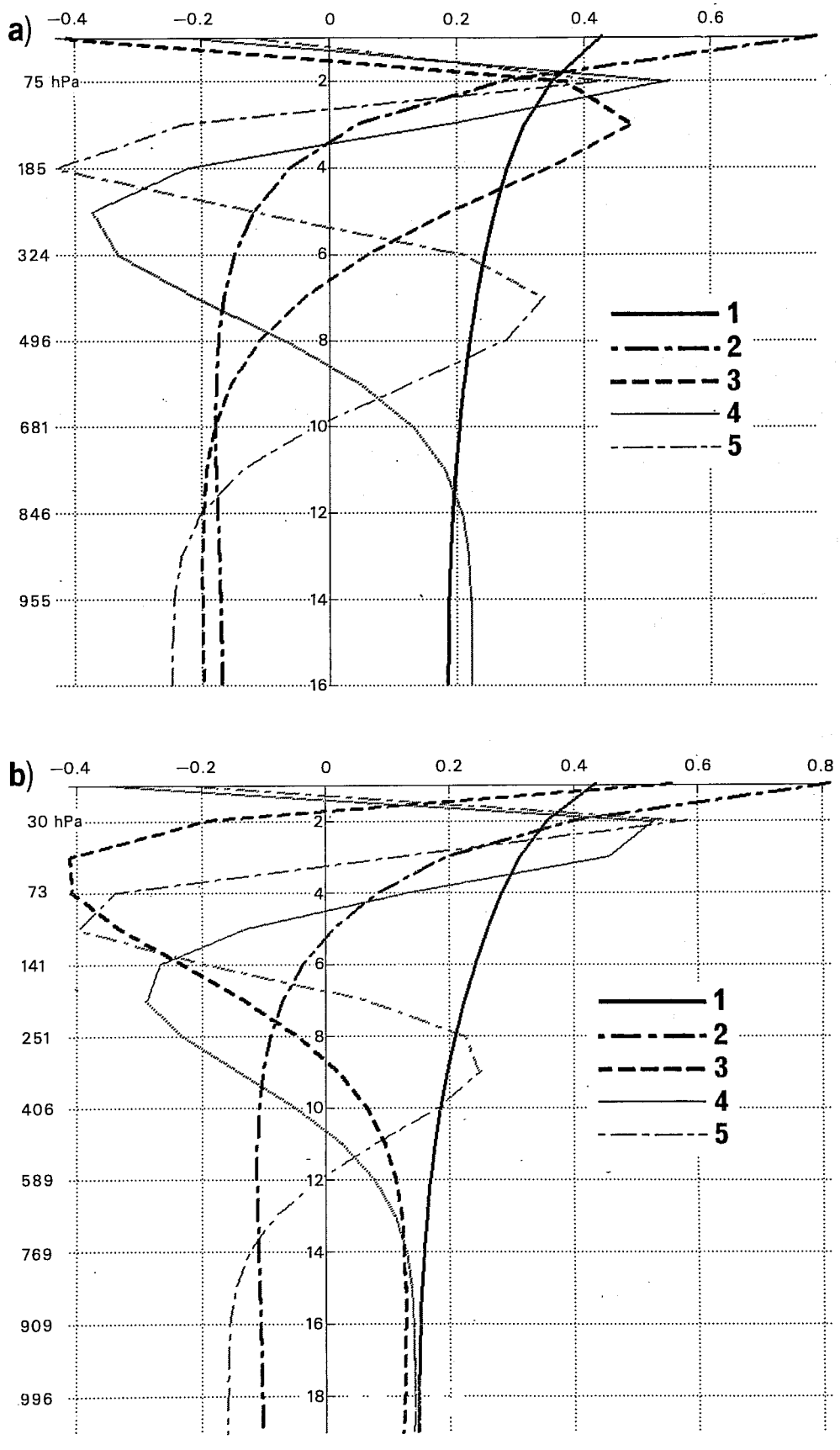

Fig. 2 The structure of the first five vertical modes for the 16 (a) and 19 (b) level version of the ECMWF model. Rounded pressure values are calculated with a surface pressure of 1000 hPa.

barotropic components of the flow. The second mode (also called the first internal) changes sign near the tropopause. The third mode divides the troposphere into two regions; this is important when describing low level inflow and upper tropospheric outflow, as present in deep tropical convection. In general, vertical mode k has k-1 sign changes. With increasing k the region of maximum amplitudes moves towards lower levels. The high vertical modes describe only shallow structures close to the lower boundary.

2.1.4 Vertical decoupling

The vectors $\underline{D}$ and $\underline{h}$ in (25) are vertically coupled, as the matrix $\underline{\underline{B}}$ has non zero off-diagonal elements. In order to decouple (25), we apply a similarity transform. First we expand any arbitrary vector $\underline{X}$ in terms of the vertical normal modes

$$\underline{X} = \underline{\underline{M}}\,\underline{\tilde{X}} \tag{29}$$

where $\underline{\underline{M}}$ is a matrix whose K columns are the K eigenvectors (vertical modes) of matrix $\underline{\underline{B}}$ and $\underline{\tilde{X}}$ is the vector of vertical mode amplitudes of $\underline{X}$.
Inserting (29) into (25) and multiplying from the left with $\underline{\underline{M}}^{-1}$ yields

$$\frac{\partial \underline{\tilde{h}}}{\partial t} = - \underline{\underline{M}}^{-1}\,\underline{\underline{B}}\,\underline{\underline{M}}\,\underline{\tilde{D}} + \underline{\underline{M}}^{-1}\,\underline{N}_p \tag{30}$$

The similarity transform $\underline{\underline{M}}^{-1}\,\underline{\underline{B}}\,\underline{\underline{M}}$ reduces $\underline{\underline{B}}$ to its spectral matrix, which has the eigenvalues $\bar{\phi}_k$ of $\underline{\underline{B}}$ in its main diagonal and has zero elements otherwise. Therefore, we can write (30) in component form.

$$\frac{\partial \tilde{h}_k}{\partial t} = - \bar{\phi}_k\,\tilde{D}_k + \tilde{N}_{pk} \tag{31}$$

where $\tilde{h}_k$, $\tilde{D}_k$ and $\tilde{N}_{pk}$ are the components of vertical mode k. The coupled equation (25) are thus transformed to a sequence of K decoupled equations. Formally, (31) is similar to the linearised continuity equation of a shallow water model, with the mean depth of the fluid replaced by the eigenvalues $\bar{\phi}_k$ of $\underline{\underline{B}}$.

2.2 Horizontal Treatment

2.2.1 Basic equations

The equations (1) - (3) are completed by the vorticity and divergence equation, which can be expressed as

$$\frac{\partial \underline{\zeta}}{\partial t} + \beta \underline{v} + f\underline{D} = \underline{N}_{\zeta} \tag{32}$$

$$\frac{\partial \underline{D}}{\partial t} - f\underline{\zeta} + \beta \underline{u} + \nabla^2 \underline{h} = \underline{N}_{D} \tag{33}$$

where $\underline{\zeta}$ and $\underline{D}$ are the vectors of vorticity and divergence at the K model levels, $\underline{u}$ and $\underline{v}$ are the vectors of the zonal and meridional wind components. All the nonlinear terms are contained in $\underline{N}_{\zeta}$ and $\underline{N}_{D}$. The Coriolis parameter is indicated by f and β denotes $\frac{df}{dy}$. Note that the linear terms on the left hand side of (32) and (33) are not vertically coupled. Expanding all variables in terms of the vertical normal modes therefore directly leads to:

$$\frac{\partial \tilde{\zeta}_k}{\partial t} + \beta \tilde{v}_k + f \tilde{D}_k = \tilde{N}_{\zeta} \tag{34}$$

$$\frac{\partial \tilde{D}_k}{\partial t} - f\tilde{\zeta}_k + \beta \tilde{u}_k + \nabla^2 \tilde{h}_k = \tilde{N}_{D} \tag{35}$$

Together with (31), (34) and (35) form a system of uncoupled equations for the k-th amplitude of a vertical normal mode expansion which is formerly equivalent to a shallow water model.

2.2.2 Horizontal structure equation

As a first step, the vorticity, divergence and the wind components u and v are expressed in terms of streamfunction ψ and velocity potential χ.

$$\zeta = \nabla^2 \psi \tag{36}$$

$$D = \nabla^2 \chi \tag{37}$$

$$u = -\frac{\sqrt{1-\mu^2}}{a} \frac{\partial \psi}{\partial \mu} + \frac{1}{a\sqrt{1-\mu^2}} \frac{\partial \chi}{\partial \lambda} \tag{38}$$

$$v = \frac{1}{a\sqrt{1-\mu^2}} \frac{\partial \psi}{\partial \lambda} + \frac{\sqrt{1-\mu^2}}{a} \frac{\partial \chi}{\partial \mu} \tag{39}$$

$$\mu = \sin \theta \tag{40}$$

where a is the radius of the earth and λ and θ are geographical longitude and latitude.

Next, we expand ψ, χ and h in terms of spherical harmonics.

$$\begin{pmatrix} \psi \\ \chi \\ \\ h \end{pmatrix} = \sum_{m=-M}^{M} \sum_{n=|m|}^{N(m)} \begin{matrix} [n(n+1)]^{-\frac{1}{2}} \\ i[n(n+1)]^{-\frac{1}{2}} \\ \\ \frac{\sqrt{\bar{\phi}_k}}{a} \end{matrix} \begin{pmatrix} \psi_{m,n} \\ \chi_{m,n} \\ \\ h_{m,n} \end{pmatrix} P_{m,n}(\mu) e^{im\lambda} \qquad (41)$$

where M and N are the truncation limits for the zonal and meridional expansions and $i=\sqrt{-1}$. $P_{m,n}(\mu)$ are the associated Legendre polynomials with zonal and total wavenumber m and n. The factors in front of the spherical harmonic coefficients $\psi_{m,n}$, $\chi_{m,n}$ and $h_{m,n}$ facilitate the subsequent analysis as they lead to a symmetric horizontal structure matrix.

As the spherical harmonics are eigenfunctions of the Laplace operator on a sphere, we get

$$\nabla^2 P_{m,n}(\mu) e^{im\lambda} = -\frac{n(n+1)}{a^2} P_{m,n}(\mu) e^{im\lambda} \qquad (42)$$

Two other useful relations for Legendre polynomials are

$$\mu P_{m,n} = \delta_{m,n} P_{m,n-1} + \delta_{m,n+1} P_{m,n+1} \qquad (43)$$

$$(1-\mu^2) \frac{dP_{m,n}}{d\mu} = (n+1) \delta_{m,n} P_{m,n-1} - n \delta_{m,n+1} P_{m,n+1} \qquad (44)$$

with

$$\delta_{m,n} = \left(\frac{n^2-m^2}{4n^2-1}\right)^{\frac{1}{2}} \qquad (45)$$

Inserting (36)-(45) into (31), (34) and (35) and at the same time dropping all reference to the vertical normal mode expansion except for the equivalent depth, $\bar{\phi}_k$, yields:

$$\frac{\partial}{\partial t} \chi_{m,n} = i2\Omega[-\delta_{m,n} \gamma_n \psi_{m,n-1} - \delta_{m,n+1} \gamma_{n+1} \psi_{m,n+1} + \frac{m}{n(n+1)} \chi_{m,n} + \frac{\sqrt{\bar{\phi}_k n(n+1)}}{2\Omega a} h_{m,n}] + \frac{i a^2}{\sqrt{n(n+1)}} Q_{D_{m,n}} \qquad (46)$$

$$\frac{\partial}{\partial t} \psi_{m,n} = i2\Omega[-\delta_{m,n} \gamma_n \chi_{m,n-1} - \delta_{m,n+1} \gamma_{n+1} \chi_{m,n+1} + \frac{m}{n(n+1)} \psi_{m,n}] - \frac{a^2}{\sqrt{n(n+1)}} Q_{\zeta_{m,n}} \qquad (47)$$

$$\frac{\partial h_{m,n}}{\partial t} = i2\Omega \frac{\sqrt{\bar{\phi}_k n(n+1)}}{a2\Omega} \chi_{m,n} + \frac{a}{\sqrt{\bar{\phi}_k}} Q_{h_{m,n}} \qquad (48)$$

where γ_n is given by

$$\gamma_n = \sqrt{\frac{(n-1)(n+1)}{n^2}} \tag{49}$$

Obviously, there is a separate set of equations for each zonal wavenumber m. With respect to the wavenumber n, (46)-(48) imply a coupling between different waves. Therefore, the system (46)-(48) has to be treated simultaneously for all n within the truncation N(m). One further simplification follows from the symmetry properties of the associated Legendre functions. If j = n-m is even, they are symmetric around the equator; if n-m is odd they are anti-symmetric. Therefore, we can combine the variables in (46)-(48) into two symmetry classes:

$$j=n-m \begin{matrix}\text{even}\\ \text{odd}\end{matrix} \qquad h_{m,n},\ \chi_{m,n} \begin{matrix}\text{symmetric}\\ \text{antisymmetric}\end{matrix} \text{ and } \psi_{m,n} \begin{matrix}\text{antisymmetric}\\ \text{symmetric}\end{matrix}$$

Defining a vector $\underline{X}$ which holds $\chi_{m,n}$, $\psi_{m,n}$ and $h_{m,n}$ for all n in the respective symmetry class, (46)-(48) can be expressed in matrix form as

$$\frac{\partial \underline{X}}{\partial t} = i2\Omega\, \underline{\underline{A}}\,\underline{X} + \underline{Q} \tag{50}$$

where $\underline{Q}$ is the vector of non linear terms.

The elements of vector $\underline{X}$ are given by (j=0,1,2...)

symmetric flow	antisymmetric flow
$x_{3j} = \chi_{m,2j+m}$	$x_{3j} = \psi_{m,2j+m}$
$x_{3j+1} = h_{m,2j+m}$	$x_{3j+1} = \chi_{m,2j+m+1}$
$x_{3j+2} = \psi_{m,2j+1+m}$	$x_{3j+2} = h_{m,2j+m+1}$

The elements of matrix $\underline{Q}$ are defined correspondingly. Matrix $\underline{\underline{A}}$ is symmetric ($a_{\ell,r} = a_{r,\ell}$). Its non zero upper triangular elements are given by (j=0,1,..)

symmetric		antisymmetric
$a_{3j,3j}$	$= \frac{m}{(2j+m)(2j+m+1)}$	$= a_{3j,3j}$
$a_{3j+2,3j+2}$	$= \frac{m}{(2j+m+1)(2j+m+2)}$	$= a_{3j+1,3j+1}$
$a_{3j,3j+2}$	$= -\delta_{m,2j+1+m}\gamma_{2j+1+m}$	$= a_{3j,3j+1}$
$a_{3j+2,3j+3}$	$= -\delta_{m,2j+2+m}\gamma_{2j+2+m}$	$= a_{3j+1,3j+3}$

$$a_{3j,3j+1} = \frac{1}{2\Omega a}\left[\bar{\phi}_k(2j+m)(2j+m+1)\right]^{\frac{1}{2}};\quad a_{3j+1,3j+2} = \frac{1}{2\Omega a}\left[\phi_k(2j+m+1)(2j+m+2)\right]^{\frac{1}{2}}$$

The orders n_s and n_a of (50) for the symmetric and antisymmetric case are

$$n_s = 2\left|\frac{N-m}{2}\right| + 2 + \left|\frac{N-m+1}{2}\right| \tag{51}$$

$$n_a = 2\left|\frac{N-m+1}{2}\right| + \left|\frac{N-m}{2}\right| + 1 \tag{52}$$

where the symbol $|\,|$ stands for integer truncation

2.2.3 Horizontal normal modes

The horizontal normal modes are the eigenvectors of matrix $\underline{\underline{A}}$. The eigenvalues of $\underline{\underline{A}}$ are the free frequencies ν of these modes. They can be divided into three classes: the eastward travelling gravity modes ($\nu<0$), an equal number of westward travelling gravity modes ($\nu>0$) and the remaining class of the slow, westward moving Rossby modes. For the zonal mean (m=0), all the slow modes have zero frequency. The meridional index n of the modes can be determined in terms of their frequency. For Rossby modes, the frequency decreases with decreasing meridional scale, whereas for gravity modes it increases with decreasing scale. From symmetry considerations it follows that the "symmetric" system includes the odd indexed Rossby modes and the even indexed gravity modes, while the "antisymmetric" system include the even indexed Rossby and odd indexed gravity modes. In Table 2, the periods of some of the gravest modes for zonal wavenumber m=1 and for $\bar{\phi}_1=115510 m^2/sec^2$ (left) and $\bar{\phi}_3 = 8301.6 \frac{m^2}{sec^2}$ (right) are given for a model with a triangular truncation at total wavenumber 63.

	k=1			k=3		
	Rossby	westw. grav.	eastw. grav.	Rossby	westw. grav.	eastw. grav.
n=0	27.9	12.7	-29.6	44.5	22.9	-119.0
1	114.0	9.9	-12.5	368.9	17.8	- 31.9
2	190.9	8.1	- 8.7	589.9	15.3	- 21.0
3	286.8	6.6	- 6.9	796.4	13.7	- 16.9
4	405.9	5.6	- 5.7	988.7	12.7	- 14.6
5	549.1	4.8	- 4.9	1170.0	12.0	- 13.0

Table 2 Free periods in hours of gravest Rossby and gravity modes for zonal wavenumber m=1 and external mode k=1 (left) and second internal mode k=3 (right)

Horizontally, the modes are characterised by their specific coupling between mass and wind field. For Rossby modes, the extra-tropical mass - and windfield is in a quasi-geostrophic balance. Gravity modes are highly divergent. In the tropics, where the geostrophic relation breaks down, normal

modes still define a relation between mass and wind. A detailed discussion of the horizontal structure for various normal modes is given by Kasahara (1976). The large scale modes, which suffer least from truncation, bear a close resemblance to Hough functions (Longuet-Higgins, 1968). The Rossby mode and eastward gravity mode with index n=0 are special as neither from their relation between mass- and wind fields, nor from their frequency characteristic can they be classified as Rossby or as inertia-gravity modes. The Rossby mode for n=0, which is also called the "mixed Rossby gravity mode" looks like a gravity mode at lower latitudes but like a Rossby mode at higher latitudes. For the gravest symmetric eastward gravity mode (Kelvin mode) the u-component is in approximate geostrophic balance whilst the v-component of the wind is very small. A detailed discussion of these two modes can be found in Matsuno (1966).

3. NON-LINEAR NORMAL MODEL INITIALISATION

The calculations described so far need to be done only once. The results, i.e. the normal modes of the model and their free frequencies are then stored for later use in the actual initialisation process.

3.1 Model equations in normal mode form

The non-zero off diagonal elements in matrix $\underline{\underline{A}}$ imply a coupling between the indices n for a particular zonal wavenumber m. In order to decouple the system we apply a transform similar to the one in Section 2.1.4. We define a modal matrix $\underline{\underline{E}}$ whose columns contain the eigenvectors of $\underline{\underline{A}}$. Any vector $\underline{X}$ can be expressed in terms of the normal modes as

$$\underline{X} = \underline{\underline{E}}\underline{Y} \tag{53}$$

where $\underline{Y}$ contains the normal mode amplitudes of $\underline{X}$. They can be computed from:

$$\underline{Y} = \underline{\underline{E}}^{-1}\underline{X} \tag{54}$$

As $\underline{\underline{A}}$ is a symmetric matrix, its eigenvectors are orthogonal.

Therefore the inversion of $\underline{\underline{E}}$ can be done by simple transposition.

Inserting (53) into (50) and multiplying from the left with $\underline{\underline{E}}^{-1}$ yields

$$\frac{d\underline{Y}}{dt} = i2\Omega\underline{\underline{E}}^{-1}\underline{\underline{A}}\underline{\underline{E}}\underline{Y} + \underline{\underline{E}}^{-1}\underline{Q} \tag{55}$$

The similarity transform $\underline{\underline{E}}^{-1}\underline{\underline{A}}\underline{\underline{E}}$ reduces $\underline{\underline{A}}$ to its spectral matrix, whose main diagonal elements hold the eigenvalues ν of $\underline{\underline{A}}$ whilst all other elements are zero. Thus, (55) can be written in component form

$$\frac{dY_j}{dt} = i2\Omega\nu_j Y_j + q_j \tag{56}$$

These are the model equations in normal mode form. Thus, we have transformed a set of coupled partial differential equations to a sequence of uncoupled ordinary differential equations. The first term on the right hand side of (56) describes the linear contribution to the time rate of change of the normal mode amplitude Y_j, q_j represents the projection of all nonlinear tendencies on mode j. When using (56), we have to bear in mind that there is a set of equations for all combinations of zonal wavenumbers m and vertical modes k.

3.2 Initialisation condition

Machenhauer (1977) proposed to set the initial time tendencies of the gravity mode coefficients to zero. This requires

$$Y_j = \frac{iq_j}{2\Omega\nu_j} \qquad (j \in GR; \text{ where GR denotes the set of gravity modes}) \tag{57}$$

As the non linear terms q_j depend upon the interaction of gravity mode coefficients Y_j, (57) is a nonlinear algebraic system. It can be solved iteratively by computing the nonlinear terms from the analysis, then deriving new gravity mode coefficients from (57), using the new coefficients for a renewed computation of the nonlinear terms q_j and so on.

This iteration scheme can be expressed as

$$Y_j^{\ell+1} = \left(\frac{iq_j}{2\Omega\nu_j}\right)^{\ell} \qquad (j \in GR) \tag{58}$$

where ℓ is the iteration count.

The actual implementation follows Andersen (1977), who proposed a method which conveniently circumvents the explicit calculation of the nonlinear terms.

The finite difference analogue of (56) is

$$q_j = \frac{Y_j(\Delta t) - Y_j(0)}{\Delta t} - i2\Omega\nu_j Y_j \tag{59}$$

Inserting (58) into (59) leads to

$$Y_j^{\ell+1} - Y_j^{\ell} = i\,\frac{Y_j^{\ell}(\Delta t) - Y_j^{\ell}(0)}{2\Omega\nu_j \Delta t} \qquad (j \in GR) \tag{60}$$

which relates the time tendency of a gravity mode coefficient to the initialisation change to be made to it. Explicit calculation of the nonlinear terms is thus avoided. Only a model timestep is required to compute the time tendencies.

As all mass field information is absorbed into $\underline{h}$, we need a method for partitioning the initialisation changes to $\underline{h}$ into changes of the temperature T and surface pressure p_s. Eliminating the divergence from the linear form of (15) and (25) yields:

$$\frac{\partial \ell n p_s}{\partial t} = s^T \underline{\underline{B}}^{-1} \frac{\partial \underline{h}}{\partial t} \tag{61}$$

Applying (61) to differences rather than to differentials leads to an expression for the initialisation changes in surface pressure. The temperature changes can then be calculated from (23).

To summarise, one pass through the initialisation process consists of the following steps (assuming that the normal modes of the model are already available).

- Run the model for one timestep to compute the time tendencies.
- Compute the tendencies of $\underline{h}$ (23)
- Project the time tendencies into vertical normal model space.
- Compute the vector $\underline{X}$
- Project into horizontal normal mode space (54)
- Compute the changes to the gravity mode coefficients (60)
- Project back from horizontal normal mode space (53)
- Decompose vector $\underline{X}$
- Project back from vertical normal mode space (29)
- Decompose change to $\underline{h}$ into changes to $\ell n p_s$ and T (61), (23).

4. INCORPORATION OF DIABATIC EFFECTS

The nonlinear term q_j in (58) contains the contribution from the nonlinear dynamical tendencies and from all the parameterised physical processes. Unfortunately, in early applications of the scheme, it soon turned out (Williamson and Temperton, 1981) that the iteration process (60) diverges when including the physical tendencies in the model timestep. A convergence criterion can easily be derived from (60) by requiring:

$$\left| \frac{Y_j^{\ell}(\Delta t) - Y_j^{\ell}(o)}{\Delta t} \right| \leq \left| 2\,\Omega\,\nu_j \right| \qquad (62)$$

Thus, divergence can first be expected for small values of ν_j, i.e. for the higher internal modes on large horizontal scales. The criterion (62) also suggests that using a basic state that is as stable as possible will improve the convergence properties, as it results in larger values for the free frequencies ν_j. The other limiting factor is the size of the total model tendencies. The physical tendencies from the convection scheme are particularly difficult to handle as they can be quite large and they mainly project on internal modes. Furthermore, they are discontinuous during the course of the iteration.

As a consequence, most early NMI schemes used only the adiabatic tendencies. Unfortunately, this largely suppressed the diabatically driven tropical circulations in the initialised analyses (Temperton, 1981). In fact, one of the main criticisms of the ECMWF "MAIN" FGGE III-b analyses is the weak divergent circulation (Lorenc and Swinbank, 1984) resulting from the use of an adiabatic initialisation scheme.

In the following sections we will first investigate the balance in the tropics in order to find out to what extent an initialisation condition like (57) is applicable. Then we will propose a suitable diabatic scheme, which does not suffer from convergence problems. Finally, we will discuss the performance of this scheme.

4.1 The balance in the tropics

A study of the balance of the atmosphere immediately runs into a problem. Ideally, one would require the exact knowledge of all the gravity and Rossby mode amplitudes in order to verify a particular initialisation condition for the gravity modes. However, the amplitudes of the gravity modes cannot be

determined to the required accuracy by an analysis system. Otherwise, there would be no need for an initialisation scheme.

Fortunately, we can reduce the uncertainty by concentrating on the structures best handled by an analysis scheme. As shown by Daley (1985) and Julian (1984), the ECMWF analysis scheme has more skill in analysing divergent flow on the largest scales than on shorter scales. Random fluctuations can further be reduced by looking at time mean fields rather than at individual analyses.

Fig. 3 shows monthly mean fields of uninitialised velocity potential fields. The 200 hPa level has been chosen because of the good data coverage by aircraft and satellite reports. The velocity potential mostly brings out the best analysed large scale component of the divergent wind field. The 00Z field for July 1985 (Fig. 3a) is characterised by zonal wavenumber 1 pattern with outflow over Indonesia and convergence in the Atlantic/African area. The 12Z figure (Fig. 3b) stay very similar, suggesting that the large scale divergent flow is quasi-stationary on a daily time scale. This is also confirmed by the fields for the intermediate hours 06Z and 18Z (not shown). The 12Z mean field for August 1985 (Fig. 3c) is still similar to the July maps. The outflow over Indonesia has intensified and slightly shifted in position. Thus, Fig. 3 seems to indicate that the large scale component of the divergent flow at 200 hPa is quasi-stationary. It varies at most on a seasonal time scale. The inspection of daily maps leads to similar conclusions. This is also evident from the corresponding figures shown by Lau (1984) for the FGGE special observing periods.

As normal modes describe a global coupling between mass and wind field, it is not sufficient to look at the wind field only in discussing balance. In the following we shall discuss the time evolution of individual gravity mode coefficients. Because of the problems in analysing gravity modes we shall take a forecasting model as a substitute for the atmosphere and track some gravity modes during a forecast. Fig. 4 shows harmonic dials for the gravest eastward (Fig. 4a) and westward (Fig. 4b), second internal gravity mode of zonal wavenumber 1 for a one day forecast. The light curve is the time evolution of the coefficient for the first day of a forecast started from an uninitialised analysis. The heavy curve describes the evolution between day 10 and 11 of the same forecast. The complex gravity mode coefficient is

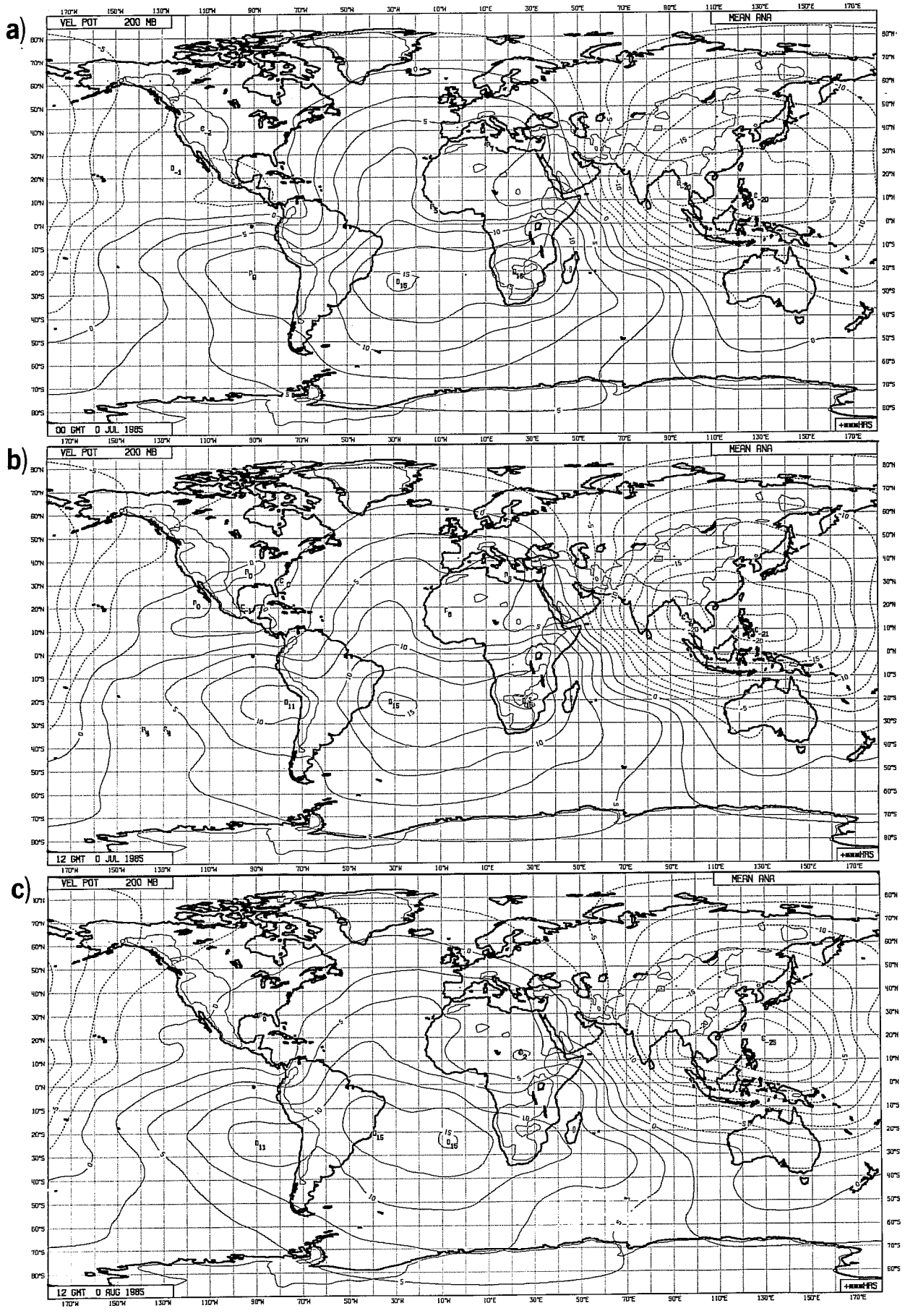

Fig. 3 Monthly mean uninitialised velocity potential at 200 hPa. a) 00 GMT, July 1985; b) 12 GMT, July 1985; c) 12 GMT August 1985. Contour interval is 10^6 m^2/sec.

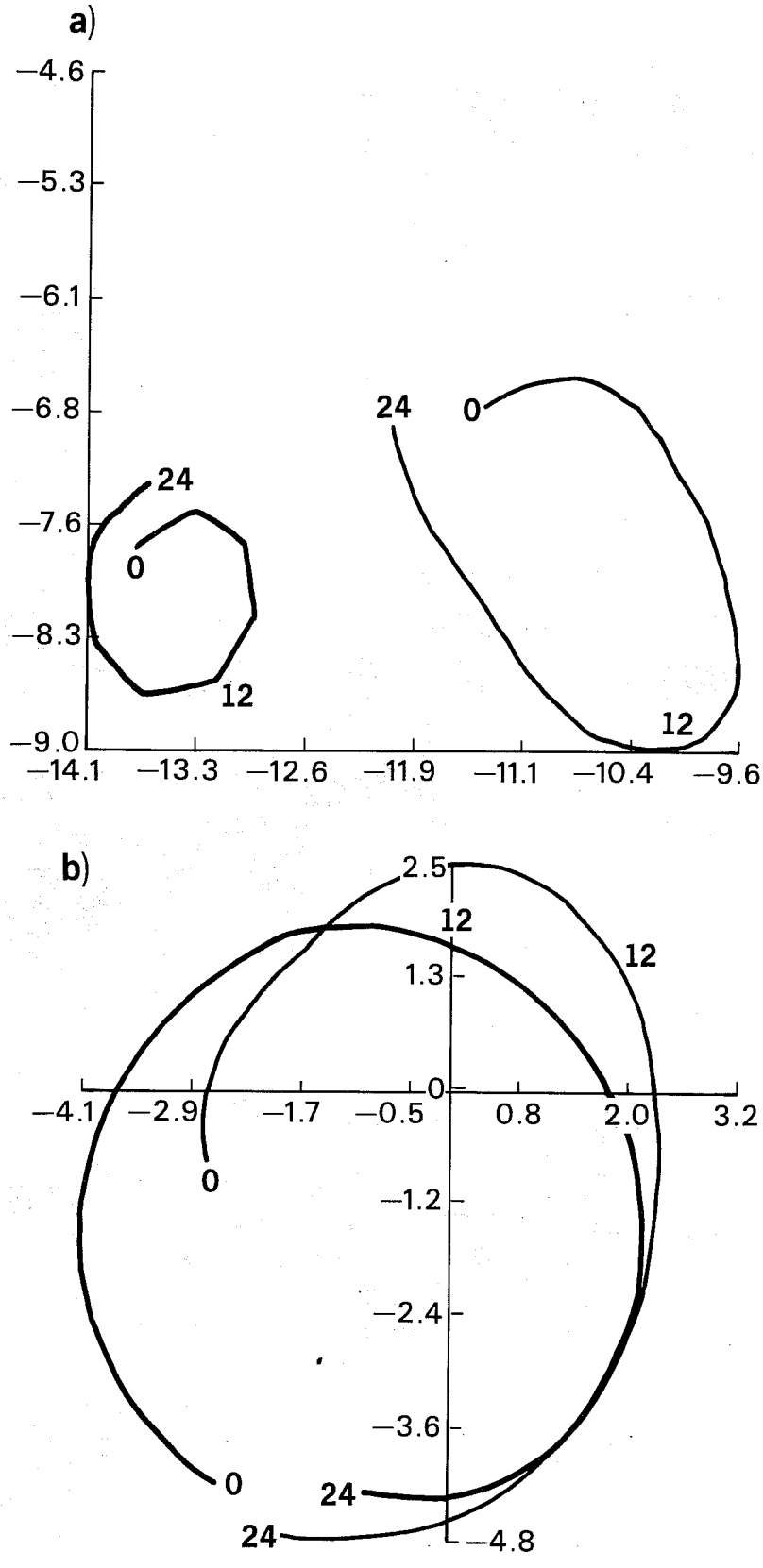

Fig. 4 Harmonic dial for second internal, zonal wavenumber 1, gravest symmetric, eastward (a) and westward (b) gravity modes. Light curve shows time evolution between day 0 and 1, full curve between day 10 and 11 of a forecast started from an uninitialised analysis. Clockwise rotation indicates westward propogation. Units on the coordinates are arbitrary, but comparable between the 2 dials.

plotted every timestep. Clockwise rotation indicates westward propagation. Because of the low equivalent depth of 830 m these modes are equatorially trapped. The gravest eastward mode is also called the Kelvin mode. At first sight it is clear that none of these modes is stationary. Especially for the westward mode the travelling component is as large as the stationary one. Between day 10 and 11 (Fig. 4b, full curve) the westward mode shows a regular westward propagation with a period of one day. This signal is also present during the early stages of the forecast. (Fig. 4b, light curve). It is, however, superimposed by other components. Interestingly enough, the Kelvin mode (Fig. 4a) which as a free wave is eastward travelling, also shows a westward propagation with a marked contribution from a one day period. This indicates that these are forced waves which have locked in with the forcing once the initial gravity wave noise is under control. As will be discussed in Section 5, the marked diurnal component is a tidal signal forced by the daily cycle in the radiation calculation but also contained in the initial data. Clearly, this signal is not stationary. The tidal component can, however, be estimated and excluded from the dials. For the actual method chosen and for the consequences this finding has for the initialisation see Section 5.

The following two figures show the time evolution of some selected gravity modes after the tidal contribution has been removed. Fig. 5 is for the gravest external symmetric modes for zonal wavenumber 1 (5a,b) and 2 (5c,d), with the eastward modes at the top (5a,c) and the westward modes in the bottom row (5b,d). Again, the light curves are for 24 hour forecasts started from the same uninitialised analysis, the full curves for the evolution between day 10 and 11 of that forecast. Clockwise rotation indicates westward propagation. The amplitudes are arbitrary, but are strictly comparable between dials. Note that the origin in the dials are not identical. The most striking features in Fig. 5 are the large transient components in the forecast started from the uninitialised analysis, thus demonstrating the need for initialisation. After ten days the transient signal has become much smaller and the modes can be regarded as approximately stationary. By this time the travelling component amounts only to a few percent of the stationary contribution. The corresponding dials for the second internal mode are given in Fig. 6. The level of noise in the early stages of the forecasts (light curves) is not as high as for the external modes. This result is not general as it only applies to one particular analysis chosen at random. As discussed

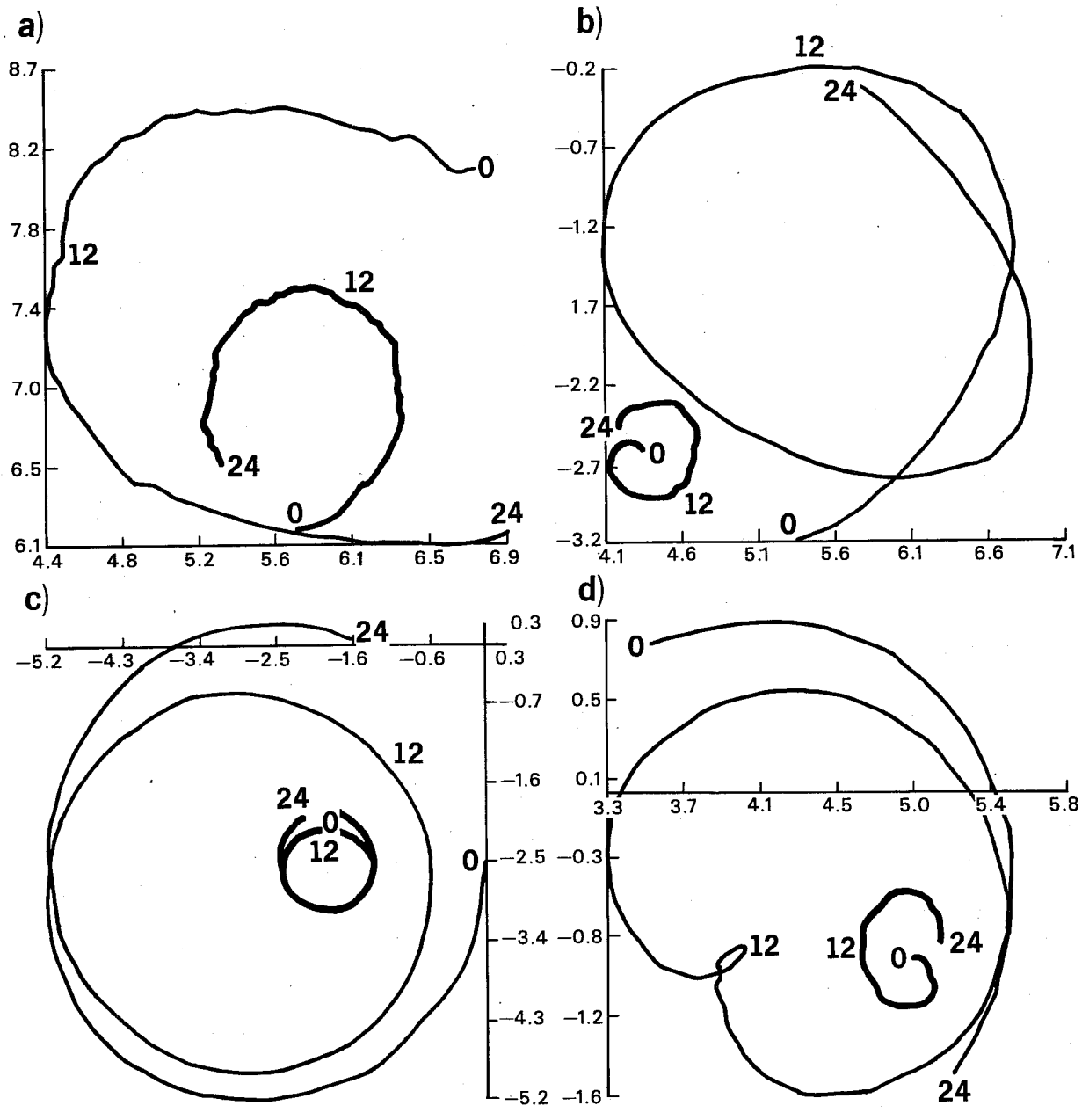

Fig. 5 Similar to Fig. 4, but for external, zonal wavenumber 1, east (a) and westward (b) gravest symmetric gravity modes. Corresponding zonal wavenumber 2 modes are given in c (east) and d (west). Tidal signals have been removed.

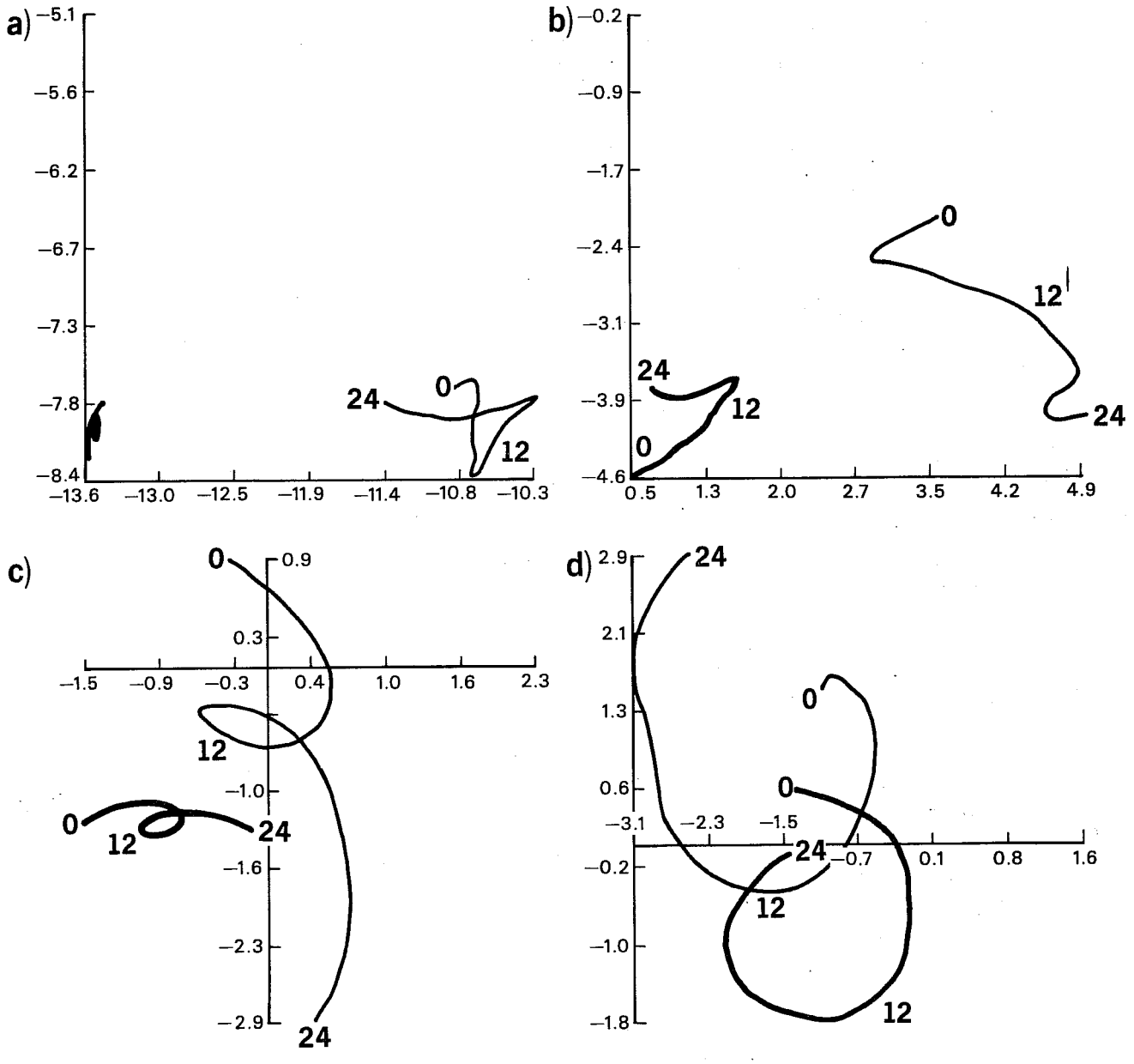

Fig. 6 Similar to Fig. 5, but for second internal modes.

in a later section, even the slow, large scale internal modes can have unrealistically large amplitudes in the uninitialised analysis. After ten days into the forecast, the modes have become quasi-stationary. In particular, the second internal Kelvin mode for zonal wavenumber 1, (Fig. 6a) which has the largest amplitude of all the modes shown, shows very little propagation. The zonal wavenumber 2 westward mode (Fig. 6d) is least stationary. Its total amplitude is, however, small. The higher internal modes (not shown) also become quasi-stationary during the forecast. Thus we conclude that both observational and model evidence seems to indicate that for practical purposes the large scale external and internal gravity modes can be regarded as stationary apart from tidal effects. In the following we shall derive a suitable diabatic initialisation condition based on this finding.

4.2 A diabatic initialisation condition

Before proposing a diabatic initialisation scheme, it is helpful to examine the solution of (56) assuming that the nonlinear term q_j can be expressed as a harmonic series with known frequencies ω. For any particular frequency ω Eq (56) then reads

$$\frac{dY_j}{dt} = i2\Omega\, \nu_j Y_j + q_j e^{i\omega t} \tag{63}$$

This is the equation for a forced harmonic oscillator. The general solution (excluding resonance) is

$$Y_j = [Y_j(t=0) - \frac{q_j}{i(\omega-2\Omega\nu_j)}]e^{i\nu_j t} + \frac{q_j}{i(\omega-2\Omega\nu_j)}e^{i\omega t} \tag{64}$$

The first term describes the transient gravity wave activity which initialisation seeks to control by defining the initial amplitude $Y_j(t=0)$ so that the term in brackets goes to zero. The second term describes the response to the forcing. Obviously, a mode can only be stationary if the forcing is stationary ($\omega \approx 0$) and if there is little or no gravity wave activity. This means that for the large scale modes discussed in the previous sub-section, the projection of the forcing on these modes must be stationary. This is an important conclusion. For non-stationary forcing a correct implementation of the initialisation condition would indeed require the knowledge of the forcing frequency ω, as indicated in the denominator of the second term in brackets in (64). Only if the stationary component of the forcing dominates the transient part can the condition (58) result in the appropriate balance.

One further qualitative conclusion can be drawn from (64). For the small scale modes, which have large frequencies ν, the initialisation condition (57) implies a reduced importance of the nonlinear terms q_j unless the quasi-stationary small scale forcing is large. The balanced amplitude Y_j will usually be small. Moreover, because of the short time scales involved, the response of these modes to a forcing will be fast so that they are quickly regenerated during a forecast. This is an important difference from the large scale modes, for which a failure to include diabatic processes in the initialisation condition can lead to long spin up times.

Based on the previous considerations, we propose the following diabatic initialisation scheme:

Step 1: Obtain an estimate of the diabatic forcing by time averaging the physical tendencies during a short forecast started from the uninitialised analysis.

Step 2: Retain only the large scale components of the projection on the "slow" gravity modes.

Step 3: Keep this forcing unchanged during the iteration process.

Step 1 is an attempt to obtain a representative estimate of the stationary component of the forcing. Operationally the time averaging is done between timesteps 3 and 10 of a forecast (2 hours of model time). The first two steps are excluded in order to avoid random contributions from the convection scheme caused by spurious instabilities in the analysis. In an assimilation scheme one could also think of using the physical forcing from the previous first guess. This would, however, perpetuate possible errors in the forcing field. The averaging period was determined empirically and is a compromise between accuracy and cost.

Step 2 further narrows the uncertainties in the forcing as it retains only the large scale components, which - as we saw - can be treated as quasi-stationary. It furthermore avoids adapting the initialised analysis to the less reliable small scale structures generated by the parameterisation schemes of the model. In practice, only forcing components which project on

inertia-gravity modes with periods longer than 11 hours are retained. Again this parameter was chosen empirically. Experiments using the unfiltered forcing field in the ECMWF system were not successful. Forecast quality was found to be insensitive to the precise choice of the filtering period, as long as the large scale components of the forcing were retained. In practice, the use of this upper bound on the frequency of the retained gravity components is equivalent to a 3-dimensional spatial filter on the forcing.

Finally, step 3 assures numerical stability of the scheme. As there is no interaction between the forcing and the iteration, the convergence properties are identical to an adiabatic scheme. Thus, with $\bar{q}_j$ being the representation of the time averaged, filtered projection of the diabatic forcing on mode j and with subscript a indicating adiabatic tendencies, equation (60) can be rewritten as

$$Y_j^{\ell+1} - Y_j^{\ell} = i \frac{\frac{1}{\Delta t}\left[Y_j^{\ell}(\Delta t) - Y_j^{\ell}(0)\right]_a + \bar{q}_j}{2\Omega\nu_j} \qquad (65)$$

Note, that $\bar{q}_j$ does not depend on the iteration count ℓ. It contains the tendencies from the following parameterised physical processes: vertical diffusion, radiation, deep and shallow convection and large scale condensation.

In order to give an impression of the accumulated physical tendencies resulting from this procedure, Fig. 7a shows the diabatic heating at model level 8 ($\approx$ 500 hPa) for 00 GMT on June 11 1979 together with the observed convective index as given by Murakami (1983) in Fig. 7b. Indices of 4 and greater denote very active convection and significant rainfall. The observed elongated pattern off the Chinese coast is well reproduced by the model. The activity in the Bay of Bengal is shifted northward in the model. The convection west off Sumatra is well captured whereas the branch extending northeast towards Borneo is missing in the model. Good agreement is again found for the western Pacific Ocean. On the whole, the agreement between the observed and modelled convective activity seems acceptable for this example. The effect of the gravity mode filtering is demonstrated in Fig. 8. A cut-off period of 5 hours (Fig. 8a) preserves all the major centres of the original fields without introducing excessive cooling. Note that the amplitude reduction is not only a function of the horizontal, but also of the vertical

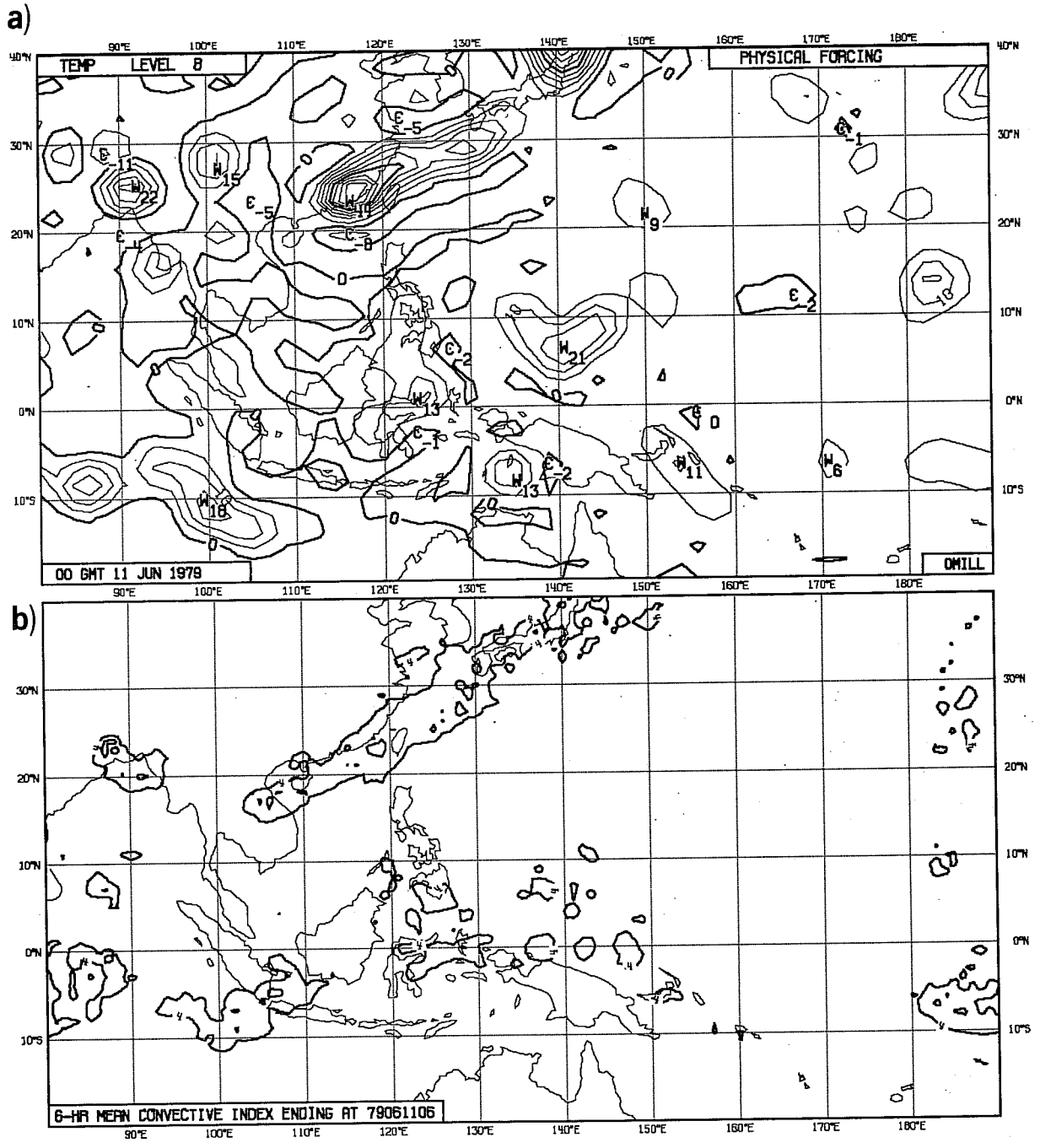

Fig. 7 a) Model generated diabatic heating in level 8 (≈500 hPa) as computed for the diabatic initialisation (averaged during a 2 hour forecast started 00 GMT, 11.6.79). Contour interval is 5 deg/day.

b) 6 hour mean convective index as given by Murakami (1983). Contour interval is 4.

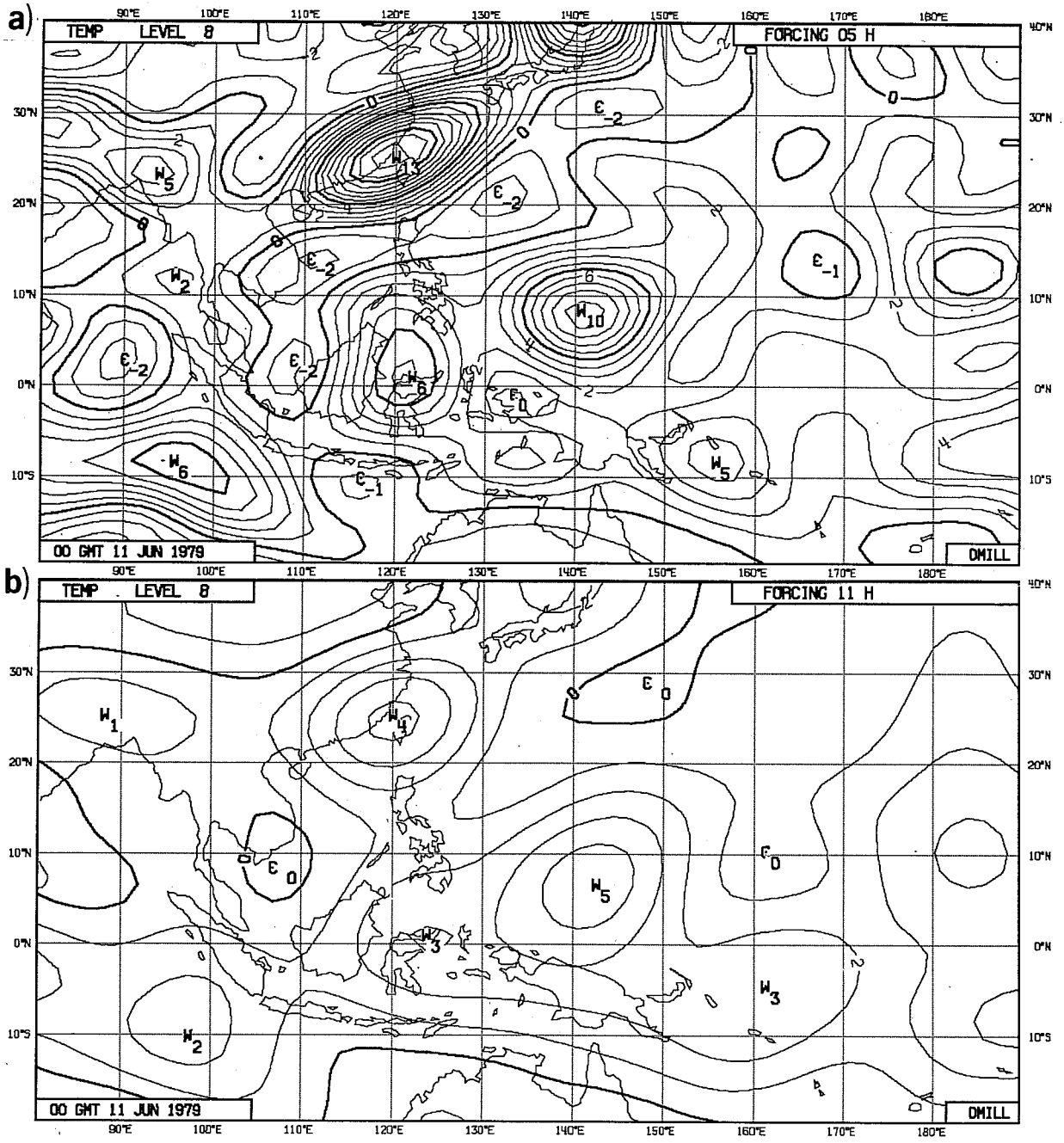

Fig. 8 Projection of the diabatic heating in level 8 on gravity modes with free periods longer than 5 hours (a) and 11 hours (b). Contour interval is 1 deg/day.

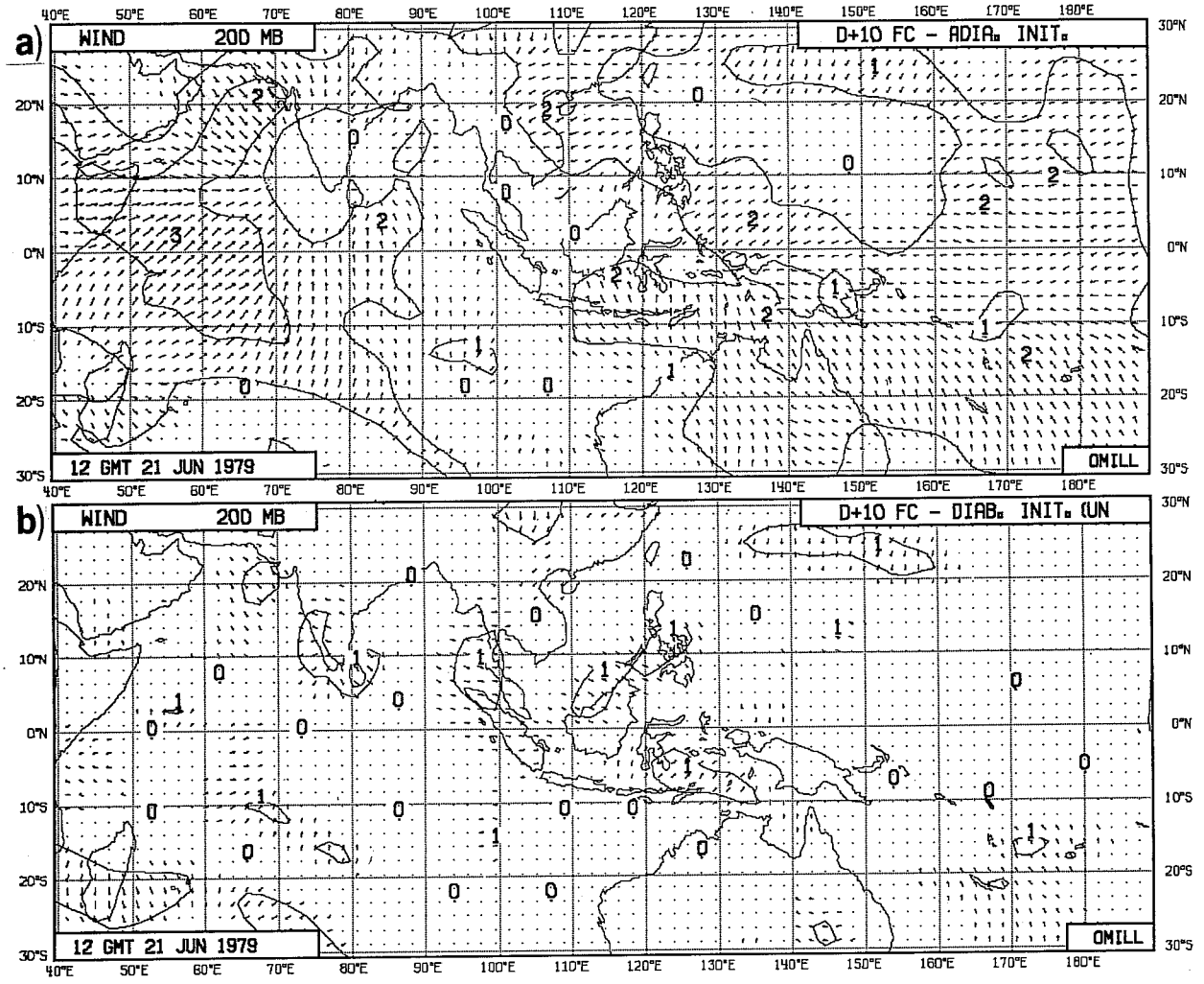

Fig. 9 Changes made to the 200 mb wind field of a 10 day forecast by an adiabatic (a) and diabatic (b) initialisation scheme. The forecast was started at 12 GMT, 11.6.79. Isolines give the wind speed with an interval of 1m/sec.

scale. Shallow structures are less damped than deep ones. A cut-off period of 11 h, as used operationally, leads to a further smoothing of the heating fields, (Fig. 8b) but still retains the major centres of activity without introducing spurious cooling. Before discussing the performance of the scheme in a data assimilation system, we shall examine the initialisation changes made to a 10 day forecast. Ideally these changes should be small, as excessive gravity wave activity should have died out with later steps of the forecast. Fig. 9 shows the initialisation changes to the 200 hPa wind field of a ten day forecast verifying at 12Z, 21.6.1979. For the adiabatic initialisation scheme using 5 vertical modes (Fig. 9a) there are changes up to 3m/sec on a large horizontal scale. The initialisation effectively reduces the large scale outflow over India and Indonesia. With the diabatic version of the scheme presented in the previous chapters, the changes are much smaller (Fig. 9b). For this test the full diabatic tendencies without any filtering were used. As we see there are still changes on small horizontal scales, thus again highlighting the inappropriateness of the initialisation condition for non-stationary small scale features, as discussed in Section 4.1. The finding that the large scale diabatic heating is important for describing the tropical balance is at variance with results reported by Errico, 1984. For the NCAR general circulation model he reached the somewhat surprising conclusion that "For no modes does heating by any process appear to participate in a balance of forces". Unfortunately, he did not discuss the performance of the NCAR model in simulating the observed quasi-stationary large scale divergent circulation. This highlights the point that in this context diagnostics derived from a model should be interpreted with some care. A proper test of an initialisation procedure can only be done within a data assimilation scheme.

4.3 The performance of the diabatic scheme in data assimilation

In the following the performance of the diabatic ECMWF initialisation scheme will be discussed under four aspects:

- the control of noise
- the changes made to the analysed fields
- the quality of forecasts.
- the spin-up problem

4.3.1 Noise control

Fig. 10a shows the evolution of surface pressure during a 24 hour forecast started from the uninitialised (full line) and diabatically initialised (dashed line) analysis for a gridpoint in the northern Rocky Mountains. The uninitialised forecast is contaminated with high frequency noise, which leads to unrealistic surface pressure variations. The initialised forecast predicts the slow rise in pressure without the superimposed high frequency oscillations. The orography does not seem to cause any particular problems. Fig. 10b gives similar curves for a point off the Norwegian coast. The forecast range is extended to 5 days. Again, the uninitialised forecast is noisy. It takes about 3 days into the forecast to dampen the gravity wave activity. Note that both forecasts are very close to each other in describing the synoptic development. Finally, Fig. 10c shows the vertical velocity at model level 8 for the same point during a 1 day forecast. While surface pressure is dominated by the external modes, the vertical velocity reflects noise in internal modes. There are large oscillations of ω in the forecast started from the uninitialised analysis. By contrast, the evolution of ω in the initialised forecast is smoother, thus showing that the initialisation scheme has some skill in controlling internal gravity wave activity.

A further indication of the effective noise control brought about by the diabatic initialisation is given in Fig. 11. It shows the field of instantaneous surface pressure tendencies, together with the reported values as registered during the 3 hours preceeding the analysis time. Note that the observed pressure tendencies are not used in the ECMWF analysis system. They are diagnostically derived from (4) using the analysed wind and surface pressure fields. Allowing for the small time difference, the tendencies computed from the initialised analysis (Fig. 11a) fit the reported value quite well. The area of falling pressure in front of a cyclone approaching the British Isles is verified in amplitude and phase by the reports. Also, the area of rising pressure in the Atlantic is supported by the few observations in this area. When calculating the pressure tendencies from the uninitialised analysis, there is little agreement between this field and the observations (Fig. 11b). Note that the contour interval has been increased from 1hPa/3h in Fig. 11a to 5hPa/3h in Fig. 11b. There are many small scale structures with excessively high tendency values. It is almost impossible to make synoptic

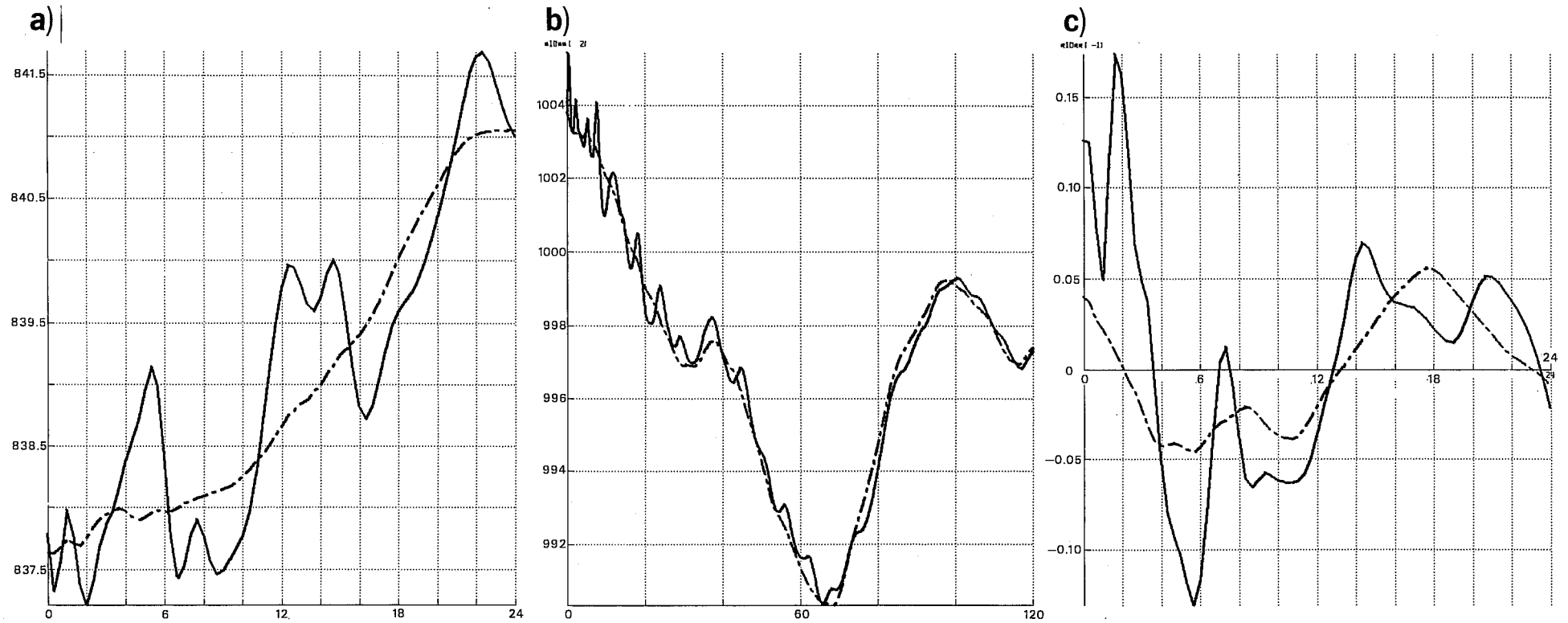

Fig. 10 Time evolution of surface pressure (a,b) and vertical velocity (c) during forecasts started from the uninitialised (full) and initialised (dashed) analysis. a) 24 hours forecast of surface pressure for a point in the northern Rocky Mountains, b) evolution of p_s during a 5 day forecast for a point off the Norwegian coast, c) Evolution of ω in level 8 during a 1 day forecast for the same point as in b).

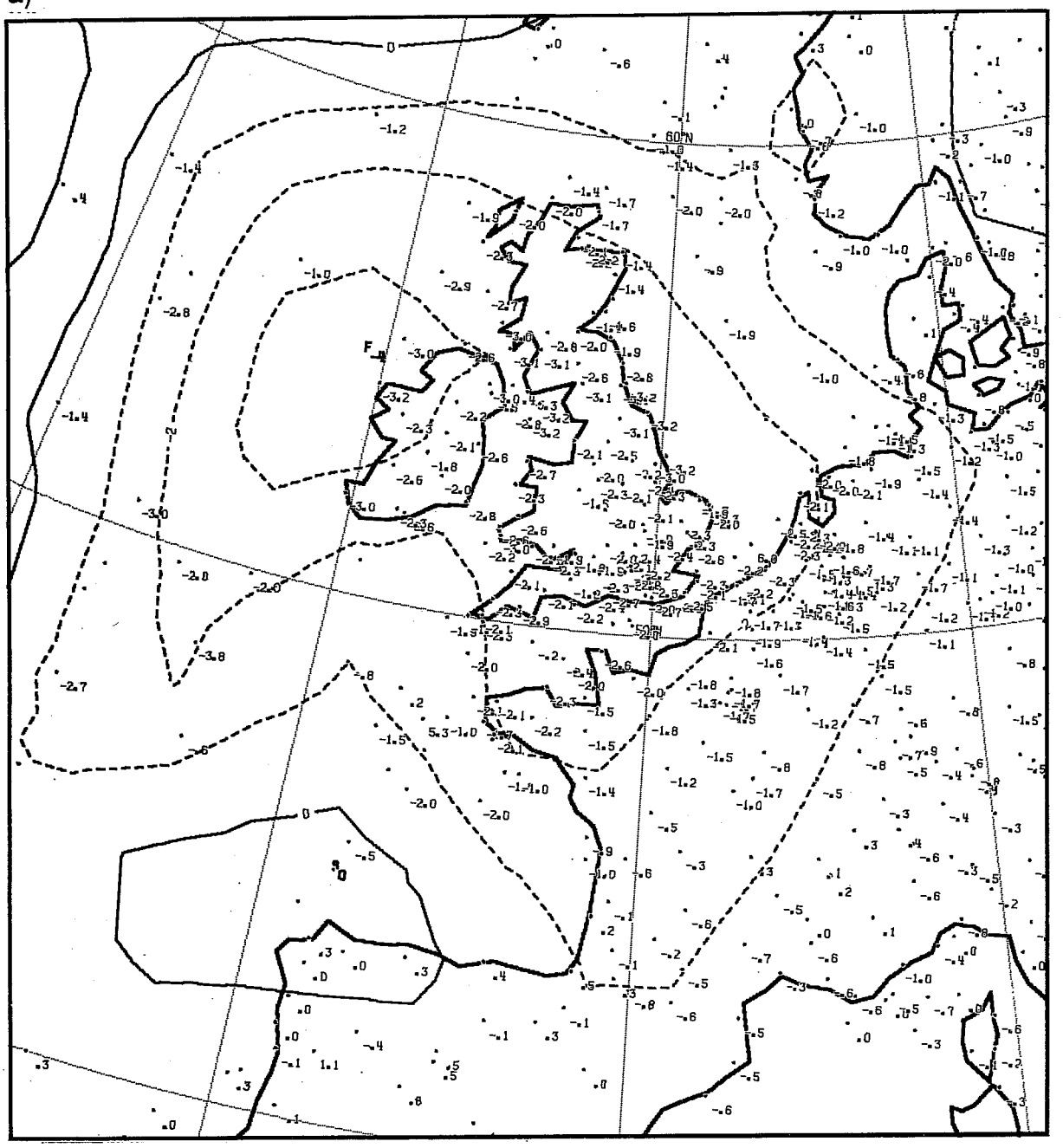

Fig. 11 Field of instantaneous surface pressure tendencies together with the 3-hourly reported values. a) tendencies computed from initialised analysis. Contour interval is 1 hPa/3 h.

b)

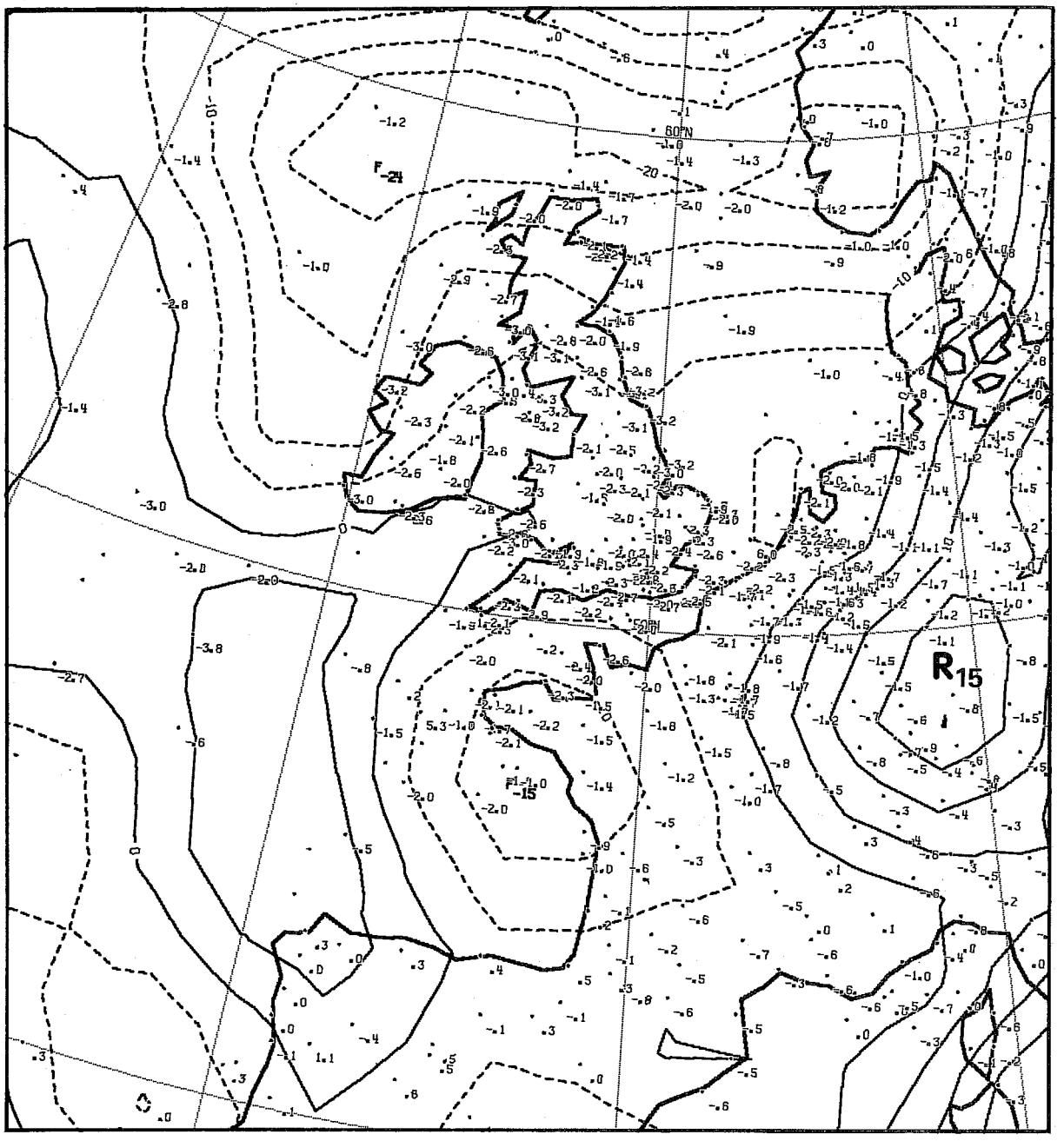

Fig. 11 (Cont) b) tendencies as computed from the uninitialised analysis. Contour interval is 5 hPa/3 h.

sense of this field. A typical horizontal scale of the noise seems to be around 700 km. The level of noise in the uninitialised analysis is hardly surprising as the analysis scheme approximates the global nonlinear three dimensional constraints between the variables by simple linear local relations. A further source of imbalance is the difference in data selection between neighbouring analysis boxes and in different vertical slabs within the same analysis box. For a description of the latest version of the analysis scheme see Shaw et al. (1984).

4.3.2 Initialisation changes to the analysis

In general, initialisation changes to the analysed fields can have their origin in three areas:

i) Failure of the analysis scheme to get the analysis close to the slow manifold (Leith, 1980). This can either be caused by erroneous data or by the numerous simplifications in the analysis method.

ii) Weaknesses in the model formulation, which would result in initialisation changes even if point i) above would not apply.

iii) Errors in the initialisation scheme itself.

Usually, all three areas contribute to initialisation changes and it often is not easy to isolate a particular process.

A typical example for point iii) is the suppression of diabatically driven circulations when using an adiabatic initialisation scheme. Many early implementations of the normal mode method suffered from this problem. As an example, Fig. 12a shows the monthly mean, initialised, zonally averaged, meridional wind component for 12Z, May 1979 as calculated from the "Main" FGGE analyses produced by ECMWF. For a description of the assimilation scheme used for the "Main" analyses see Bengtsson et al., 1982. The adiabatic initialisation, which was used for the "Main" production, almost entirely wiped out the upper tropospheric return flow of the Hadley cell. Also, the tropical vertical velocities are very small (Fig. 12c) when using an adiabatic initialisation scheme. By contrast, the "Final" assimilation produces a much

more vigorous Hadley cell (Figs. 12b,d). The "Final" assimilation basically is a re-analysis of certain episodes from the FGGE year with the 1985 version of the ECMWF assimilation system. The upper tropospheric return flow has increased from 0.5 to 2m/sec and the vertical velocity from .005 to .02 pa/sec in the tropical troposphere. Although the assimilation system used for the "Final" runs differs in many respects from the early version used for the "Main" production, (Uppala, 1986) the inclusion of diabatic tendencies is mainly responsible for the strengthening of the Hadley cell. This was confirmed by independent tests (Wergen, 1982).

Another indication of the intensification of the divergent circulation is shown in Fig. 13, which gives the monthly mean velocity potential field at 200 hPa for May 1979. The first two panels are taken from Lau, 1984. They show the uninitialised fields as produced by GFDL (top) and ECMWF (middle) for the "Main" runs. Generally, the ECMWF divergent flow is smoother but weaker than the GFDL field. On the other hand, the ECWMF "Final" field (Fig. 13c) shows a considerably increased divergent circulation; especially over Indonesia and South-America. Note that the "Final" ECMWF field (Fig. 13c) is initialised. Thus the initialised "Final" velocity potential shows stronger gradients than both the "GFDL" and "ECMWF" "Main" uninitialised fields.

It is interesting to compare the changes the analysis makes to the first guess to the changes made to the analysis by the initialisation. Ideally, the initialisation increment should be smaller than the analysis increment. Otherwise, either the analysis increment is unbalanced or the initialisation scheme is defective. For the northern hemisphere 500 mb height field, Hollingsworth et al. (1986) demonstrated that the major part of the evolution is described by the forecast model within the ECMWF data assimilation system. The analysis increments are generally smaller and the initialisation changes are smaller still. Fig. 14 gives the global seasonal mean analysis (Fig. 14a) and initialisation (Fig. 14b) increment for the 200 hPa wind averaged for 00Z of June, July and August 1984. The mean analysis increments are generally small in the northern extra-tropics. However, in the tropics and in the southern hemisphere values around 5m/sec can be found. The initialisation increment is much smaller, generally of the order 1m/sec. This suggests, that most of the information contained in the data has been accepted by the initialisation. This also applies for the tropics, where the initialisation

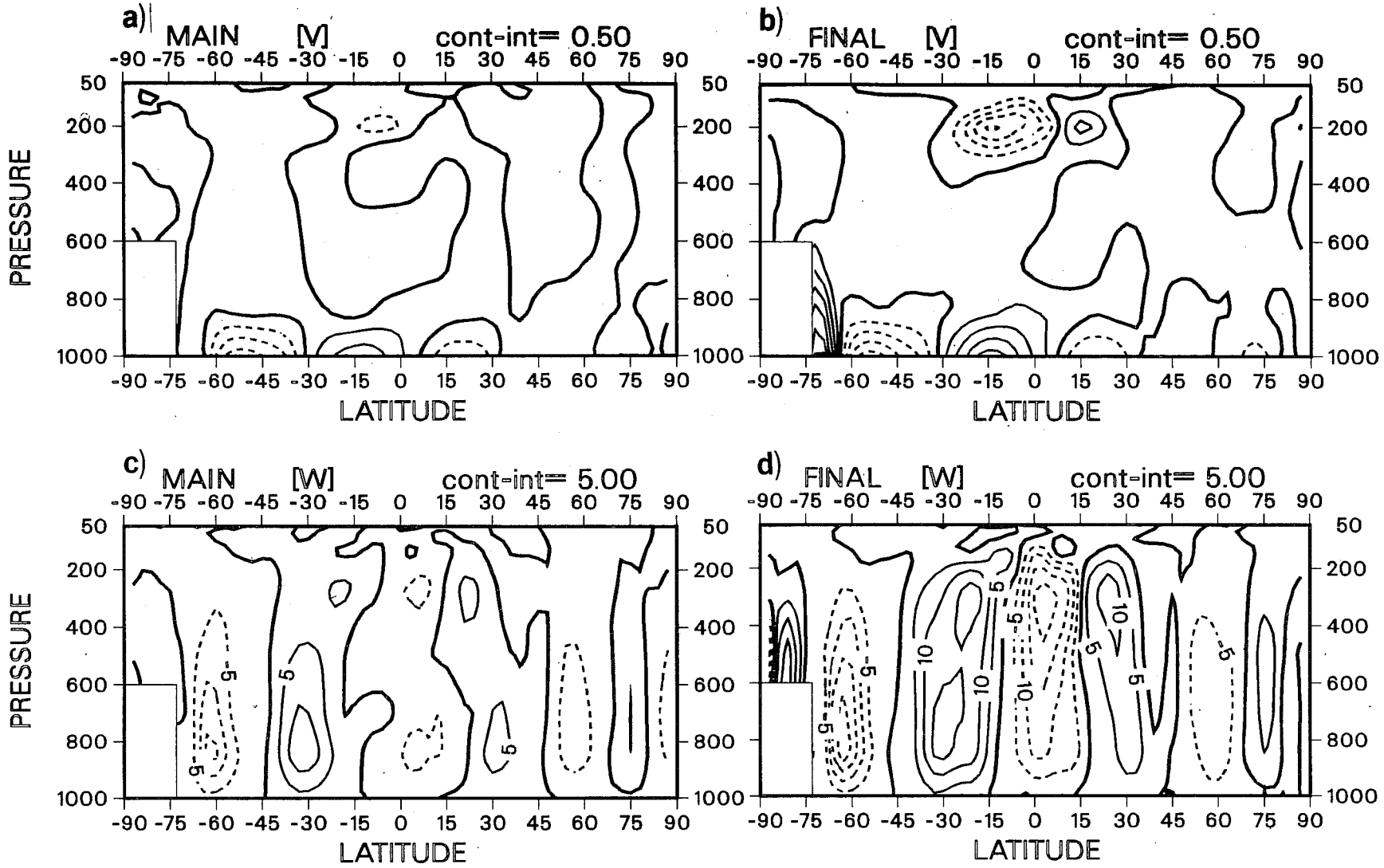

Fig. 12 May 1979 monthly mean latitude-pressure cross section for "Main" (a,c) and "Final" (b,d) analyses, a,b) zonal mean meridional velocities, contour interval 0.5 m/sec, c,d) zonal mean vertical velocity ω, contour interval 5 10^{-3} Pa/sec.

$\overline{\chi}$

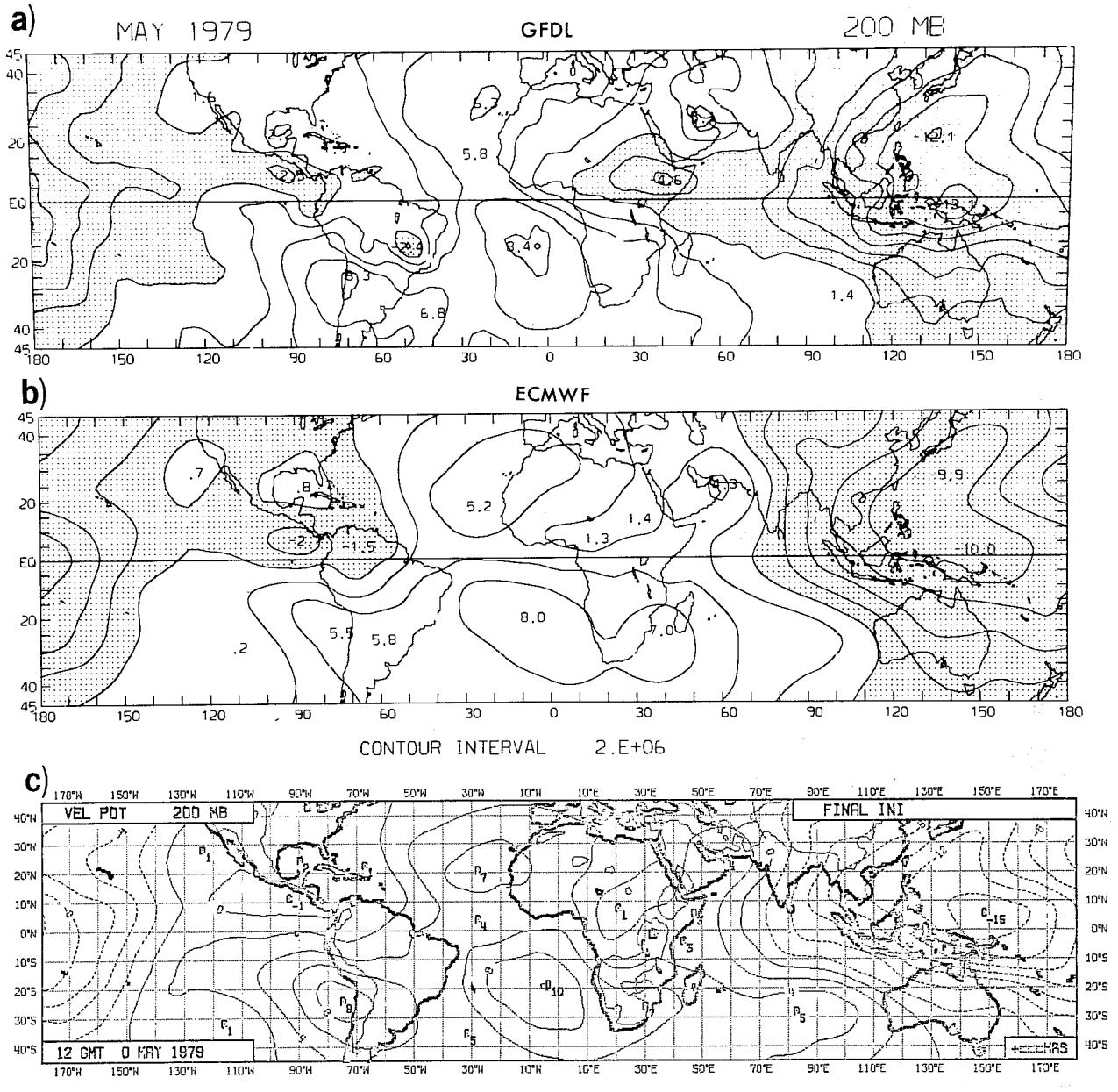

Fig. 13 May 1979 monthly mean 200 hPa velocity potential. a) uninitialised GFDL analysis, b) uninitialised "Main", c) initialised "Final" ECMWF analysis. Contour interval is 10^6 m^2/sec. a,b are taken from Lau, 1984.

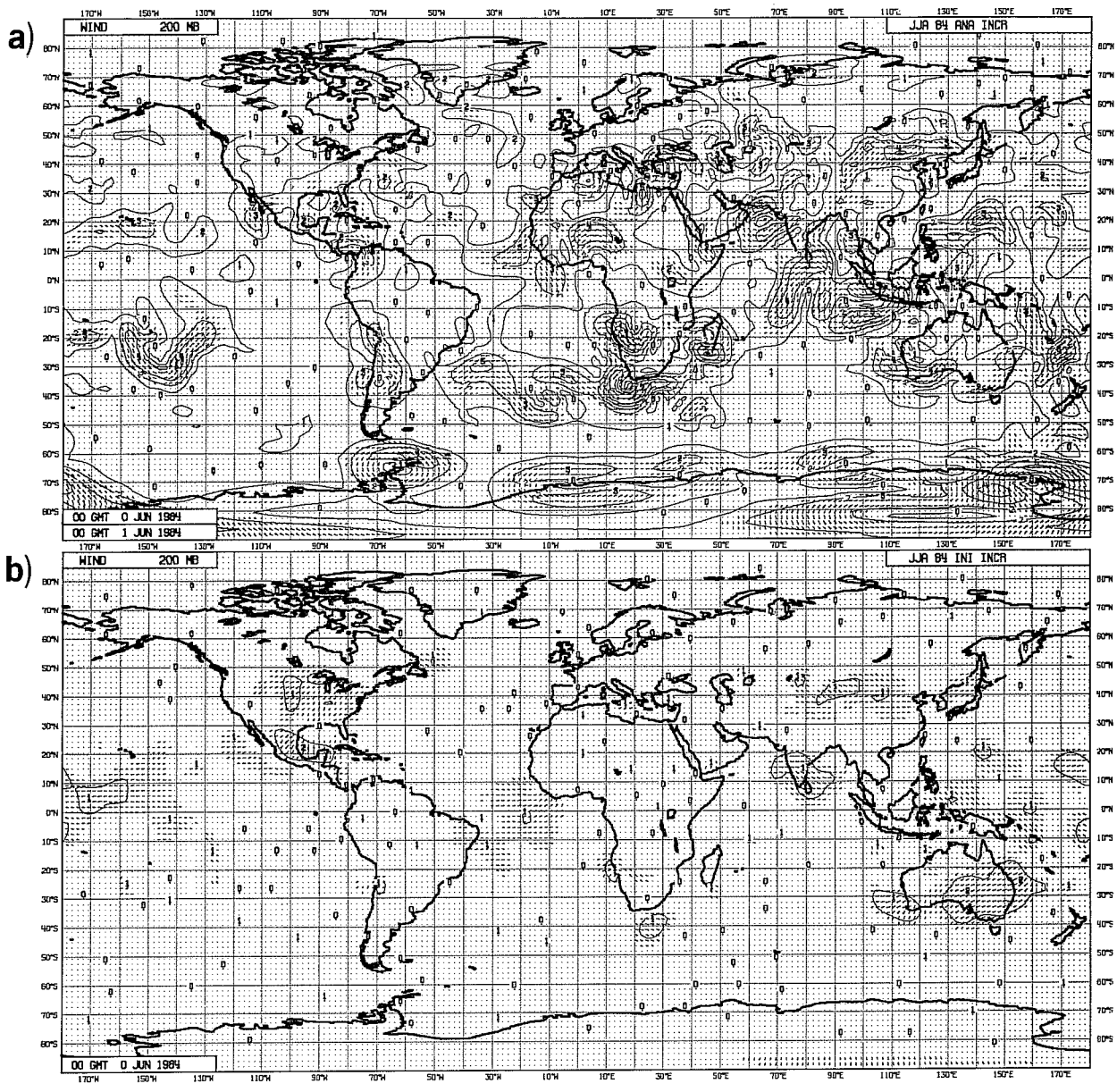

Fig. 14 June 1984 00 GMT, monthly mean analysis increment (a) and initialisation increment (b) for 200 hPa wind fields. Isolines give wind speed in 1 m/sec.

increment is frequently a mirror image of the analysis increment if an adiabatic initialisation is used. The inclusion of diabatic tendencies in the initialisation is essential for retaining the analysed information in the tropics.

The most critical variable with respect to initialisation changes is the divergence. Fig. 15 shows the June, July, August 1984 00Z mean divergence at 200 hPa for the uninitialised (Fig. 15a) and initialised (Fig. 15b) fields over Indonesia. The patterns are very similar. Extremes are slightly reduced in the initialised fields. There are also some areas where the initialisation results in a modest increase in amplitude. From this it would seem that neither the analysis nor the initialisation suffer any longer from systematic deficiencies, at least not in the upper tropospheric wind field.

Next we shall look at the vertical structure of the initialised fields. For this, we show zonal cross-sections rather than zonal averages. While zonal averages are useful to highlight gross features, they are prone to sampling errors for variables such as the meridional and vertical velocity, which frequently change sign in the zonal direction. In a zonal average day and night time as well as continental and maritime regimes of circulation are all lumped together.

Fig. 16 shows a longitude-pressure cross section of the meridional average (20°N-5°N) of the initialised divergence (Fig. 16a) and vertical velocity (Fig. 16b) for 00Z, Summer 1984 between 65° and 180°E. The most prominent feature in the divergence field is the strong maximum associated with convective outflow concentrated around 150 hPa. In the boundary layer there is strong convergence. A secondary maximum of convergence can be found around the 400 hPa level between 90°E and 100°E and 110°E and 125°E. This vertical structure implies a maximum vertical velocity at 300 hPa (Fig. 16b). Between 90°E and 100°E there is a secondary maximum in ω around 850 hPa. Although this complicated vertical structure disagrees with some long-held views of the tropical atmosphere (Newell et al., 1974) there is observational evidence from special observing campaigns which support the results in Fig. 16. For instance, Thompson et al. (1979) reported a secondary maximum of convergence around the 400 hPa level for the GATE dataset. Johnson and Young (1983) (using winter MONEX data) computed a ω profile with a maximum at 450 hPa for

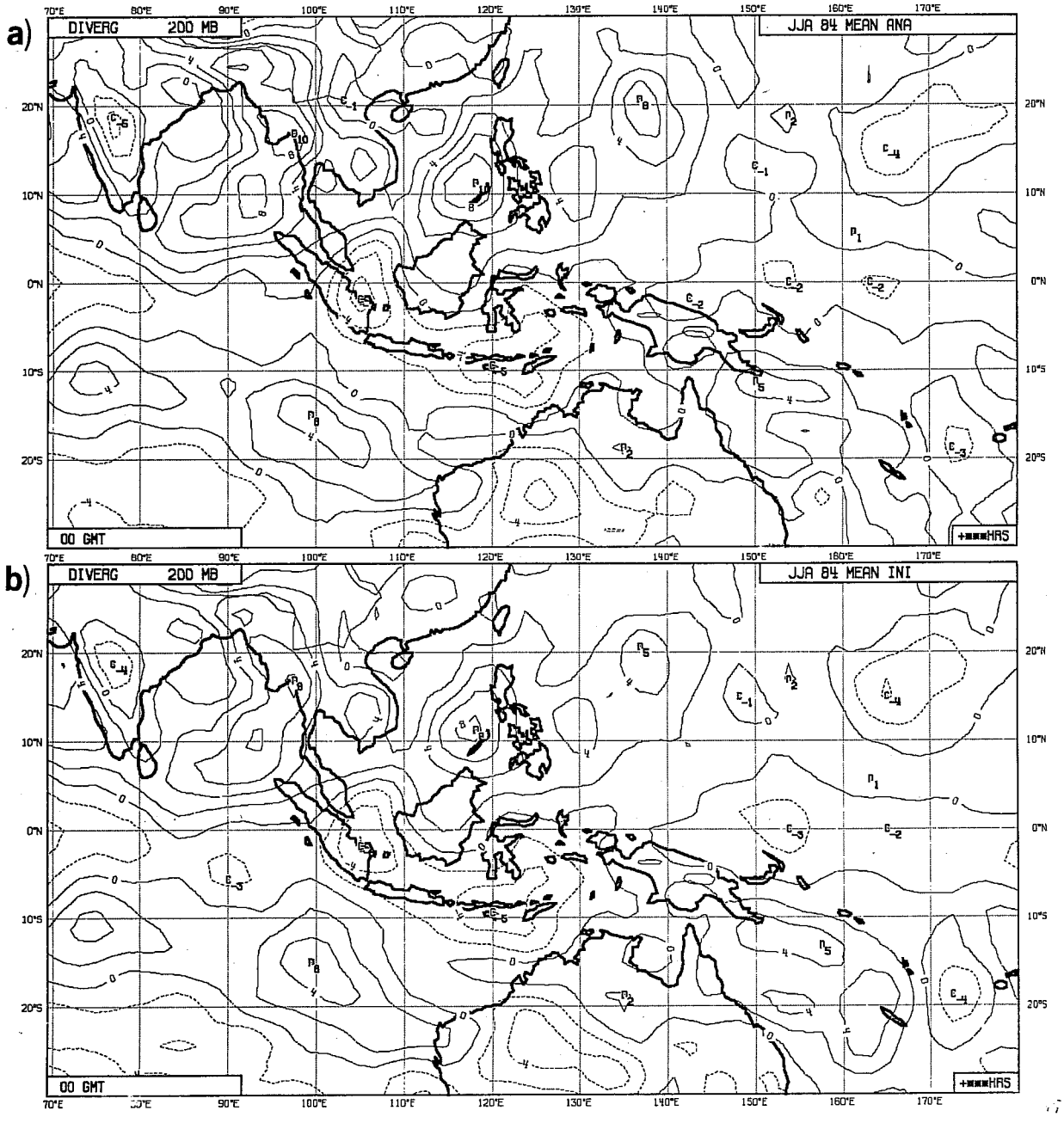

Fig. 15 June, July, August 1984 mean 200 hPa divergence for 00 GMT. a) uninitialised analysis b) initialised analysis. Contour interval is 10^{-6} sec^{-1}.

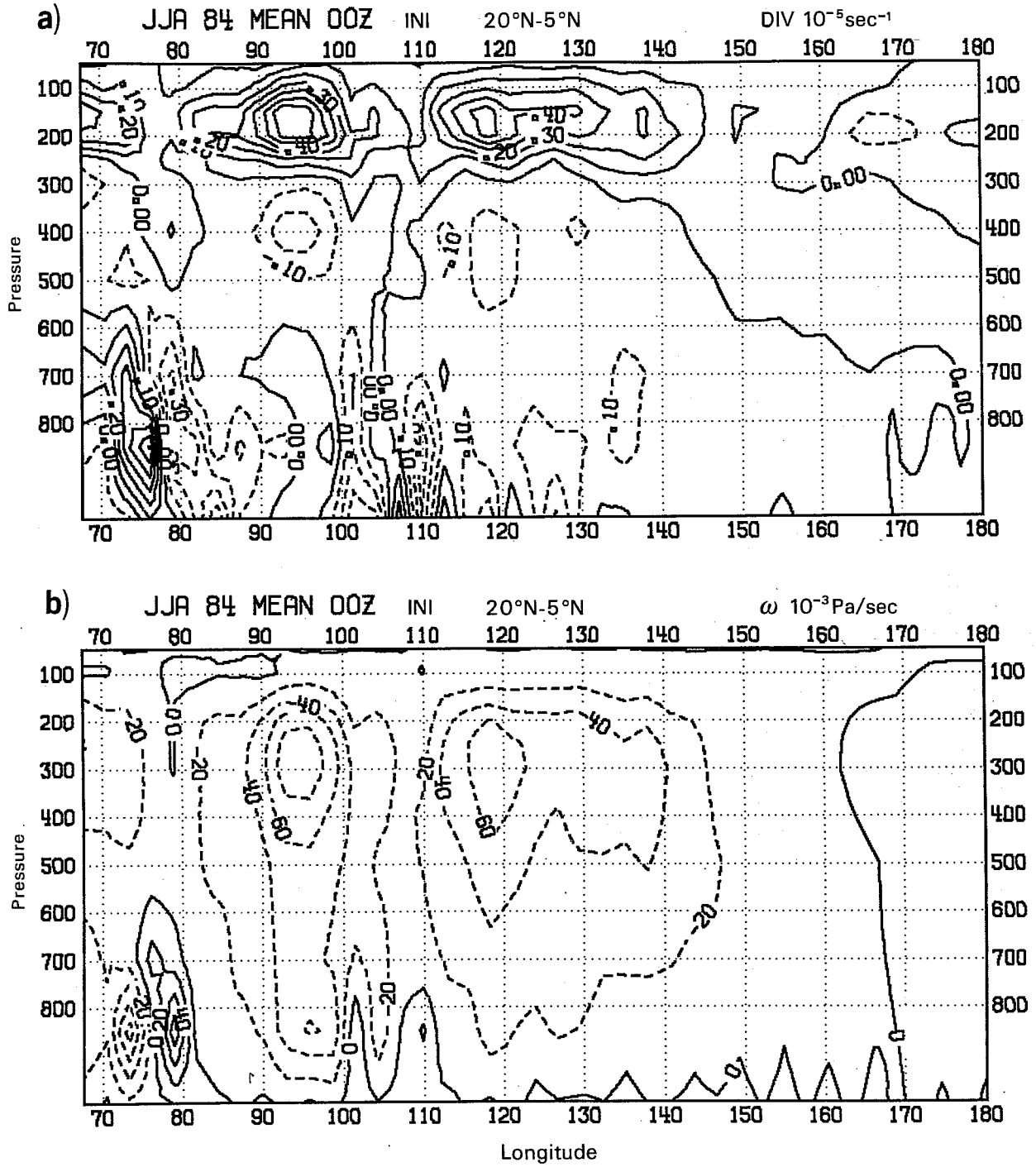

Fig. 16 Longitude pressure cross section of JJA 84 mean initialised divergence (a) and vertical velocity ω (b), averaged between 5°N and 20°N. Contour interval is 10^{-5} sec^{-1} (a) and 10^{-3} Pa/sec (b).

0800 local time and at 300 hPa for 1400 local time. Both profiles show a small secondary maximum around 900 hPa. The observed amplitudes agree very well with the values given in Fig. 16.

Despite the agreement between the initialised fields and the calculations based directly on observations, there remain some reservations about the detailed structure of the initialised tropical fields. One is the quality of the diabatic heating field used in the initialisation. Any deficiency in the parameterisation package will be reflected in the initialised fields to some extent. Experiments with a different convection parameterisation (Betts and Miller, 1984) indicate, however, that the differences are small. This is partly because of the horizontal filtering of the physical tendencies, which retains only the more reliable large scale components. Another problem concerns the uncertainties in using single level data in the analysis scheme. For example, it is not clear how best to spread the information from cloud track winds vertically. There is a problem with the height assignment for this data. These reports also produce systematic under-estimates of wind speed (Källberg 1985). Nevertheless, they are almost the only source of information about the wind field in large areas of the tropics.

As only a limited number of vertical modes is initialised, spurious structures in the vertical can also be introduced by the initialisation scheme. Operationally only the first 5 vertical modes are initialised at ECMWF. Therefore, "noise" contained in the higher modes remains uncontrolled. When transforming from the vertical normal mode space back to physical space this can lead to some arbitrary structures. The question, how many vertical modes to initialise will be addressed in Section 6.

4.3.3 Forecast impact

While closeness of the initialised and uninitialised analysis and the effective noise control are desirable features of an initialisation scheme, they do not necessarily guarantee satisfactory performance of the scheme within a data assimilation system. For instance, initialisation changes can be substantially reduced by initialising fewer horizontal and/or vertical modes. This does, however, not necessarily mean that the ensuing forecasts are better, as they might be contaminated with noise from the uninitialised

modes. Similarly, the forecasts can also suffer from excessive noise control; e.g. by not making a proper distinction between Rossby and gravity modes when applying a scheme which is only based on frequency.

Therefore, a thorough testing of any modification can only be done within a data assimilation scheme. The most critical parameter is the quality of the short range forecast used as a first-guess for the next analysis. Ideally, any improvement in the initialisation should be reflected in the ensuing forecast. The improvement in the first guess will be directly reflected in the quality of the next analysis through better quality control decisions. The easiest way to test the quality of initialisation and first guess fields is to compare them to the observations after erroneous reports have been eliminated. Fig. 17 shows the RMS fit to tropical radiosonde data of the initialised analysis (left) and of the 6 hour first guess (right) for the zonal (a,b) and meridional (c,d) wind components and for the height field (e,f). On average, about 120 reports were available at each analysis time. The curves with squares are for the adiabatically initialised analysis, those with circles are for the diabatic initialisation. The results are valid for the 00Z fields, averaged between 26.12.78 and 28.12.78. Quite clearly, the diabatically initialised fields are closer to the observed values than the adiabatic fields which confirms the results discussed in the previous sub-section. Most importantly, the improvement is maintained through the 6 hour forecast. This is demonstrated by the closer fit of the forecast started from the diabatically initialised analysis. The signal in the u-component is somewhat obscured by the rapid growth of forecast errors both in Rossby and gravity modes, in the middle atmosphere. Nevertheless, a positive impact can be found in the boundary layer and close to the tropopause. For the v-component and for the height field most of the improvement in the initialisation is reflected in the forecast.

There is also a positive impact on the forecasts beyond 6 hours. This is demonstrated in Fig. 18 which shows monthly mean operational forecast scores before and after the introduction of the diabatic initialisation on 21.9.82. The light full and heavy lines gives the absolute correlation of vector wind at 200 hPa in the tropics for day 1 and day 2. During September 1982 the scores improved by about 3%. The dashed curve gives the northern hemisphere anomaly correlation of 500 hPa height for day 2. It also shows a slight

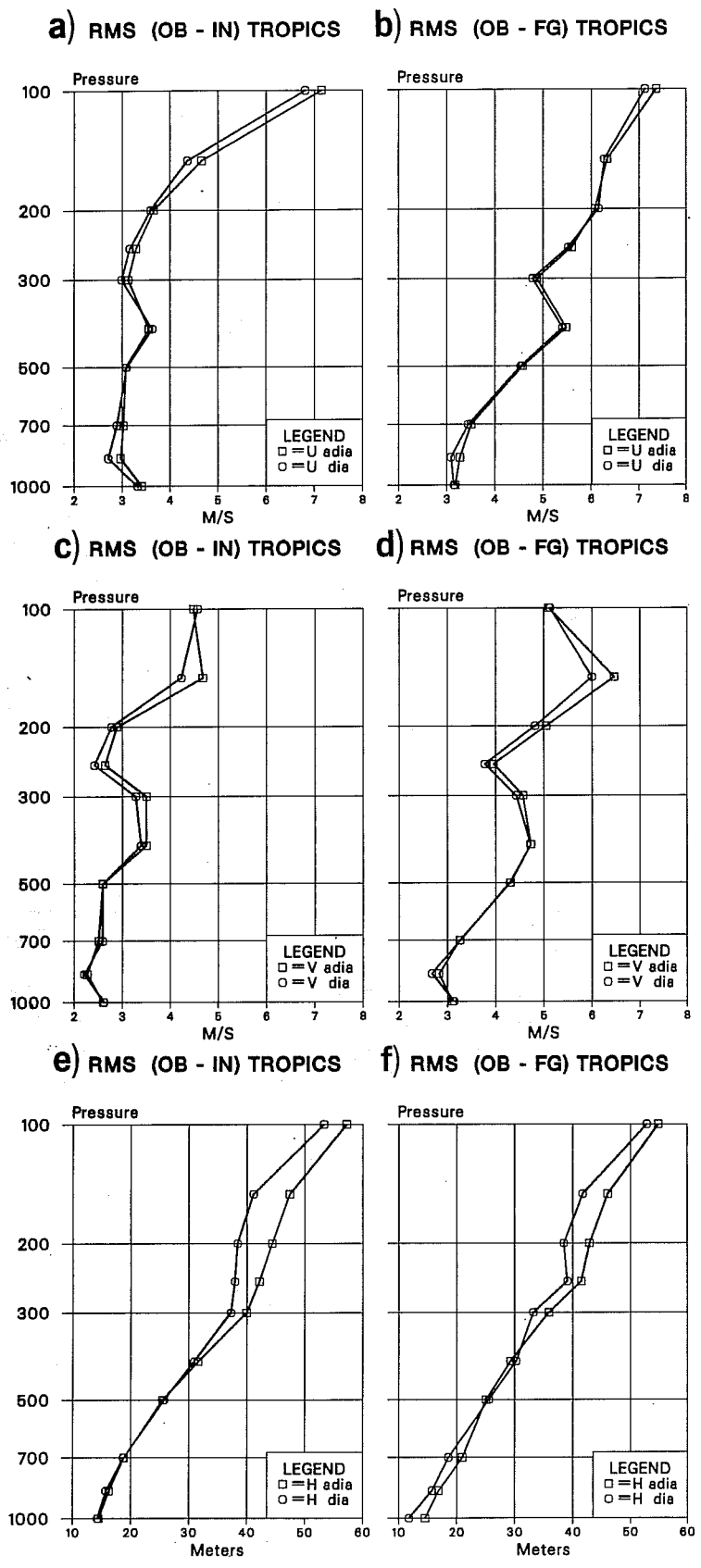

Fig. 17 RMS fit of initialised analysis (left) and first guess (right) to screened tropical radiosonde data, averaged for 00 GMT from 26.12.78 to 28.12.78. Squares give fit for adiabatic, circles for diabatic initialisation scheme. a) initialised, b) first guess zonal wind component; c) initialised, d) first guess meridional wind component; e) initialised, f) first guess geopotential.

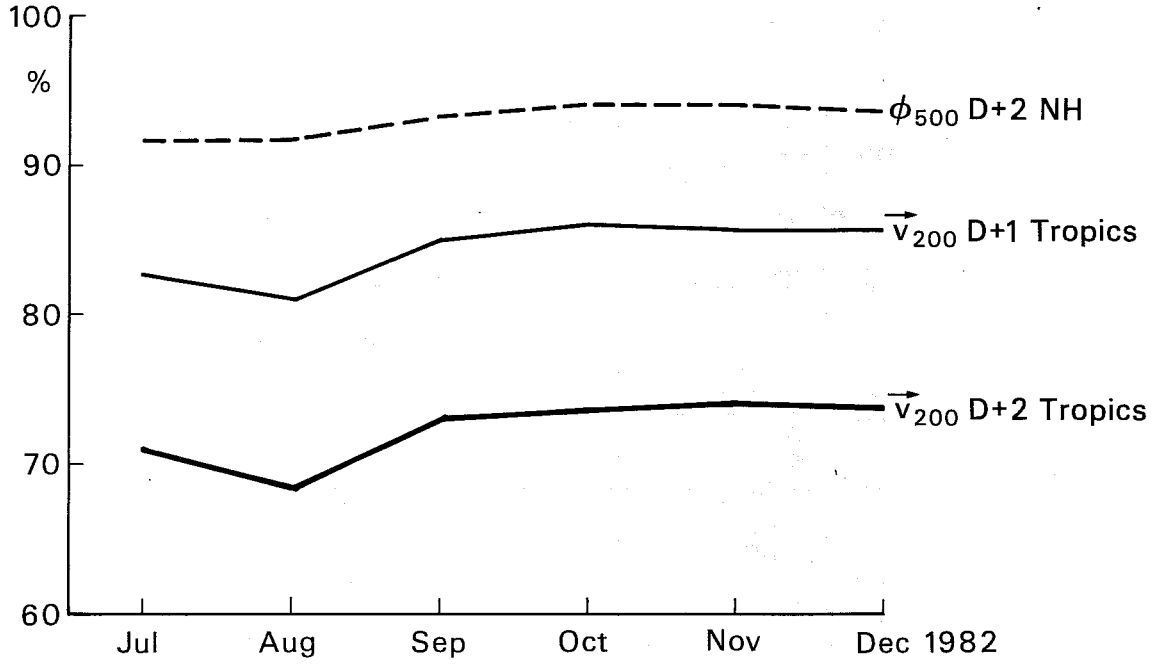

Fig. 18 Scores for operational forecasts between July and December 1982. Dashed: Anomaly correlation of 500 hPa D+2 height forecast averaged between 20°N and 22.5°N; absolute correlation of 200 hPa D+1 (light) and D+2 (heavy) wind field forecast in the tropics.

improvement during September 1982. As the forecasts are verified against the initialised analyses, part of the improvement is due to a more realistic verifying analysis.

4.3.4 The spin-up problem

A matter of ongoing concern is the so-called "spin-up" problem arising from the length of time it takes the model to fully develop a divergent circulation and to reach a balanced hydrological budget. It is sometimes argued that the initialisation negatively influences the spin-up. The following two figures (Figs. 19 and 20) are meant to shed some light on this problem. They show the convective rain accumulated between 00 and 12 hours and between 24 and 36 hours into the forecast. The forecasts were started from the initialised and from the uninitialised analyses. Fig. 19 is for the Indonesian area. During the first 12 hours the precipitation patterns are already well established for the initialised forecast (Fig.19a). The corresponding forecast started from the uninitialised analysis (Fig. 19b) shows a similar pattern, although the rain-band extending northeast from the Philippines is less well organised. Later in the forecast, the precipitation pattern is similar to the earlier pattern in each forecast respectively (Fig. 19c,d), thus indicating that the precipitation was already well spun-up during the first 12 hours of the forecast. The picture is fundamentally different for the east Pacific. Initially, there is little precipitation in the ITCZ area, both with initialised (Fig. 20a) and in the uninitialised (Fig. 20b) forecast. However, 24 hours later, the convective precipitation along the ITCZ is well established. Qualitatively, there is little difference between uninitialised and initialised forecasts.

From this it would seem that the spin-up problem is more severe in some areas than in others. Compared to this, the impact of the initialisation is small. At present, it is not clear what causes the large variability. Apart from differences in flow type, differences in data coverage could be responsible. In the east Pacific area the analysis mainly relies on satellite data. Cloud track winds are very difficult to use because they are single level data and they suffer from bias and height assignment problems (Källberg, 1985). Furthermore, it is not clear whether the temperature retrievals from satellites are accurate enough and have sufficient vertical resolution to

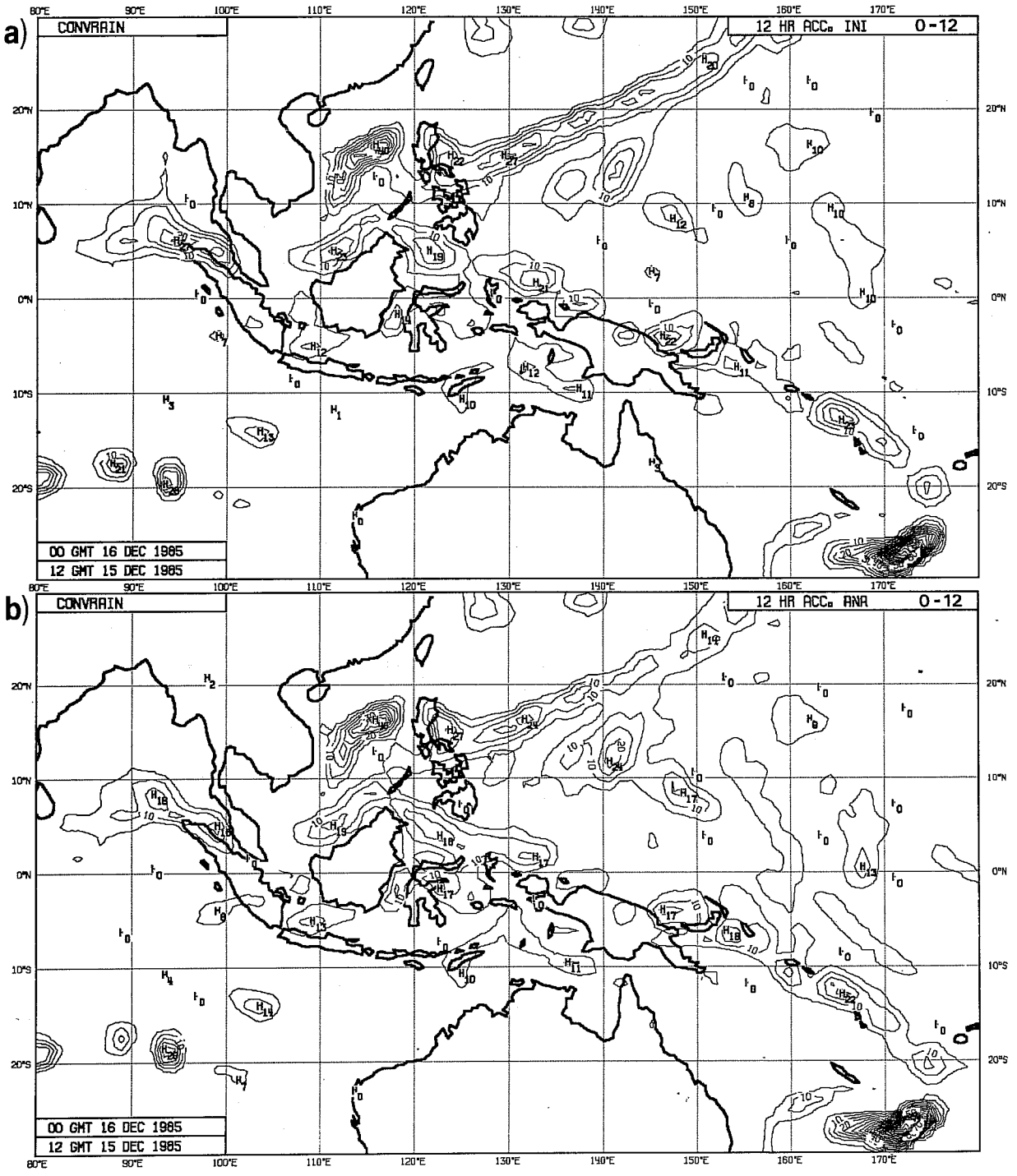

Fig. 19 12 hour accumulated convective precipitation for forecasts from 12 GMT, 15.12.85. a) initialised, precipitation between 0 and 12 hours, b) uninitialised, precipitation between 0 and 12 hours, c) initialised precipitation between 24 and 26 hours, d) uninitialised, precipitation between 24 and 26 hours.

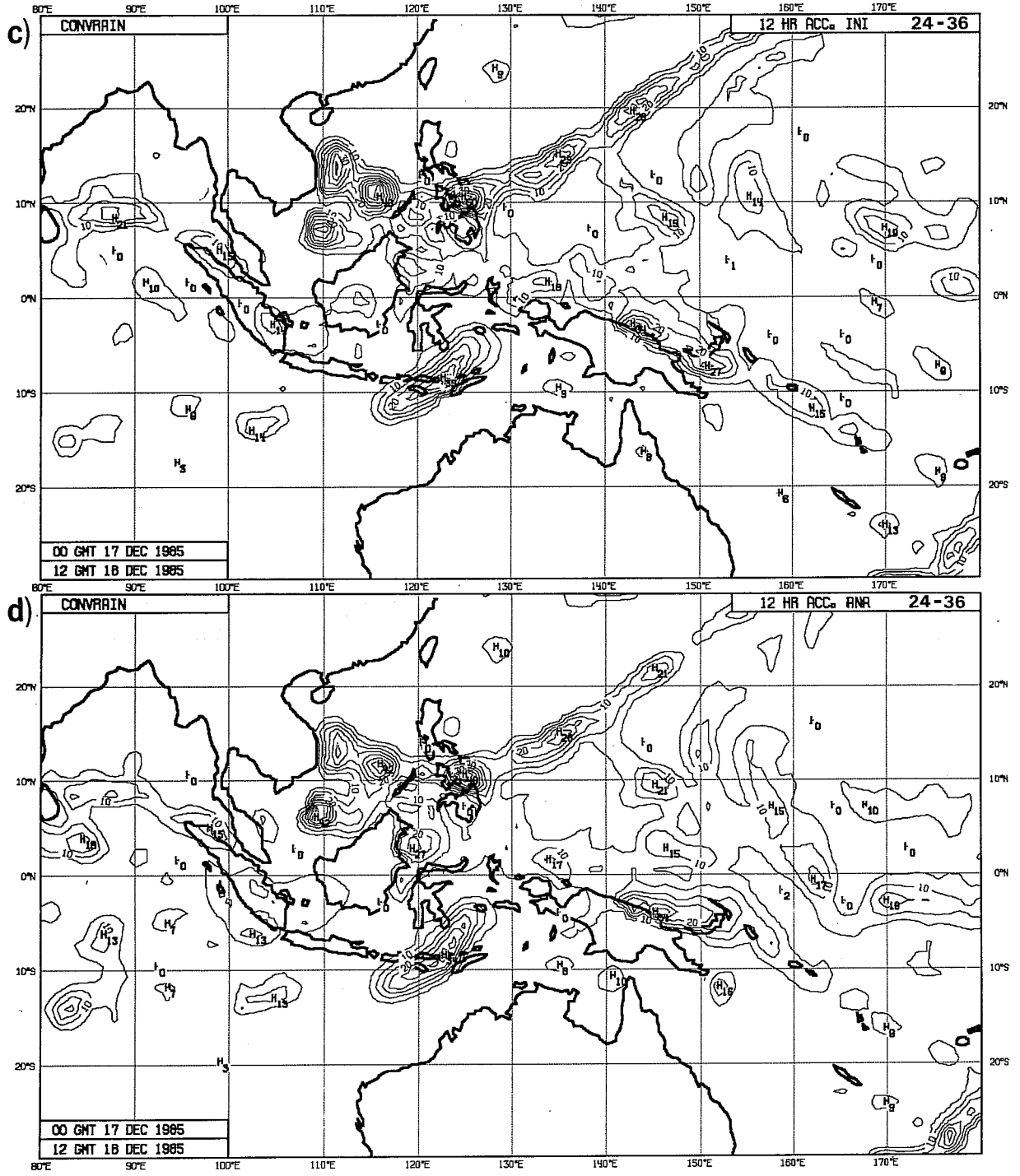
c)
CONVRAIN
12 HR ACC. INI
24-36
00 GMT 17 DEC 1985
12 GMT 18 DEC 1985
d)
CONVRAIN
12 HR ACC. ANA
24-36
00 GMT 17 DEC 1985
12 GMT 18 DEC 1985
80°E
90°E
100°E
110°E
120°E
130°E
140°E
150°E
160°E
170°E
20°N
10°N
0°N
10°S
20°S

Fig. 19 (Cont)

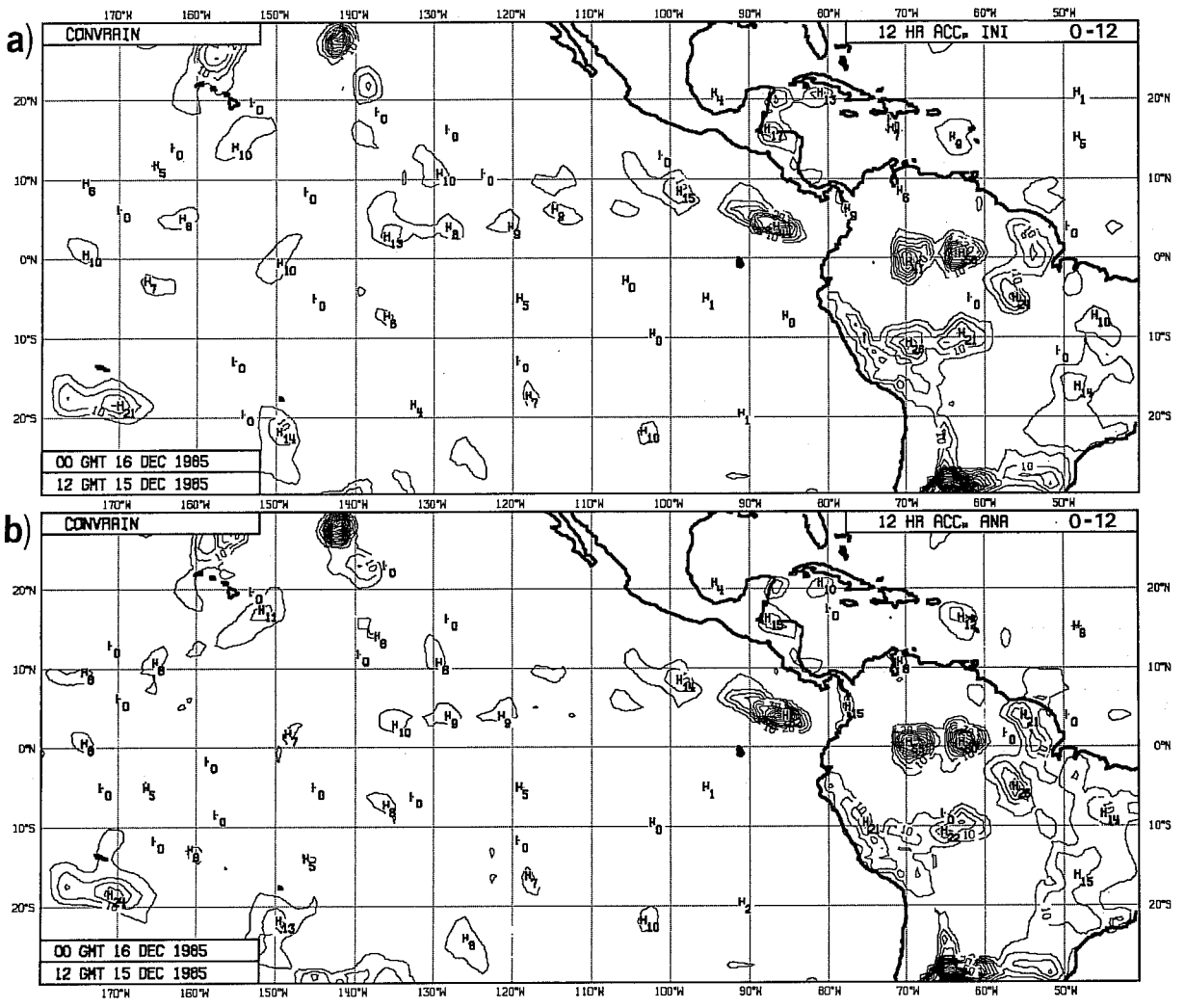

Fig. 20 Similar to Fig. 19, but for East Pacific area.

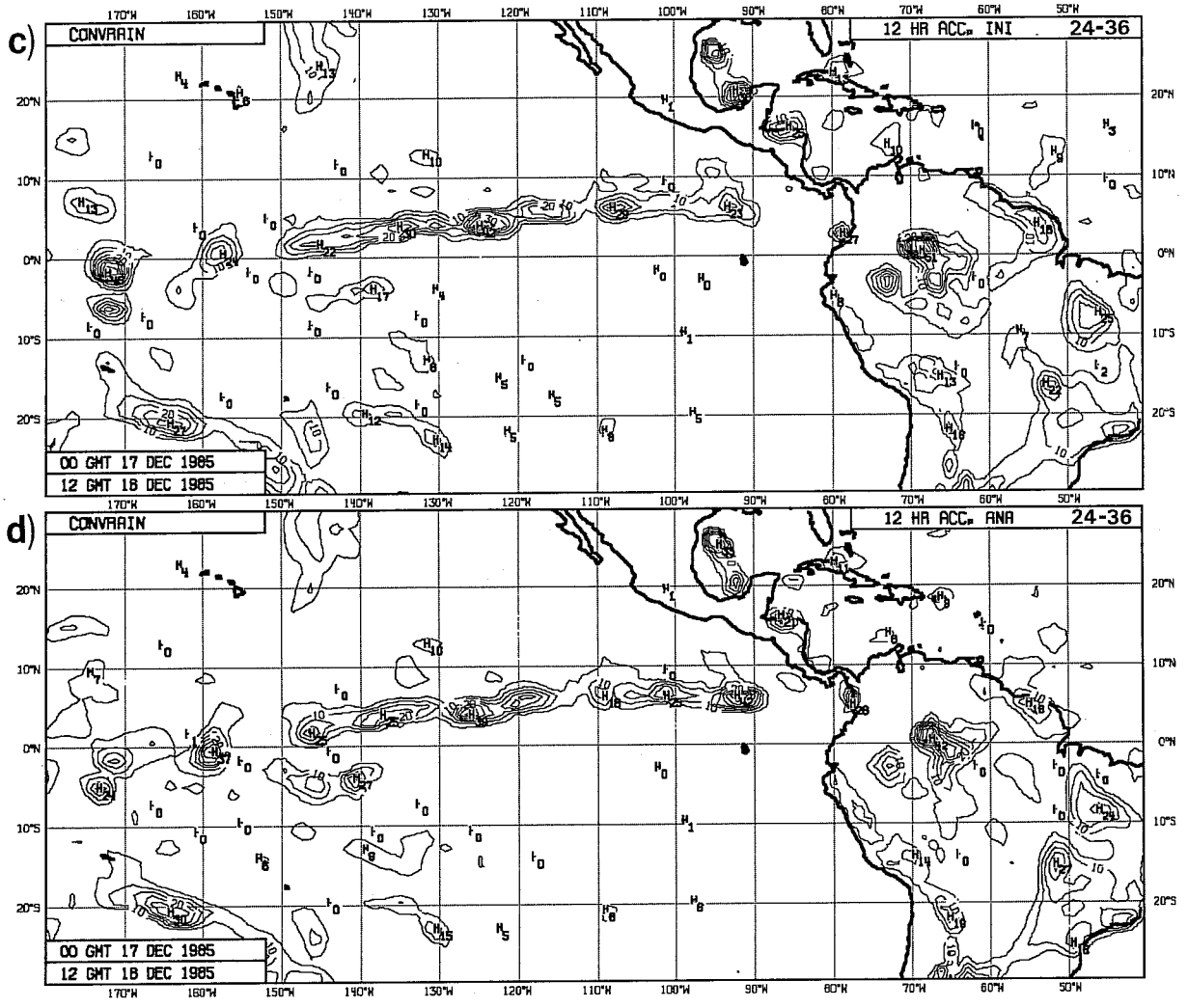
c)
CONVRAIN
12 HR ACC. INI
24-36
00 GMT 17 DEC 1985
12 GMT 18 DEC 1985
d)
CONVRAIN
12 HR ACC. ANA
24-36
00 GMT 17 DEC 1985
12 GMT 18 DEC 1985

Fig. 20 (Cont)

consistently correct the first guess. On the other hand, the data coverage in the Indonesian area is quite different as there are a number of radiosondes and numerous surface reports which are likely to lead to a better definition of the three-dimensional correction field.

Quite generally, the demands on an analysis scheme are very subtle in the context of data assimilation and the spin-up problem in particular. Apart from the requirements to fit the basic fields such as mass and wind, the parameterisation packages expect a consistent correction of a combination of derived quantities. For instance, the Kuo convection scheme depends on a precise specification of the initial moisture convergence together with the matching static stability. The boundary layer scheme requires a consistent definition of vertical wind shear, and stability. Without a dense, three-dimensional, high quality data coverage, analysis schemes are likely to upset some of these internal model balances. This is not to mention weaknesses in the parameterisation schemes themselves.

5. INITIALISATION CHANGES TO THE TROPICAL MASS FIELD

5.1 The problem

So far, we have not touched upon the handling of tropical mass field information by the initialisation. As we shall see, there is an extra complication which requires special attention.

The problem is highlighted in Fig. 21, which shows the RMS fit of analysis (circles) initialisation (triangles) and first guess (squares) height fields to tropical radiosonde data for 12Z, averaged for January 1984. The analysis scheme brings about a large correction of the first guess. The initialisation, however, wipes out most of this correction, so that the initialised analysis is closer to the first guess than to the uninitialised height analysis. This is largely caused by the rejection of tropical surface pressure data by the initialisation.

From the geostrophic adjustment theory, one might argue, this result is to be expected. After all, in the tropics the mass field adjusts to the wind field at least for barotropic structures. On the other hand, because of the good data coverage, surface pressure is one of the best analysed parameters and ideally one would like to retain this information. Attempts to overcome the problem have so far all been based on purely mathematical concepts. Daley (1978) proposed a variational normal mode initialisation scheme for a barotropic model. It allowed one to control the changes made to the analysed fields; albeit at the cost of modifying Rossby as well as gravity modes. Temperton (1984) proposed a similar scheme for the baroclinic ECMWF gridpoint model. While these schemes managed to limit the initialisation changes, they did not lead to any significant improvement in the subsequent forecasts. Temperton (1984) suggested that it might be more rewarding to find out what causes the rejection of tropical mass data and to remove that deficiency from the analysis initialisation cycle rather than imposing arbitrary mathematical constraints. This line of thought will be taken up here.

It is instructive to look at the mean initialisation changes to the 1000 hPa height field. Fig. 22a shows the June, July, August 1985 mean increment for 00Z while Fig. 22b is valid for 06Z. The striking feature of these maps is a tropical zonal wavenumber 2 pattern. At 00Z we have negative values in the South Pacific, positive values in the Atlantic, negative in the Indian Ocean

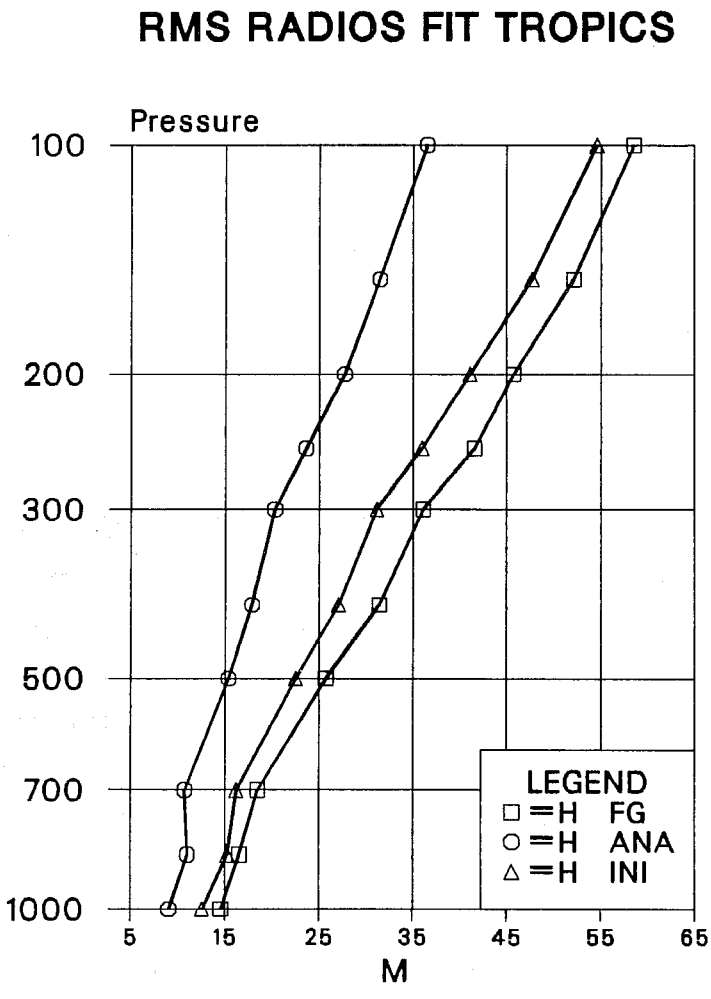

Fig. 21 RMS fit of analysis (circles), initialised analysis (triangles) and first guess (squares) to tropical radiosonde data for 12Z, January 1984.

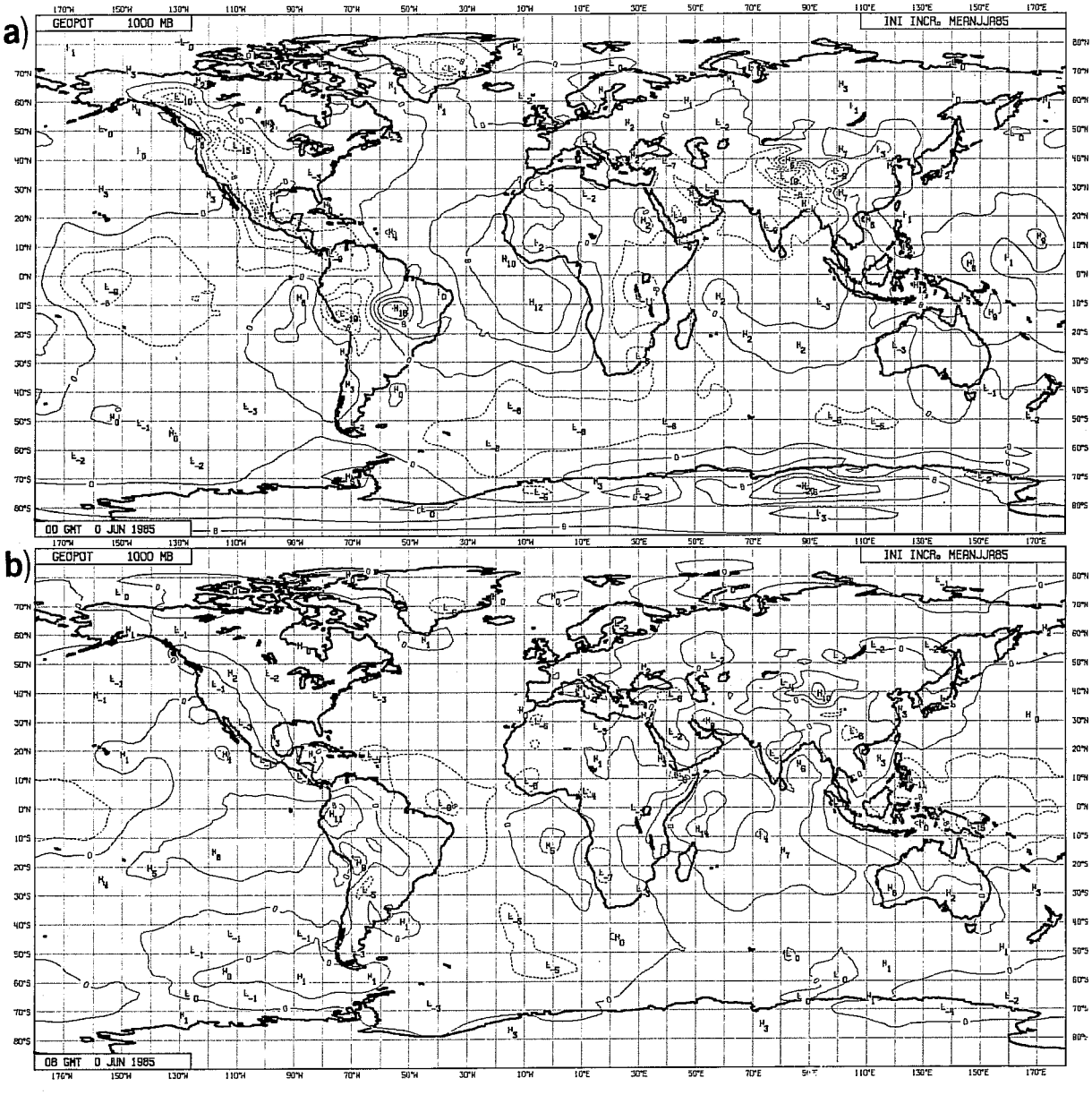

Fig. 22 Mean June, July and August 1985 initialisation increment of the 1000 hPa height field for 00 GMT (a) and 06 GMT (b). Contour interval is 4m.

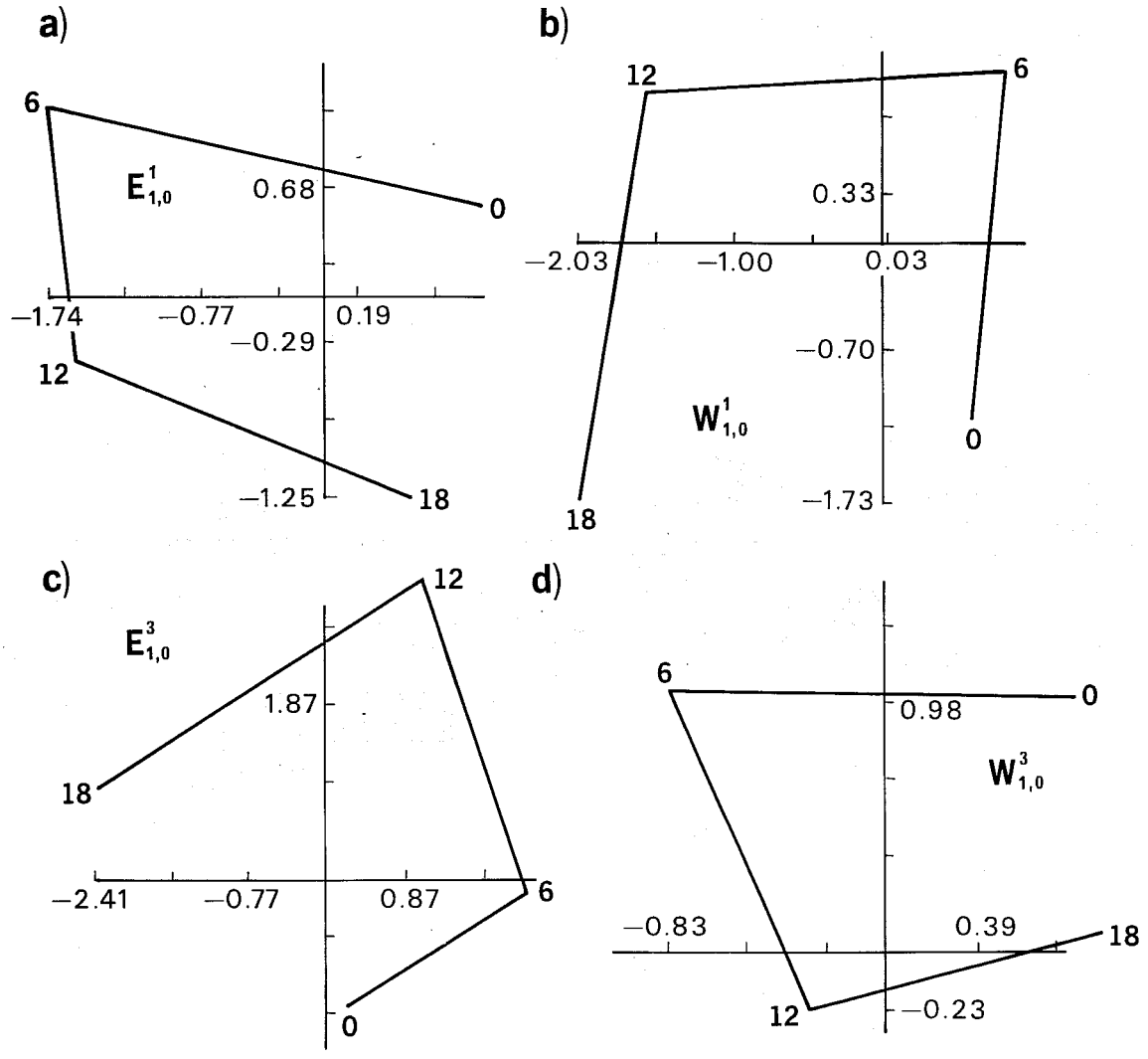

Fig. 23 Harmonic dials of mean June 84 initialisation changes for zonal wavenumber 1 at the 4 daily analysis times (00, 06, 12, 18 GMT). a) external Kelvin mode, b) external, gravest symmetric westward gravity mode, c) second internal Kelvin mode, d) second internal, gravest symmetric westward gravity mode.

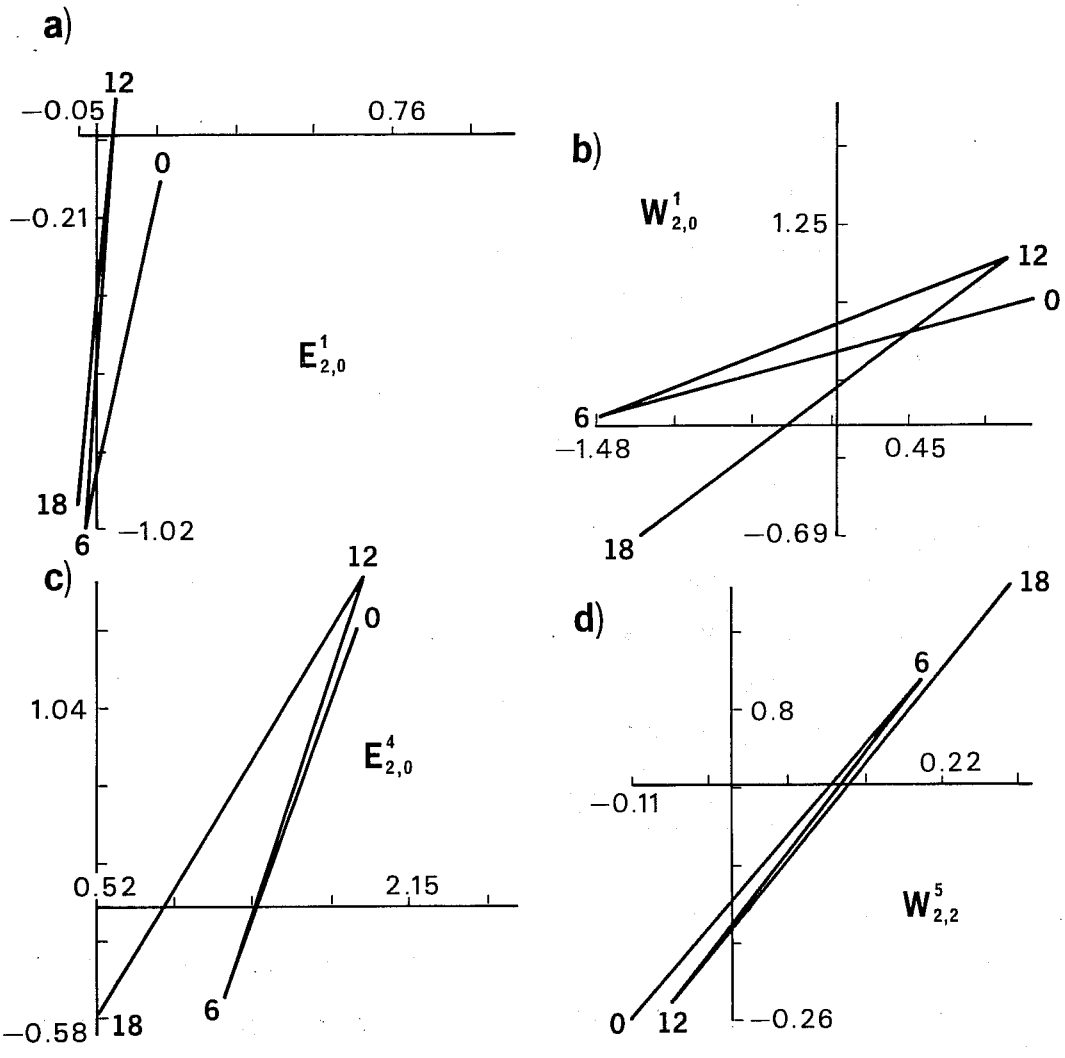

Fig. 24 Harmonic dials of mean June 84 initialisation changes for zonal wavenumber 2 at the 4 daily analysis times (00, 06, 12, 18 GMT). a) external Kelvin mode, b) external, gravest symmetric westward gravity mode, c) third internal Kelvin mode, d) fourth internal, second gravest symmetric westward gravity mode.

and again positive in the West Pacific. Six hours later the pattern has changed sign with positive values in the East Pacific and Indian ocean and negative values in the Atlantic and West Pacific. The amplitude is of the order of 10m, which is about the climatological variability of the 1000 hPa height field in the tropics.

Some further insight into this process can be obtained by looking at the initialisation changes to individual gravity mode coefficients. Fig. 23 gives harmonic dials for zonal wavenumber 1 coefficients, valid for the mean June 1984 increments. Each dial indicates the mean changes at the four daily analysis times (18, 00, 06, 12 GMT). On these dials counter clockwise rotation indicates westward propagation. Numbers on the coordinates are arbitrary, but are comparable between different dials. The external Kelvin mode (Fig. 23a) shows a regular westward propagation with a period of 24 hours. The second internal Kelvin mode (Fig. 23c) behaves similarly. As free modes, Kelvin modes travel eastward. The fact that the signal in the initialisation changes propagates westward for these modes implies a corresponding westward propagating forcing. The gravest symmetric external (Fig. 23b) and second internal (Fig. 23d) westward gravity modes also show a regular westward propagation with a period of 24 hours. Some selected dials for zonal wavenumber 2 gravity modes are shown in Fig. 24. Basically, the coefficients oscillate between two states. Within six hours the signal has propagated by half a wavelength. With a time resolution of six hours, no statement about the direction of propagation can be made. Eastward (Fig. 24a,c) and westward (b,d) modes are similar in behaviour. All vertical modes contribute, with the third internal Kelvin mode (Fig. 24c) having the largest amplitude.

5.2 The cause of the problem

There is a straightforward explanation for all these findings: the initialisation condition $\dot{Y}=0$ is not appropriate for the atmospheric tides. Instead of requiring stationarity for the gravity mode projection of the tidal signal, one should allow it to propagate westward with the movement of the sun. As already pointed out in the context of the diabatic initialisation, the Machenhauer condition is only appropriate if the forcing is quasi-stationary. This is clearly not the case if the radiation scheme simulates the diurnal cycle of the sun. Also, the observational data reflect

the presence of tidal activity in the analysis and thus imply transient tidal components in the model tendencies.

Atmospheric tides are mostly thermally excited by the absorption of solar radiation by ozone and water vapour. Mainly zonal wavenumber 1 and 2 modes are excited. Due to the vertical distribution of the absorbers, the diurnal zonal wavenumber 1 pressure wave is largely trapped, whereas the semi-diurnal wave can propagate vertically (Chapman and Lindzen, 1970). Therefore, the semi-diurnal wave dominates in the surface pressure field. Chapman and Lindzen (1970) quote amplitudes of 1.22 hPa and .22 hPa for the dominant, first two gravest symmetric spherical harmonics of the semi-diurnal surface pressure oscillation. For the corresponding harmonics of the diurnal wave they give .46 and .21 hPa.

5.3 A possible solution

An obvious way to avoid the problem discussed above would be to exclude the tidal signal from the initialisation. With $\dot{Y}_t$ denoting the tidal component of the time tendencies, the initialisation condition (65) can then be re-written as

$$Y_j^{\ell+1} - Y_j^{\ell} = \frac{\frac{i}{\Delta t}\left[Y_j^{\ell}(\Delta t) - Y_j^{\ell}(0)\right]_a + \bar{p}_j - \dot{Y}_t}{2\Omega\nu_j} \qquad (66)$$

Note that $\dot{Y}_t$ as well as the physical tendencies $\bar{q}_j$ are assumed to be independent of the iteration count ℓ.

This still leaves us with the problem how to determine $\dot{Y}_t$. A convenient and stable estimate can best be obtained by a timeseries analysis. For zonal wavenumber m=1 we need to isolate the westward travelling waves with a period of one day. For zonal wavenumber 2 the relevant period is 12 hours. These are the dominant components for the atmospheric tides. Other harmonics, e.g. the zonal wavenumber 3 semi-diurnal wave, have considerably smaller amplitudes (Chapman and Lindzen, 1970).

With $\dot{Y}_j$ denoting the timeseries of gravity mode tendencies ending at the actual analysis date J, an estimate of the tidal component $\dot{Y}_{t_J}$ for that time

can be obtained from

$$\dot{Y}_{t_J} = \frac{1}{J} \sum_{j=1}^{J} \dot{Y}_j \, e^{i \frac{\pi m}{2} j} \qquad (67)$$

In (67) it is assumed that the entries in the series are six hours apart. The length J of the series has to be determined experimentally. It has to be long enough to avoid aliasing. On the other hand it should not mask the seasonal variability of the tides. For operational implementation a length of ten days was chosen. The analysis (67) is performed for all vertical modes being initialised. In the meridional direction it is applied for the first four symmetric and anti-symmetric modes. As noted earlier the computation of the tidal tendencies is only done for zonal wavenumber m=1 and m=2.

5.4 Results

The proposed scheme was tested in a 5 day data assimilation. Fig. 25 shows the RMS fit of the initialised (left) and of the first guess (right) height field averaged over the last 3 days of the assimilation. Squares depict the standard scheme, circles are for the test with the special handling of the tides in the initialisation. Excluding the tides from the initialisation improves the initialised tropical height field RMS fit by about 5m. The improvement increases in the upper troposphere. In the six hour forecasts, most of the improvement in the lower troposphere is maintained. Around the 300 hPa level the positive impact becomes smaller, but on the whole the exclusion of the tides from the initialisation results in a better tropical surface pressure forecast.

The impact of the modification on the evolution of the predicted tropical surface pressure is shown in Fig. 26. It gives traces for 24 hours forecasts started from the uninitialised analysis (full), from the standard diabatic initialisation (dashed-dotted) and from the initialisation with the special handling of the tides (dashed). At .93°N and 11°W (Fig. 26a) the tidal initialisation is initially closer to the uninitialised analysis and captures the semi-diurnal pressure variation better than the standard initialisation, especially in the early stages of the forecast. It does not, however, suffer from the noise problems of the uninitialised analysis. Similar conclusions hold for a point in the tropical Pacific (Fig. 26b) which again shows a more pronounced semi-diurnal pressure wave for the "tidal" initialisation. It is

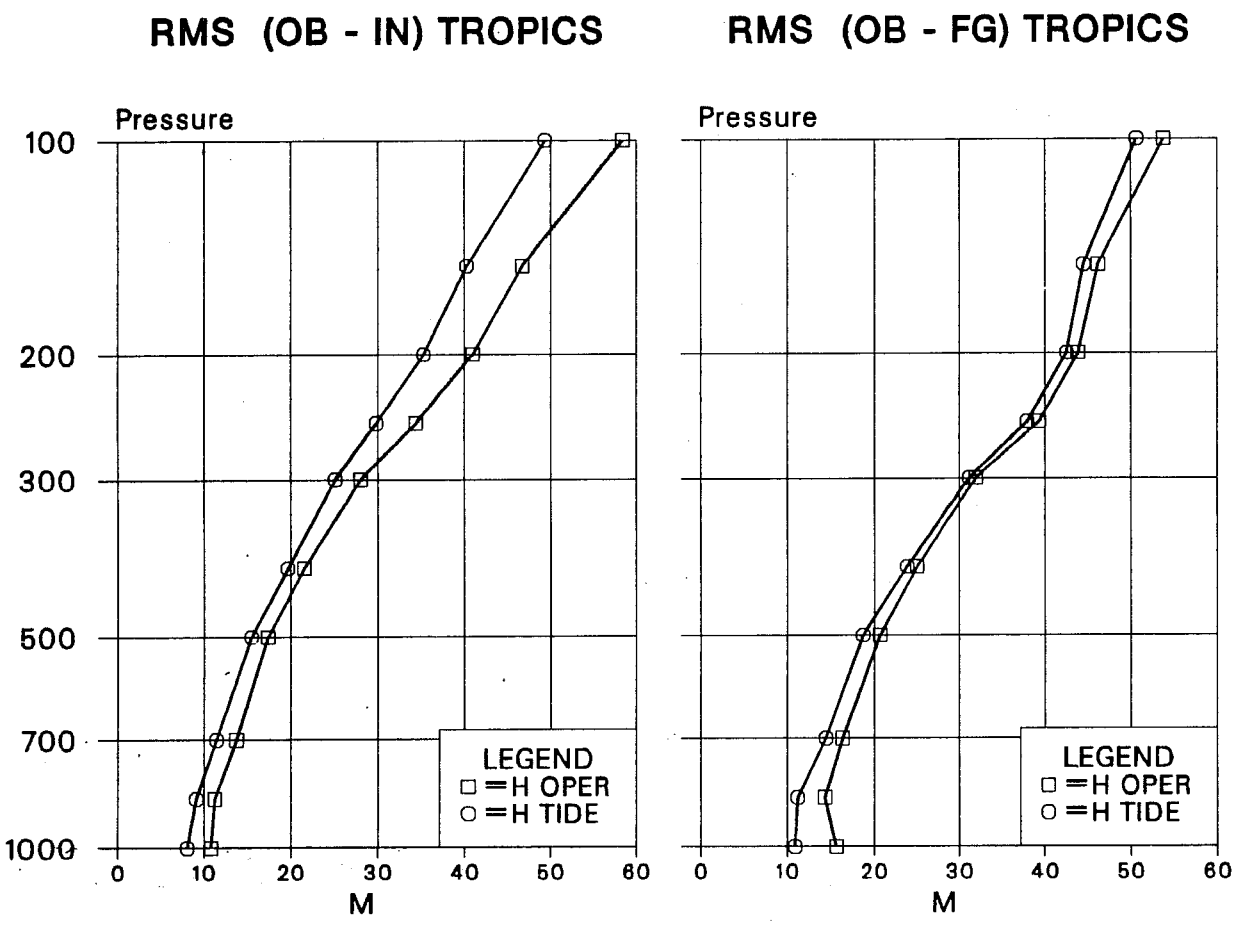

Fig. 25 RMS fit of the initialised height analysis (left) and first guess (right) to screened tropical radiosonde data. Average for 12 GMT, 13.3.85-15.3.85. Square: standard scheme, circles: test with special handling of tidal tendencies.

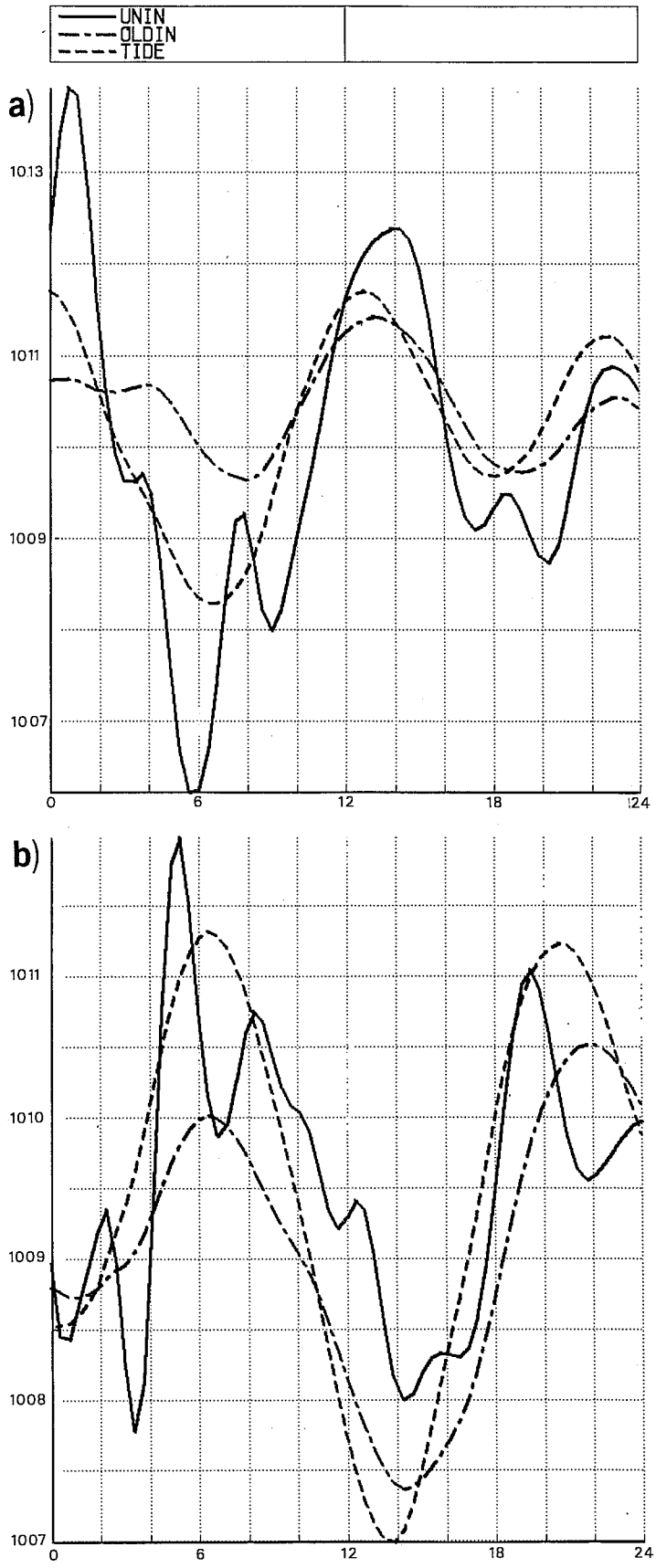

Fig. 26 Evolution of surface pressure, for a point at 0.93°N, 11°W (a) and at 0.93°N, 144°W. (b) for a forecast from 12 GMT, 15.3.85 started from the uninitialised analysis (full), the standard initialisation (dashed-dotted) and from the test scheme (dashed).

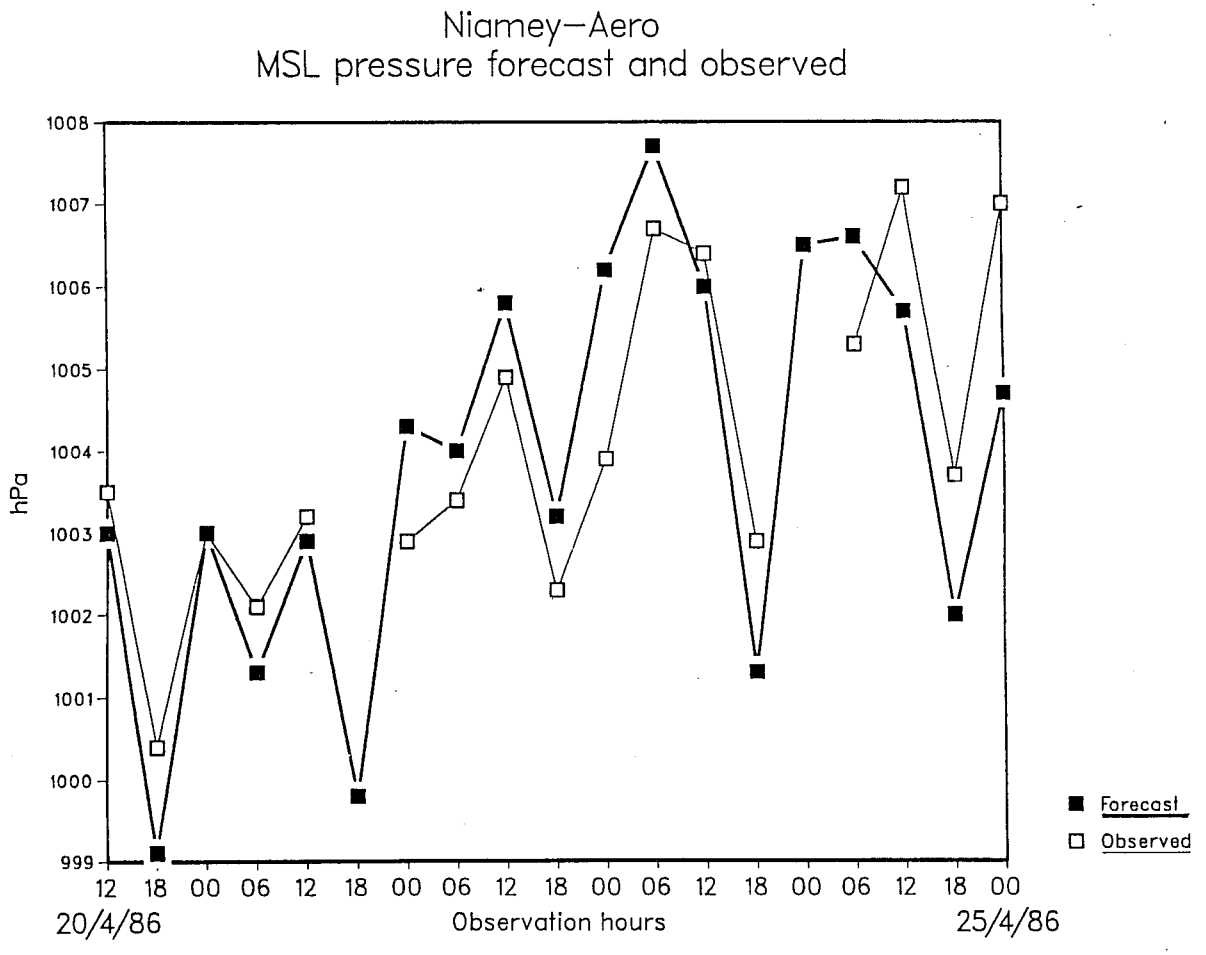

Fig. 27 Predicted (full squares) and observed (open squares) surface pressure at Niamey (13°N, 2°E) between 12 GMT, 20.4.86 and 00 GMT, 25.4.86. (Humphreys, pers. comm.)

instructive to compare the predicted surface pressure evolution to the observed values. Fig. 27 shows the corresponding curves for the station Niamey in Niger (13°N, 2°E) (Humphreys, Pers. comm). The model captures most of the semi-diurnal oscillations and of the superimposed longer term trend.

The assimilation system benefits from the improved surface pressure forecasts mainly through a reduced need for corrections to the mass field. Most of the mass information over the tropical continents is from SYNOP reports. While it is easy to use them to correct the surface pressure, there are large uncertainties as to how to spread the information vertically. By improving the first guess this problem can be alleviated.

6. SOME ADDITIONAL EXPERIMENTS

6.1 On the use of a cut-off period

An attractive idea to circumvent the problem of the severe damping of divergent circulations by an adiabatic scheme in the tropics is to introduce a cut-off period into the initialisation process. Modes with free periods longer than that cut-off period are not initialised. As shown by Puri (1983) the tropical divergent circulation is mainly described by some large scale internal inertia-gravity modes. These modes have long periods and it seems inappropriate to identify them with noise. Therefore, they could perhaps be excluded from the initialisation process. This would automatically avoid the substantial amplitude reduction brought about by an adiabatic initialisation. However, using a cut-off period places a large burden on the analysis system, as it is now the only means to control the inertia-gravity wave activity in the assimilation scheme.

To test whether this can cause problems a number of assimilations have been run. Fig. 28 shows the results for an experiment run from 28.3.86, 12 GMT to 30.3.86, 12 GMT. It depicts the RMS fit of initialised analysis (left) and first guess (right) to tropical radiosonde data for the last cycle of the experiment. Top panels are for the u-, bottom panels for the v-component. The line joined by circles shows the fit for an initialisation scheme which did not initialise the Kelvin mode and its westward travelling counterpart for zonal wavenumbers smaller than 10 and for vertical modes 3 to 5. It is compared to the operational diabatic scheme (squares). For the initialised analysis (left panels) there is little to choose between the two methods. However, the first guess started from the cut-off initialisation is inferior to the diabatic run. It fits the data less well in the upper troposphere. Cloud track winds supply most of the wind observations at these levels. Fig. 28 suggests that in the ECMWF system this information has a projection on large scale internal gravity modes, which, if not initialised, can lead to "noise" problems in the assimilation cycle.

This large scale "noise" not only affects the short-range forecast but also leads to some detrimental effect in the medium range. Fig. 29 shows the error in the zonal mean wind for a forecast from the diabatic (Fig. 29a) and from the cut-off scheme (Fig. 29b). The fields are time averages for the last half of a 10 day forecast. In the tropics and in the northern hemisphere

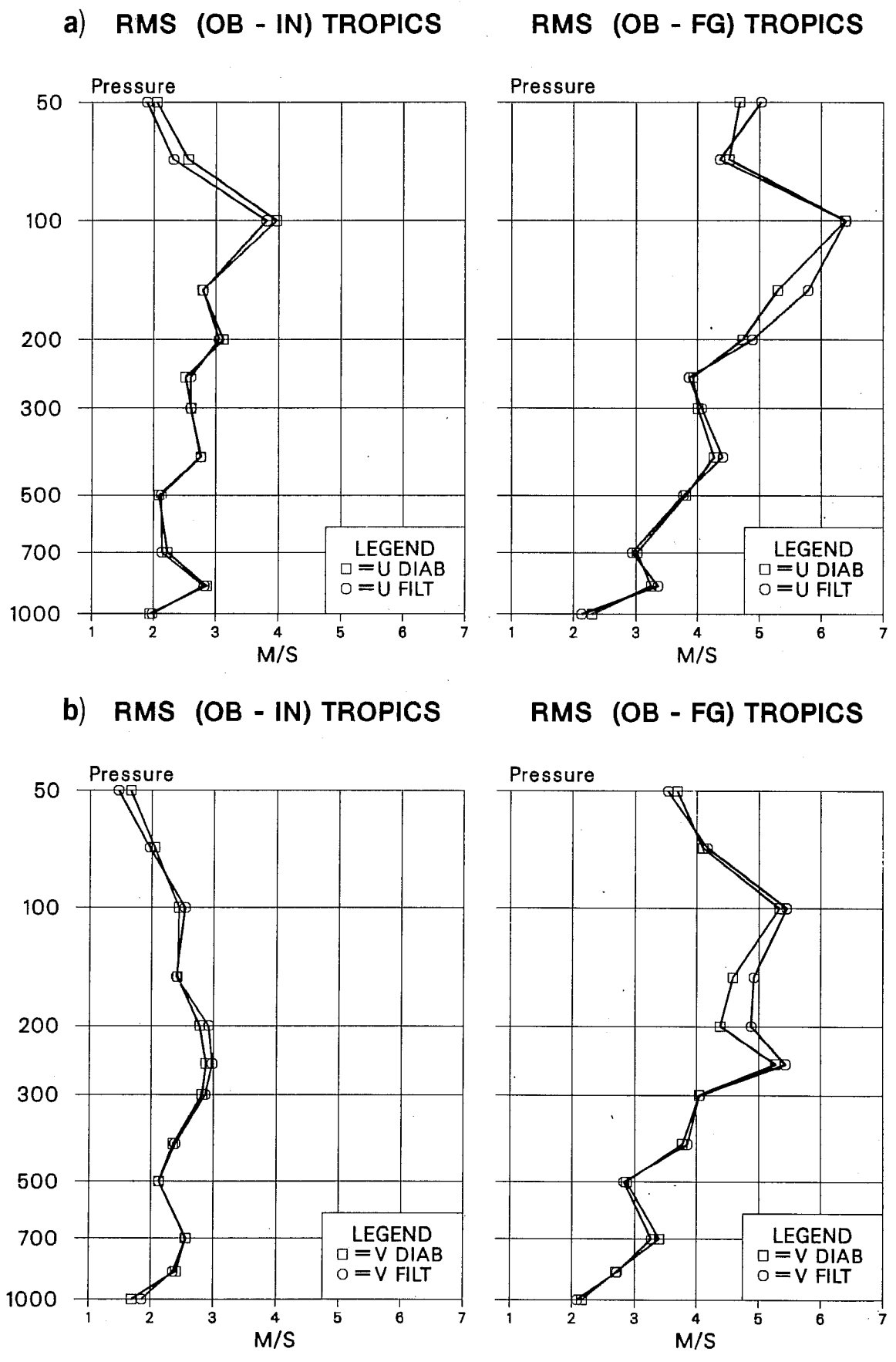

Fig. 28 RMS fit of initialised (left) and first guess (right) fields for 12 GMT, 30.3.86 to tropical radiosonde data. a) zonal, b) meridional wind component. Squares depict standard diabatic scheme, dots for scheme as proposed by Puri (1983).

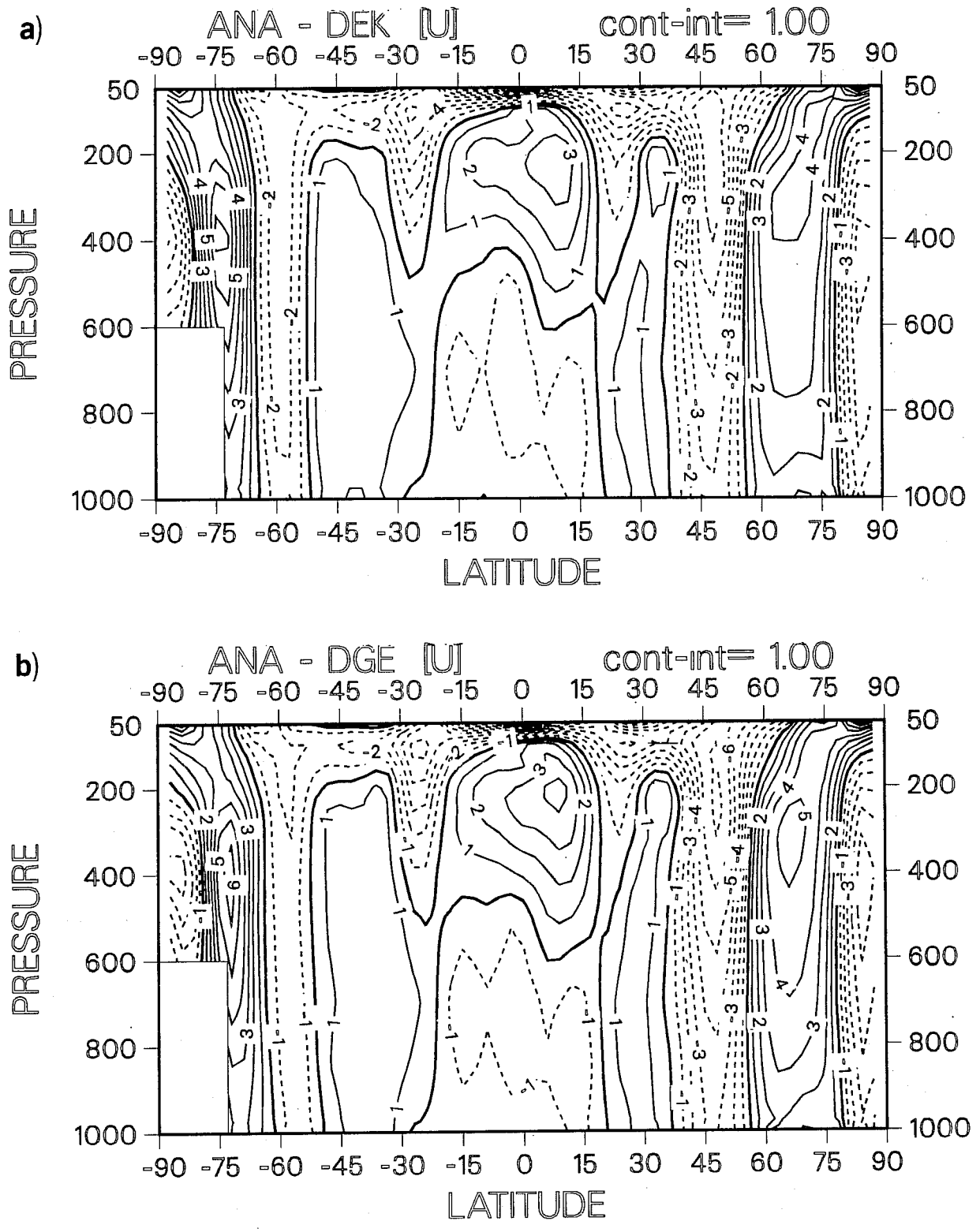

Fig. 29 Latitude-pressure cross section of zonal mean of zonal wind error, averaged between day 5 and 10 of a forecast started at 12 GMT, 30.3.86. a) from diabatic initialisation, b) from initialisation scheme as propsed by Puri (1983). Contour interval is 1 m/sec.

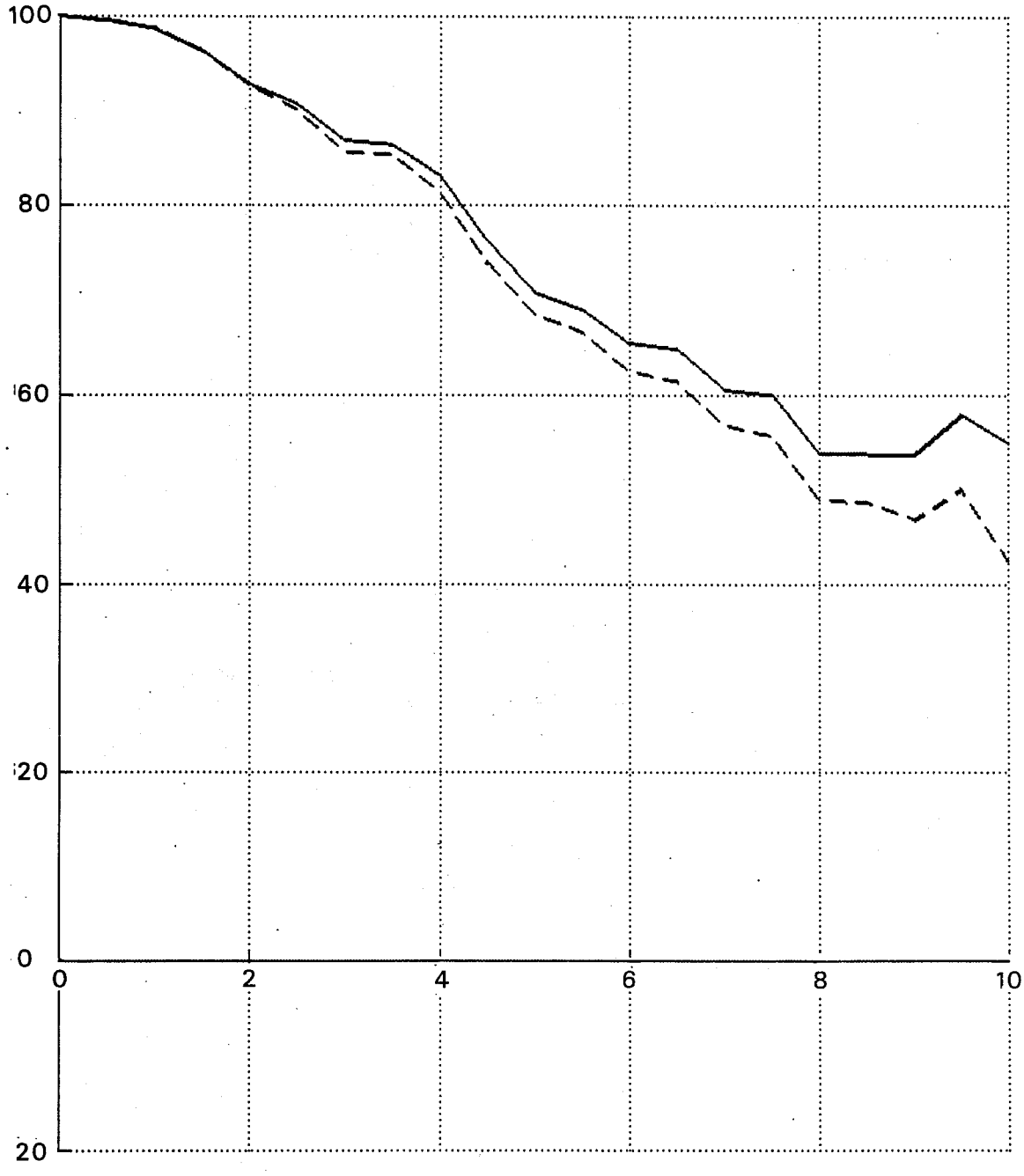

Fig. 30 Anomaly correlation of height for zonal wavenumber 1 to 3, averaged from 200 to 1000 hPa and from 20°N to 90°N. Initial date: 12 GMT, 17.9.84. Full: forecast started from diabatically initialised analysis, dashed: forecast from initialisation after Puri (1983).

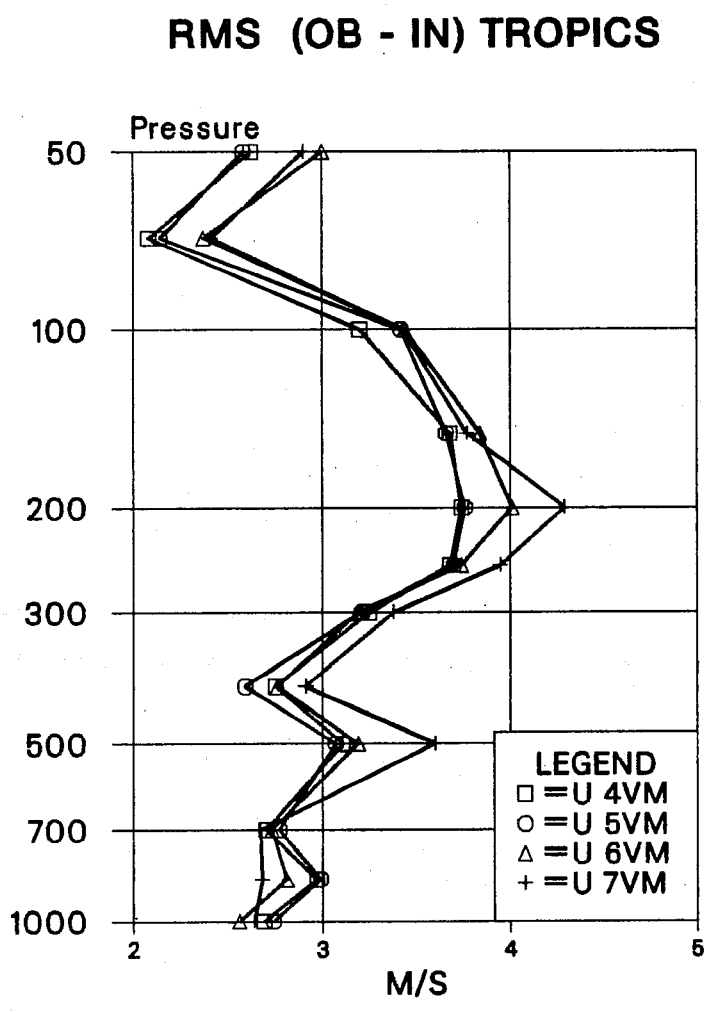

Fig. 31 RMS fit of initialised zonal wind field to tropical radiosonde data, valid for 12 GMT, 26.2.85. Squares: 4 vertical modes initialised, circles: 5 vertical modes, triangles: 6 vertical modes, crosses: 7 vertical modes.

upper tropospheric errors are smaller in the forecast started from the diabatic initialisation.

Similar experiments were run over the last 5 years whenever there was a major change to the ECMWF forecasting system. However, the conclusions were always similar. Furthermore, the problems became more evident if the assimilation was run over a longer period. As an example, Fig. 30 shows the zonal wavenumber 1 to 3 anomaly correlation of height for the northern hemisphere, averaged from 1000 to 200 hPa for a forecast started from a diabatic initialisation (full) and from a cut-off scheme (dashed). The latter was preceeded by a 5 day data assimilation from 12 Z, 12.9.84 to 12 Z, 17.9.84. The forecast from the cut-off scheme scores less well, which again highlights problems with the control of large scale internal inertia-gravity waves in the assimilation phase.

It was this finding which motivated the investigation into the performance of the optimum interpolation scheme in analysing planetary scale normal modes (Cats and Wergen, 1983). They concluded, that there are substantial errors in analysing these modes. The main error source was shown to be the poor data coverage, but there were also systematic weaknesses in the formulation of the analysis scheme. As expected, errors were largest for the gravity modes. From this it would seem that there is little hope in controlling the gravity wave activity within an assimilation system by the analysis scheme only. As discussed before, the ECMWF assimilation system benefits from the extra control of the gravity waves brought about by the diabatic initialisation. It thus relies on the better analysed Rossby modes and on the large scale components of the physical forcing.

6.2 How many vertical modes to initialise?

A decision on the number of vertical modes to be initialised is usually based on their free frequency. According to this argument, the higher internal inertia-gravity modes should only be initialised, if their free frequency is smaller than that of the fastest (external) Rossby mode for the same horizontal indices m and n. For the ECMWF model this would suggest to include 5 vertical modes in the initialisation process. However, the argument pays no attention to the amount of "noise" actually contained in the higher vertical modes and to the appropriateness of the initialisation condition $\dot{Y}=0$ for these

modes. Therefore, a number of one day data assimilations were run, in which the number of vertical modes to be initialised was varied from 4 to 7. All experiments were run with the 19-level model and the standard diabatic initialisation scheme. Fig. 31 shows the RMS fit of the initialised zonal wind component to tropical radiosonde data for the last cycle in the experiment (26.2.85, 12Z). In the stratosphere and upper troposphere the best fit is obtained by initialising 4 or 5 modes. Initialising 6 or 7 modes fits the data less well. A notable exception is the boundary layer, where initialising more vertical modes has a positive effect. This perhaps indicates that the initialisation condition $\dot{Y}=0$ is applicable in the boundary layer; a finding also reported by Errico (1984).

The impact of the number of initialised vertical modes on the vertical structure of the ω field is shown in Fig. 32. It depicts longitude-pressure cross sections of the initialised analysis, averaged between 22°N and 5°N for the last cycle of the assimilation. There are 3 major centres of rising motion at 105°E, 150°E and 207°E which are similar for all 4 initialisations. The centre at 105°E has a double structure, whereas the remaining areas show a simple maximum of rising motion around 400 hPa. The 4 mode initialisation (Fig. 32a) shows more detail in the ω field, which seems, however, to be unbalanced, as it is removed when initialising more vertical modes. Overall, Fig. 32 demonstrates that the number of vertical modes included in the initialisation has only a modest impact on the structure of the divergent wind field in the tropics.

Forecast quality turned out to be rather insensitive to the number of initialised vertical modes. Fig. 33 shows the anomaly correlation of height for the northern hemisphere, averaged from 1000 to 200 hPa. By and large, the forecast started from the assimilation with only 4 vertical modes being initialised (heavy) scores best whereas initialising 7 modes (light) slightly degrades the forecasts. In the early stages of the forecasts there is very little difference. This was also confirmed by the fit of the first guess to the data (not shown) during the assimilation phase. On the whole, Fig. 33 suggests that initialising only 4 vertical modes might be sufficient. A firm recommendation should, however, be preceded by much larger data assimilations, preferably in different situations, both with respect to flow type and data coverage. Furthermore, it should be pointed out that this result only applies

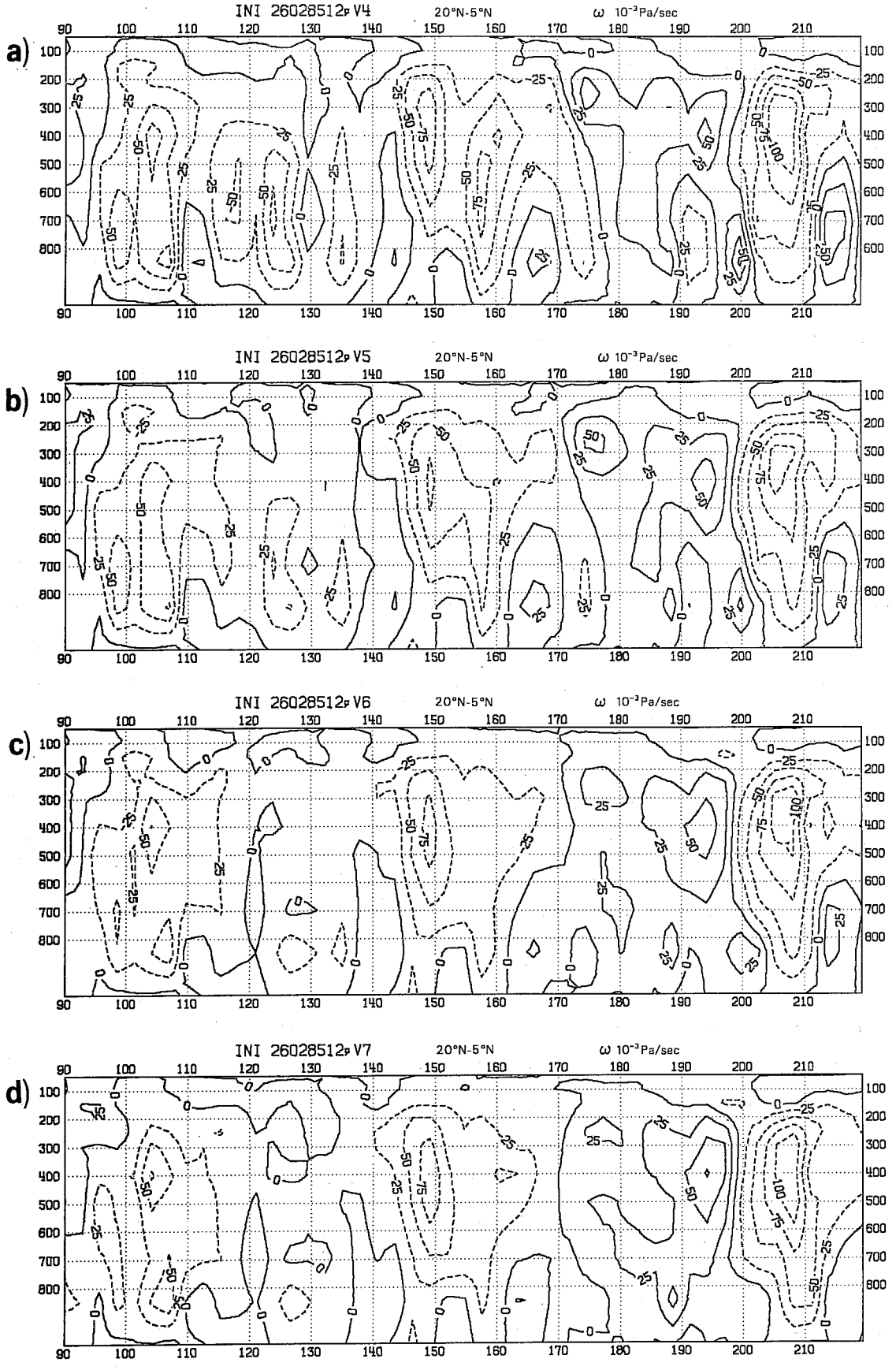

Fig. 32 Longitude and pressure cross-section of meridional average (22°N-5°N) of vertical velocity ω computed from initialisation with 4(a), 5(b), 6(c) and 7(d) vertical modes included. Fields are valid for 12 GMT, 26.2.85. Contour interval is 10^{-3} pa/sec.

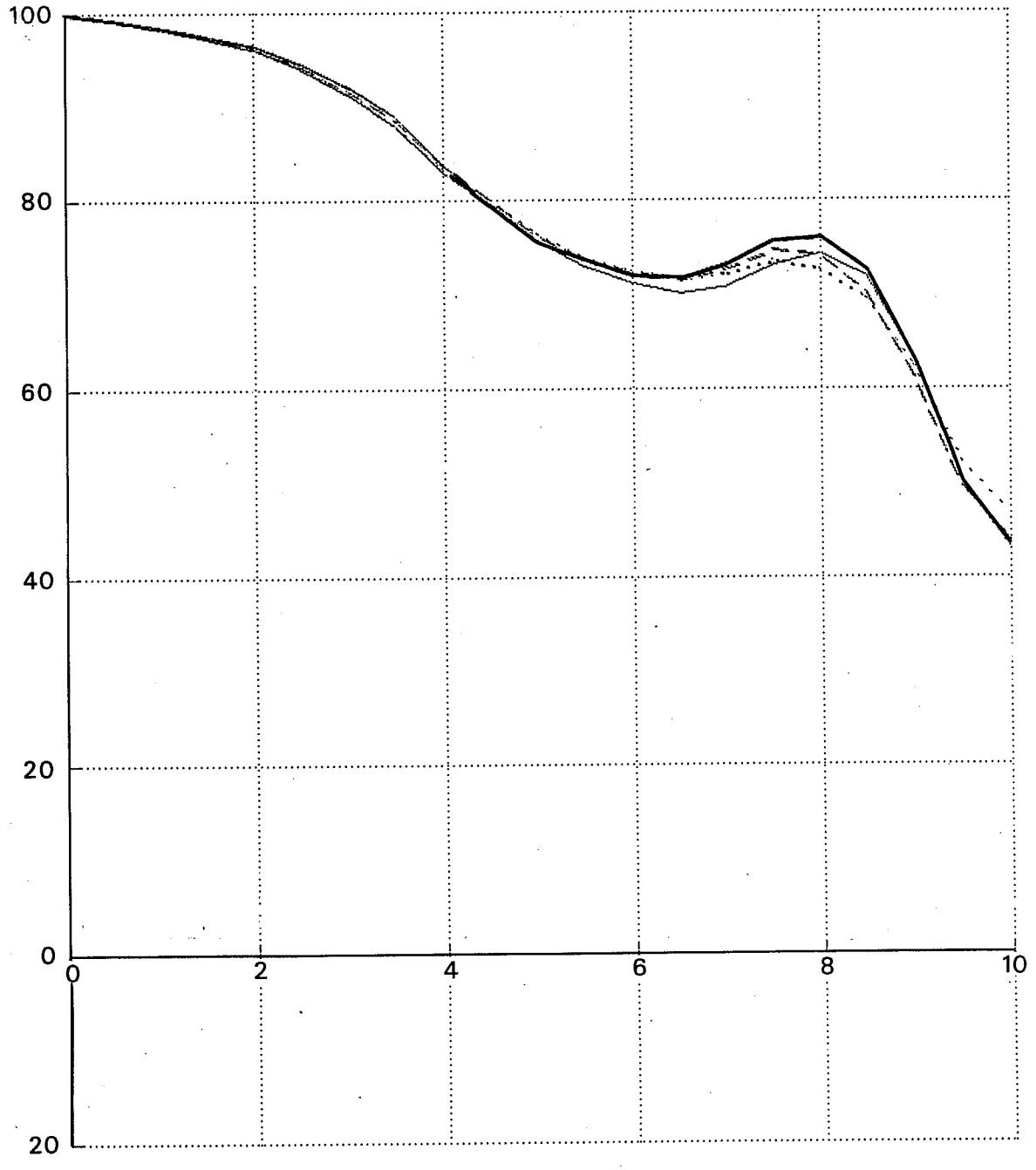

Fig. 33 Anomaly correlation of height, averaged from 200 to 1000 hPa and from 20°N to 90°N for 10 day forecasts started after data assimilation with 4 (heavy), 5 (dashed), 6 (dotted) and 7 (light) vertical modes included in the initialisation.

for the present version of the ECMWF assimilation system (May 1986). Conclusions might differ for future versions of it as indeed for assimilation schemes of other operational forecasting centres.

7. CONCLUSIONS AND OUTLOOK

The normal modes of a spectral model with a hybrid vertical coordinate were derived. Apart from a slightly more complicated linearisation process for the vertical structure equation, the implementation of an initialisation scheme for such a model followed the usual σ-model approach.

A diabatic initialisation scheme was proposed. It was based on the finding that the large scale external and internal inertia-gravity modes are - apart from tidal effects - quasi stationary. The performance of the scheme was discussed and it was shown that it successfully controls noise in the forecasts. Furthermore, the introduction of diabatic tendencies into the initialisation process significantly reduced the damping of divergent circulations as experienced when using an adiabatic scheme. The diabatic initialisation also led to some improvement in forecast quality - both in the short - and in the medium range. In an example, the spin-up problem was shown to be more pronounced in some areas than in others. Compared to this local variability, the effect of the initialisation on the spin-up was small.

The problem of systematic rejection of tropical surface pressure data by the initialisation was shown to be caused by a mishandling of the tides. A suitable modification to the initialisation condition was derived and its performance assessed.

Finally, some additional experiments on the use of a cut-off period and on the number of vertical modes to be initialised were presented. Not initialising some planetary scale internal modes turned out to have a detrimental effect on the forecast. Concerning the number of vertical modes, the experiment seemed to favour slightly a scheme with 4 vertical modes. However, the impact on the forecast was generally small.

A problem still outstanding with NMI is the initialisation of transient gravity modes. A proper application of the standard initialisation condition would require the knowledge of the time history of these modes. At present, it is not clear, how important this aspect is. Another area of concern is the change the initialisation makes to the analysed fields and the implication this has for diagnostic studies. While one can argue what the main purpose of the analysis is, it is clear that the initialised analysis should mainly be

judged by the quality of the subsequent forecast. Quite generally, the best analysis for numerical weather prediction is not necessarily the best for diagnostic purposes. When a closer fit to the observations matters, the uninitialised analysis is probably a better choice.

On the whole, the initialisation within the ECMWF assimilation system acts as a global, 3-dimensional, nonlinear, multivariate, final sweeper before the start of the forecast. It usually leads to modest modifications of the analysed fields and thus points to areas where the analysis system has problems in defining the fields close to the slow manifold. Occasional large initialisation changes invariably point to erroneous data which have found their way into the analysis despite the various quality controls. In this way, the initialisation can serve as a monitoring tool for the global observing system.

While NMI can successfully control noise in a forecast, relying too much on this property would mean to cure the symptoms rather than the cause. Ideally, one should seek to incorporate constraints into the analysis which - ultimately - lead to a balanced analysis and thus make the initialisation redundant. Eventually, the development should aim towards a unified analysis/initialisation/forecast scheme which incorporates the time dimension into the analysis process. Present day assimilation schemes only correct the first guess. They do not yet try to come to a real time understanding why the forecast was in error and what corrective action is required.

Acknowledgement

Anthony Hollingsworth carefully reviewed the manuscript. Els Kooij patiently waited for the completion of the manuscript and then took it smoothly through the publication process. Maxine Dance bravely worked her way through my unique handwriting. The figures were done by Jocelyn Williams.

References

Andersen, J.H., 1977: A routine for normal mode initialization with nonlinear correction for a multi-level spectral model with triangular truncation. ECMWF Internal Report No. 15, 41pp.

Baer, F., 1977: Adjustment of initial conditions required to suppress gravity oscillations in nonlinear flows. Contrib.Atmos.Phys., 50, 350-366.

Bengtsson, L., 1981: Current problems in four-dimensional data assimilation. ECMWF Seminar on Data Assimilation Methods, 15-19 September 1980, 195-218.

Bengtsson, L., M. Kanamitsu, P. Kållberg, S. Uppala, 1982: FGGE 4-dimensional data assimilation at ECMWF. Bull.Amer.Met.Soc., 63, 29-43.

Betts, A.K., and M.J. Miller, 1984: A new convective adjustment scheme. ECMWF Technical Report No. 43, 68pp.

Cats, G.J., and W. Wergen, 1983: Analysis of large scale normal modes by the ECMWF analysis scheme. ECMWF Workshop on Current Problems in Data Assimilation, 8-16 November, 1982, 343-372.

Chapman, S., and R.S. Lindzen, 1970: Atmospheric Tides, thermal and gravitational. D. Reidel Publishing Company, Dordrecht, Holland, 209 pp.

Daley, R., 1978: Variational nonlinear normal mode initialisation, Tellus, 30, 201-218.

Daley, R., 1985: The analysis of synoptic field divergence by a statistical interpolation procedure. Mon.Wea.Rev., 113, 1066-1079.

Dickinson, R.E., and D.L. Williamson, 1972: Free oscillations of a discrete stratified fluid with applications to numerical weather prediction. J.Atmos.Sci, 29, 623-640.

Errico, R.M. 1984: The dynamical balance of a general circulation model. Mon.Wea.Rev., 112, 2439-2454.

Hinkelmann, K., 1951: Der Mechanismus des meteorologischen Lärmes. Tellus, 3, 285-296.

Hollingsworth, A., D.B. Shaw, P. Lönnberg, L. Illari, K. Arpe, and A.J. Simmons, 1986: Monitoring of observation and analysis quality by a data-assimilation system. Mon.Wea.Rev., 114, 861-879.

Hoskins, B.J., and A.J. Simmons, 1975: A multi-layer spectral model and the semi-implicit method. Quart.J.Roy.Meteor.Soc., 101, 637-655.

Johnson, R.H., and G.S. Young, 1983: Heat and moisture budgets of tropical mesoscale anvil clouds. J.Atmos.Sci., 40, 2138-2147.

Julian, P.R., 1984: Objective analysis in the tropics: A proposed scheme. Mon.Wea.Rev., 112, 1752-1767.

Kasahara, A., 1974: Various vertical coordinate systems used for numerical weather prediction. Mon.Wea.Rev., 102, 509-522.

Kasahara, A., 1976: Normal modes of ultra-long waves in the atmosphere. Mon.Wea.Rev., 104, 669-690.

Kållberg, P, 1985: On the use of cloud track wind data from FGGE in the upper troposphere. ECMWF Tech.Memo. No. 111, 39pp.

Lau, Ngar-Cheung., 1984: A comparison of circulation statistics based on level III-b analyses produced by GFDL and ECMWF for the special observing periods. NOAA Data Report, ERL GFDL-6, 1984.

Leith, C.E., 1980: Nonlinear normal mode initialization and quasi-geostrophic theory. J.Atmos.Sci, 37, 958-968.

Longuet-Higgins, M.S., 1968: The eigenfunctions of Laplace's tidal equations over a sphere. Phil.Trans.Roy.Soc. London, Vol. A262, No. 1132, 511-607.

Lorenc, A.C., and R. Swinbank, 1984: On the accuracy of general circulation statistics calculated from FGGE data - a comparison of results from two sets of analyses. Quart.J.Roy.Meteor.Soc., 110, 915-942.

Machenhauer, B., 1977: On the dynamics of gravity oscillations in a shallow water model, with applications to normal mode initialisation. Beitr.Phys.Atmos., 50, 253-271.

Matsuno, T., 1966: Quasi-geostrophic motions in the equatorial area. J.Met.Soc., Japan, 44, 25-42.

Murakami, M., 1983: Analysis of the deep convective activity over the western Pacific and south east Asia. Part I: Diurnal variations. J.Met.Soc. Japan, 61, 60-76.

Newell, R.E., J.W. Kidson, D.G. Vincent, and G.J. Boer, 1974: The general circulation of the tropical atmosphere. Vol. 2, The MIT Press, 371pp.

Puri, K., and W. Bourke, 1982: A scheme to retain the Hadley circulation during nonlinear normal mode initialisation. Mon.Wea.Rev., 110, 327-335.

Puri, K., 1983: The relationship between convective adjustment, Hadley circulation and normal modes of the ANMRC spectral model. Mon.Wea.Rev., 111, 23-33.

Shaw, D.B., P. Lönnberg, and A. Hollingsworth, 1984: The 1984 revision of the ECMWF analysis system. ECMWF Technical Memorandum No. 92, 69pp.

Simmons, A.J., and D.M. Burridge, 1981: An energy and angular momentum convserving finite-difference scheme and hybrid vertical coordinates. Mon.Wea.Rev., 109, 758-766.

Temperton, C., and D.L. Williamson, 1979: Normal mode initialization for a multi-level gridpoint model. ECMWF Tech.Rep. No. 11, 91pp.

Temperton, C., 1981: Design of the ECMWF normal mode initialization procedure. ECMWF Seminar on Data assimilation methods, 15-19 September 1980, 159-193.

Temperton, C., 1984: Variational normal mode initialisation for a multi-level model. Mon.Wea.Rev., 112, 2303-2316.

Thompson, Jr., R.M., S.W. Payne, E. Recker, and R.J. Reed, 1979: Structure and properties of synoptic scale wave disturbances in the intertropical convergence zone of the Eastern Atlantic. J.Atmos.Sci, 36, 53-72.

Uppala, S., 1986: The assimilation of the Final Level IIb data set at ECMWF, Part I. Reprints of the national conference on the "Scientific results of the First GARP Global Experiment, American Meteorological Society, Boston, 24-29.

Wergen, W, 1982: Initialisation. ECMWF Seminar/Workshop on the Interpretation of Numerical Weather Prediction Products, 13-17 September 1982, 31-57.

Williamson, D.L., 1976: Normal mode initialisation procedure applied to forecasts with the global shallow water equations. Mon.Wea.Rev., 104, 195-206.

Williamson, D.L., and C. Temperton, 1981: Normal mode initialisation for a multi-level grid-point model. Part II: Nonlinear aspects. Mon.Wea.Rev., 109, 744-757.

ECMWF PUBLISHED TECHNICAL REPORTS

No.1 A case study of a ten day prediction. (Arpe, K., L. Bengtsson, A. Hollingsworth and J. Janjic; September, 1976)

No.2 The effect of arithmetic precisions on some meteorological integrations. (Baede, A.P.M., D. Dent and A. Hollingsworth; December 1976)

No.3 Mixed-radix fast Fourier transforms without reordering. (Temperton, C.; February, 1977)

No.4 A model for medium-range weather forecasting - adiabatic formulation. (Burridge, D.M., and J. Haseler; March 1977)

No.5 A study of some parameterisations of sub-grid processes in a baroclinic wave in a two-dimensional model. (Hollingsworth, A.; July, 1977)

No.6 The ECMWF analysis and data assimilation scheme: analysis of mass and wind field. (Lorenc, A., I. Rutherford and G. Larsen; December, 1977)

No.7 A ten-day high-resolution non-adiabatic spectral integration; a comparative study. (Baede, A.P.M., and A.W. Hansen; October, 1977)

No.8 On the asymptotic behaviour of simple stochastic-dynamic systems. (Wiin-Nielsen, A.; November, 1977

No.9 On balance requirements as initial conditions. (Wiin-Nielsen, A.; October, 1978)

No.10 ECMWF model - parameterization of sub-grid scale processes. (Tiedtke, M., J.-F. Geleynn, A. Hollingsworth and J.-F. Louis; January, 1979)

No.11 Normal mode initialization for a multi-level grid-point model. (Temperton,C., and D. L. Williamson; April, 1979)

No.12 Data assimilation experiments. (Seaman, R.; October, 1978)

No.13 Comparison of medium range forecasts made with two parameterization schemes. (Hollingsworth, A., K. Arpe, M. Tiedtke, M. Capaldo, H. Savijärvi, O. Åkesson, and J.A. Woods; 1978)

No.14 On initial conditions for non-hydrostatic models. (Wiin-Nielsen, A.C.; November, 1978)

No.15 Adiabatic formulation and organization of ECMWF's spectral model. (Baede, A.P.M., M. Jarraud and U. Cubasch; 1979)

No.16 Model studies of a developing boundary layer over the ocean. (Okland, H.; November, 1979)

No.17 The response of a global barotropic model to forcing by large-scale orography. (Quiby, J.; January, 1980)

No.18 Confidence limits for verification and energetics studies. (Arpe, K.; May, 1980)

No.19 A low order barotropic model on the sphere with orographic and Newtonian forcing. (Källén, E.; July, 1980)

No.20 A review of the normal mode initialization method. (Du H, X.Y.; August, 1980)

No.21 The adjoint equation technique applied to meteorological problems. (Kontarev, G.; September, 1980)

No.22 The use of empirical methods for mesoscale pressure forecasts. (Bergthorsson, P.; November, 1980)

No.23 Comparison of medium range forecasts made with models using spectral or finite difference techniques in the horizontal. (Jarraud, M., C. Girard, and U. Cubasch; February, 1981)

No.24 On the average errors of an ensemble of forecasts. (Derome, J.; February, 1981)

No.25 On the atmospheric factors affecting the Levantine Sea. (Ozsoy, E.; May, 1981)

No.26 Tropical influences on stationary wave motion in middle and high latitudes. (Simmons, A.J.; August, 1981)

No.27 The energy budgets in North America, North Atlantic and Europe based on ECMWF analyses and forecasts. (Savijärvi, H.; November, 1981)

No.28 An energy and angular momentum conserving finite-difference scheme, hybrid coordinates and medium-range weather prediction. (Simmons, A.J., and R. Strüfing; November, 1981)

No.29 Orographic influences on Mediterranean lee cyclogenesis and European blocking in a global numerical model. (Tibaldi, S. and A. Buzzi; February, 1982)

No.30 Review and re-assessment of ECNET - A private network with open architecture. (Haag, A., F. Königshofer and P. Quoilin; May, 1982;)

No.31 An investigation of the impact at middle and high latitudes of tropical forecast errors. (Haseler, J.; August, 1982)

No.32 Short and medium range forecast differences between a spectral and grid point model. An extensive quasi-operational comparison. (Girard, C. and M. Jarraud; August, 1982)

No.33 Numerical simulations of a case of blocking: the effects of orography and land-sea contrast. (Ji, L.R., and S. Tibaldi; September, 1982)

No.34 The impact of cloud track wind data on global analyses and medium range forecasts. (Källberg, P., S. Uppala, N. Gustafsson and J. Pailleux; December, 1982)

No.35 Energy budget calculations at ECMWF: Part I: Analyses 1980-81 (Oriol, E.; December, 1982)

No.36 Operational verification of ECMWF forecast fields and results for 1980-1981. (Nieminen, R.; February, 1983)

No.37 High resolution experiments with the ECMWF model: a case study. (Dell'Osso, L.; September, 1983)

No.38 The response of the ECMWF global model to the El-Nino anomaly in extended range prediction experiments. (Cubasch, U.; September, 1983)

No.39 On the parameterisation of vertical diffusion in large-scale atmospheric models. (Manton, M.J.; December, 1983)

No.40 Spectral characteristics of the ECMWF objective analysis system. (Daley, R.; December, 1983)

No.41 Systematic errors in the baroclinic waves of the ECMWF model. (Klinker, E., and M. Capaldo; February, 1984)

No.42 On long stationary and transient atmospheric waves. (Wiin-Nielsen, A.C.; August, 1984)

No.43 A new convective adjustment scheme. Betts, A.K., and M.J. Miller; October, 1984)

No.44 Numerical experiments on the simulation of the 1979 Asian summer monsoon. (Mohanty, U.C., R.P. Pearce and M. Tiedtke; October, 1984)

No.45 The effect of mechanical forcing on the formation of a mesosale vortex. (Wu, G.X., and S.J. Chen; October, 1984)

No.46 Cloud prediction in the ECMWF model. (Slingo, J., and B. Ritter; January, 1985)

No.47 Impact of aircraft wind data on ECMWF analyses and forecasts during the FGGE period. 8-19 November 1979. (Baede, A.P.M., P. Kållberg, and S. Uppala; March, 1985)

No.48 A numerical case study of East Asian coastal cyclogenesis. (Chen, S.J. and L. Dell'Osso; May, 1985)

No.49 A study of the predictability of the ECMWF operational forecast model in the tropics. (Kanamitsu, M.; September, 1985)

No.50 On the development of orographic cyclones. (Radinovic, D.; June, 1985)

No.51 Climatology and systematic error of rainfall forecasts at ECMWF. (S. Tibaldi; October, 1985)

No.52 Impact of modified physical processes on the tropical simulation in the ECMWF model. (Mohanty, U.C., J.M. Slingo and M. Tiedtke; October, 1985)

No.53 The performance and systematic errors of the ECMWF tropical forecasts (1982-1984). (Heckley, W.A.,; November, 1985)

No.54 Finite element schemes for the vertical discretization of the ECMWF forecast model using linear elements. (Burridge, D.M., J. Steppeler, and R. Strüfing; January, 1986)

No.55 Finite element schemes for the vertical discretization of the ECMWF forecast model using quadratic and cubic elements. (Steppeler, J.; February, 1986)

No.56 Sensitivity of medium-range weather forecasts to the use of an envelope orography. (Jarraud, M., A.J. Simmons and M. Kanamitsu; September 1986)

No.57 Zonal diagnostics of the ECMWF 1984-85 operational analyses and forecasts. (Brankovic, C.; October, 1986)

No.58 An evaluation of the performance of the ECMWF operational forecasting system in analysing and forecasting tropical easterly wave disturbances. Part 1: Synoptic investigation. (Reed, R.J., A. Hollingsworth, W.A. Heckley and F. Delsol; September, 1986)

No.59 Diabatic nonlinear normal mode initialisation for a spectral model with a hybrid vertical coordinate (Wergen, W.; December 1986).